

**IN-PLANE CYCLIC LOAD TEST OF MASONRY WALL
WITH RC OVERLAY ON ONE FACE**

MD. IZHARUL HAQUE AZAD



DEPARTMENT OF CIVIL ENGINEERING
BANGLADESH UNIVERSITY OF ENGINEERING AND TECHNOLOGY
Dhaka, Bangladesh

November, 2022

IN-PLANE CYCLIC LOAD TEST OF MASONRY WALL WITH RC OVERLAY ON ONE FACE

A Thesis Submitted by
MD. IZHARUL HAQUE AZAD
Student ID - 1017042344

A Thesis Submitted to the Department of Civil Engineering in
Partial Fulfilment of the Requirements for the Degree of
Master of Science in Civil and Structural Engineering



DEPARTMENT OF CIVIL ENGINEERING
BANGLADESH UNIVERSITY OF ENGINEERING AND TECHNOLOGY
Dhaka, Bangladesh

November, 2022

The thesis titled “**In-Plane Cyclic Load Test of Masonry Wall with RC Overlay on One Face**” submitted by Md. Izharul Haque Azad, Roll No.: 1017042344, Session: October 2017, has been accepted as satisfactory in partial fulfilment of the requirement for the degree of **Master of Science in Civil and Structural Engineering** on the 13th November, 2022.

BOARD OF EXAMINERS



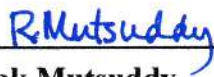
Dr. Raquib Ahsan
Professor
Department of Civil Engineering
BUET, Dhaka-1000

Chairman
(Supervisor)



Dr. Md. Delwar Hossain
Professor and Head
Department of Civil Engineering
BUET, Dhaka-1000

Member
(Ex- officio)



Dr. Rupak Mutsuddy
Assistant Professor
Department of Civil Engineering
BUET, Dhaka-1000

Member



Dr. Ismail Saifullah
Professor
Department of Civil Engineering
KUET, Khulna-9203

Member
(External)

DEDICATION

This Research Work Is Dedicated to My Beloved Parents and My Family

DECLARATION

It is hereby declared that except where specific references are made, the work embodied in this thesis is the result of an experimental investigation carried out by the author under the supervision of Dr. Raquib Ahsan, Professor, Department of Civil Engineering, BUET. Apart from where states otherwise by reference acknowledgement, the work presented is entirely by the author.

Neither the thesis nor a part of it is concurrently submitted elsewhere for the award of any degree or diploma.



Md. Izharul Haque Azad

ACKNOWLEDGEMENT

“In the name of Almighty ALLAH, The Most Gracious, The Most Merciful”

My heartiest gratitude is to Almighty ALLAH (SWT) for immense mercy on me and granting me the chance and fortitude to accomplish my thesis work satisfactorily.

I would like to express whole-hearted gratitude and obligation to my respected supervisor, Dr. Raquib Ahsan (Professor, Department of Civil Engineering, BUET). Without his rigorous direction, constructive comments, encouragement, and passionate support throughout the development of this thesis, it would not have been possible to complete it.

Sincere appreciation to Dr. Md. Delwar Hossain (Professor, and Head of the Department of Civil Engineering, BUET) for his support from the Department. The author states his gratitude to Dr. Rupak Mutsuddy (Associate Professor, Department of Civil Engineering, BUET) and Dr. Ismail Saifullah (Professor, Department of Civil Engineering, KUET) for giving their valuable comments, thoughtful insights, and suggestions for enriching the quality of this thesis work.

I am also thankful to the passed out MSc students of our department Md Aminul Islam, Abul Hasnat and Tonmoy Das for providing me the necessary information about the state of lab facilities, its limitations and sharing their work experiences with me. A special thanks to the group of Research Assistances of Dr. Raquib Ahsan Sir namely Jannat, Rakin, Sadia, Shegufta and Tasdia for assisting me unconditionally in the experimental works. Thanks and appreciation are extended to the technical staff and labors of the ‘Concrete and Materials Lab’ and the ‘Strength of the Materials Lab’ for their friendly attitude and helpful mentality during the experiment work. The research grant received for this study from the Committee for Advanced Studies and Research (CASR) of BUET, Dhaka is highly appreciated as well.

Finally, I would like to express my love, respect and appreciation to my beloved family members – Md. Mukhtar Ali (Father), Mst. Zohra Khatoon (Mother), Mst. Bodrunnesa (Aunt), Mrs. Firoza Khatun (Elder Sister), Md. Sarfaraz Ahmed (Elder Brother) and Dr. Md. Iftekhar Yunus (Elder Brother). Without their unconditional love and support, it would have been very difficult for me to accomplish my task. I am and will remain indebted to them for their motivation which has sustained me throughout the long journey of my academic life.

ABSTRACT

Unreinforced brick masonry buildings, a prevalent structural typology for residential buildings in Bangladesh, require attention to improve their seismic performance. These buildings or their wall components are rarely designed to resist lateral loads. In seismic events, they suffer severe damage causing loss of lives and properties. That is why their seismic retrofitting and strengthening is very important for the seismic resilience of Bangladesh. This research presents an experimental investigation of seismic retrofitting of unreinforced masonry walls and its findings.

In-plane cyclic loading tests, acting simultaneously with gravity loads, were conducted on a series of half-scale masonry walls of thickness 127 mm. The walls were constructed to replicate a full-scale 10 in. masonry wall with English bond conventionally used in our country. Samples with two aspect ratios (height to length ratio), namely 1.0 (1524 mm height x 1524 mm length) and 0.75 (1524 mm height x 2032 mm length), were prepared and tested under lateral cyclic loadings and their response and failure modes were observed. Then the failed samples were retrofitted and the two others were directly strengthened with a 40 mm thick RC overlay on one face having 6 mm dia. rebars provided @75 mm c/c in both directions. The cage was anchored to the wall with the help of hooks and to the base using epoxy. The lateral load carrying capacity of short walls (AR=1.0) was increased by 3.2 times for both the directly strengthened sample and the sample retrofitted after failure. For long walls (AR=0.75), the capacities increased 3.43 times and 2.85 times, respectively. The capability of undergoing a large deformation prior to failure was also improved remarkably due to the incorporation of RC overlay.

The dissipated energy for directly strengthened short walls was 11.56 times and for short walls retrofitted after failure was 9.1 times of that of the control specimens. For directly strengthened long walls, the dissipated energy was 12.34 times and that for long walls retrofitted after failure was 2.93 times. The ductility was also improved by a factor of 4.3 (for samples retrofitted after failure) and 7.45 (for direct strengthened samples) for short walls and 3.4 (for samples retrofitted after failure) and 8.9 (for direct strengthened samples) times for long walls in comparison to the control samples. The RC overlay also influenced hysteresis damping. The hysteresis damping ratio for short wall assembly ranges from 7.85% to 16.61 % when retrofitted and 10.77 % to 17.29 % when directly strengthened. In the case of the long wall control specimen, the damping ratio was 5.07 % to 13.7 % which increased

to the range of 13.01 % to 19.16 % when retrofitted and 11.89 % to 31.83 % when directly strengthened. The failure modes of the walls also changed from rocking and sliding to rocking and flexural compression, and in some cases, it was the formation of diagonal cracks. The strengthened samples exhibit a rocking type of failure and there was also a sign of corner crushing as the cracks propagated towards the toe. The test results suggest that the RC overlay improved the seismic response of unreinforced masonry (URM) walls in terms of all the parameters stated above. Regarding the influence of aspect ratio, it was found that the long walls exhibited better performance compared to the short walls with an aspect ratio equal to one.

TABLE OF CONTENTS

DEDICATION	i
DECLARATION	ii
ACKNOWLEDGEMENT	iii
ABSTRACT	iv
TABLE OF CONTENTS	vi
LIST OF FIGURES	viii
LIST OF TABLES	xii
NOTATION	xiii
LIST OF ABBREVIATIONS	xiv
Chapter 1 INTRODUCTION	1
1.1 General.....	1
1.2 Background of the Research.....	2
1.3 Core Parameters of the study	4
1.4 Objectives of the Study.....	4
1.5 Scope of the Investigation	5
1.6 Methodology of the Study	5
1.7 Outline of the Thesis.....	6
Chapter 2 LITERATURE REVIEW	8
2.1 Introduction	8
2.2 Masonry Structures.....	8
2.3 Properties of Masonry	10
2.3.1 Compressive Strength of Masonry	11
2.3.2 Tensile Strength of Masonry	13
2.3.3 Strength of Masonry in Combined Compression and Shear.....	14
2.3.4 Stress-Strain Properties of Masonry	15
2.3.5 Yield Criterion for Masonry Units.....	16
2.4 Mortar Types	17
2.5 Lateral Loads on Masonry Buildings	18
2.5.1 Seismic Loads and their Effect on Masonry Buildings	18
2.5.2 Wind Loads on Masonry	24
2.6 URM Building Stocks in Bangladesh.....	27
2.7 Behaviour of Masonry Walls under Cyclic Loading	28
2.8 Response and Failure Modes of Masonry Wall.....	29
2.8.1 Shear Failure.....	30
2.8.2 Sliding Mode	31
2.8.3 Rocking Mode	31
2.8.4 Flexural Compression Mode.....	31
2.9 Allowable Compressive and Shear Stresses in Masonry (BNBC 2020)	32
2.10 Damping Ratio and Energy Dissipation of URM under Cyclic Loads... ..	33
2.11 Strengthening Techniques of URM Walls.....	35
2.12 Experimental Investigations	38
2.12.1 Seismic Retrofitting Using FRP and GFRP.....	38
2.12.2 Seismic Retrofitting Using Ferrocement (Wire mesh)	40
2.12.3 Seismic Retrofitting PP band and other meshes	44
2.12.4 Seismic Retrofitting Using RC Overlay	46
2.13 Summary.....	51

Chapter 3	METHODOLOGY.....	53
3.1	Introduction	53
3.2	Geometry and Physical Properties of Test Specimens	53
3.3	Material Properties	55
3.3.1	Properties of Bricks	56
3.3.2	Properties of Cement	57
3.3.3	Properties of Fine Aggregates (Sands)	58
3.3.4	Properties of Coarse Aggregate	58
3.3.5	Properties of Mortar.....	59
3.3.6	Properties of Reinforcing Bars	60
3.3.7	Admixture	61
3.3.8	Timber for Formworks	61
3.4	Construction of URM Wall Specimens and their Retrofitting	61
3.4.1	Base Preparation for URM Walls	61
3.4.2	Masonry Wall Construction.....	62
3.4.3	Retrofitting Work.....	63
3.5	Test of Wall Specimens	66
3.5.1	Prism Test and Estimation of the Capacity of Masonry	67
3.5.2	Experimental Setup.....	68
3.5.3	Instrumentation	71
3.5.4	Loading Scheme	74
Chapter 4	RESULTS AND DISCUSSION.....	75
4.1	Introduction	75
4.2	Analysis of Test Results	75
4.2.1	Failure Modes of Short Wall Assemblies	75
4.2.2	Failure Modes of Long Wall Assemblies	80
4.3	Analysis of Test Data and Graphical Representations.....	87
4.3.1	Load-Deformation Response (Hysteresis Curves)	87
4.3.2	Energy Dissipation.....	94
4.3.3	Hysteresis Percentage Damping	97
4.3.4	Stiffness Degradation.....	99
4.3.5	Experimental and Theoretical Lateral Load Comparison.....	101
4.3.6	In-plane Deformation Profile of the Wall Samples	102
4.4	Comparison of Obtained Result to Literature.....	105
Chapter 5	CONCLUSIONS AND RECOMMENDATIONS	112
5.1	Summary and Conclusion.....	112
5.2	Future Recommendations	113
	REFERENCES.....	115
	APPENDIX.....	120

LIST OF FIGURES

Figure No.	Description	Pg. No.
Figure 2.1	Prehistoric architecture of masonry of ancient (Lourenco, 2014).....	9
Figure 2.2	Different types of stone masonry, a) Rubble Masonry, b) Ashlar Masonry, c) Course Ashlar Masonry (Lourenco, 2014).....	9
Figure 2.3	Typical bonds in masonry walls, a) Stretcher bond, b) Header bond, c) English bond, d) Flemish bond.....	10
Figure 2.4	Modeling strategies for masonry structures, (a) Detailed micro-modelling, (b) Simplified micro-modeling, (c) Macro-modeling (Lourenco, 2014)	10
Figure 2.5	Relationship between brick crushing strength and brickwork strength for various mortar strengths (Hendry et al., 2004).....	12
Figure 2.6	Effect of joint thickness on brickwork strength (Hendry et al., 2004) ..	13
Figure 2.7	Typical relationship between shear strength of brickwork and vertical precompression from test results (Hendry et al., 2004).....	15
Figure 2.8	Typical stress-strain curve for brick masonry (Hendry et al., 2004).....	15
Figure 2.9	Yield Criterion: (a) Typical stress-strain behaviour, (b) For brick unit (Lofti and Shing, 1994)	17
Figure 2.10	Interaction curve for bricks under biaxial compression-tension (Khoo and Hendry, 1973)	17
Figure 2.11	Global seismic hazard map showing peak ground acceleration with a probability of exceedance of 10% in 50 years (Silva et al., 2020).....	19
Figure 2.12	Tectonic setup of Bangladesh and plate boundaries (Akhter, 2010).....	20
Figure 2.13	Seismic zone map of Bangladesh (BNBC, 2020).....	21
Figure 2.14	Izmit earthquake occurred in 1999 (Turkey) (Yolalmis, 1999).....	22
Figure 2.15	Bhuj earthquake occurred in 2001 (India) (NICEE, 2001).....	23
Figure 2.16	Nepal earthquake occurred in 2015 (Nepal).....	23
Figure 2.17	Formation and pathways of storms.....	24
Figure 2.18	Basic wind speed (V, m/s) map of Bangladesh (BNBC, 2020).....	25
Figure 2.19	Cyclone storm tracks in Bangladesh (Banglapedia, 2021).....	26
Figure 2.20	Typical Construction of URM Building walls (Ansary, 2003)	27
Figure 2.21	Shear Crack Pattern for Tested Wall (Abram, 1992)	29
Figure 2.22	Flexure Crack Pattern for Tested Wall (Abram, 1992)	29
Figure 2.23	Out-of-plane behaviour of URM walls.....	30
Figure 2.24	Behaviour of URM walls under in-plane loadings	30
Figure 2.25	Failure mode of URM walls under In-plane load, (a) Sliding failure, (b) Rocking, (c) Diagonal cracking (Ghiassi et al., 2012)	31

Figure 2.26	Equivalent Viscous Damping Ratio (ξ_{eq}), and Effective Stiffness (K_{eff}) for Symmetric Hysteresis Loops (Hose and Seible, 1999).....	34
Figure 2.27	Equivalent Viscous Damping Ratio (ξ_{eq}), and Effective Stiffness (K_{eff}) for Asymmetric Hysteresis Loops (Hose and Seible, 1999)	35
Figure 2.28	Application of RC overlay on the face of URM walls (Retrofitting of DoT building at Tejgaon, Dhaka, 2019).....	38
Figure 2.29	Failure mode of samples (Mohamed et al., 2007)	39
Figure 2.30	Complete experimental setup (Saleem et al., 2016)	40
Figure 2.31	Specimen before and after retrofitting (Shah et al., 2017)	41
Figure 2.32	Complete experimental setup (Islam and Ahsan, 2019).....	42
Figure 2.33	Masonry wall sample ready for testing (Hasnat et al., 2022)	43
Figure 2.34	Wrapping walls with different mesh, (a) Steel mesh, (b) Soft polymer, (c) Geo-grid, (d) PP-band, (e) Plastic bag (Nissanka et al., 2015)	44
Figure 2.35	Application of PP bands on room (Nayak and Dutta, 2016)	45
Figure 2.36	After test condition of wall specimen (Jamshid et al., 2018)	45
Figure 2.37	Application of RC jacket on both sides of the wall (Sergey and Elena, 2011).....	46
Figure 2.38	Full setup of masonry wall for cyclic test (Sergey and Elena, 2011)	46
Figure 2.39	Typical detail of masonry wall strengthening with reinforced concrete layer (Ghiassi et al., 2012).....	47
Figure 2.40	Test setup for the shear walls (Messali et al., 2017).....	48
Figure 2.41	Crack patterns and crack width of URM walls (Mustafa et al., 2018) ..	49
Figure 2.42	Failure mode of strengthened samples (Mustafa et al., 2018).....	50
Figure 2.43	Setup for monotonic loading on wall samples (Mahmoud et al., 2019) 51	
Figure 3.1	Detailed dimensions (in mm) of a typical wall sample (short wall).....	54
Figure 3.2	Detailed dimensions (in mm) of a typical wall sample (long wall).....	54
Figure 3.3	Dimensions of reduced scale brick compared to a full size brick unit ..	57
Figure 3.4	Half-scale brick unit with side dimensions.....	57
Figure 3.5	Gradation curve for Sylhet sand and local sand	58
Figure 3.6	Gradation curve for 5 mm downgrade coarse aggregate used for RC overlay	59
Figure 3.7	Dimension and reinforcement detailing of the RCC base	62
Figure 3.8	Construction of RCC base for masonry wall.....	62
Figure 3.9	Construction of walls, (a) Construction in progress, (b) Fully prepared URM walls.....	63
Figure 3.10	Application of epoxy for anchoring rebar with base, (a) Holes in the base, (b) Marks @75 mm, (c) Applying epoxy, (d) Inserting bars	64

Figure 3.11	The 90-degree hook used for the anchoring of rebars with wall	64
Figure 3.12	Schematic detailing of reinforcement and its anchoring	65
Figure 3.13	Wall sample fully prepared for casting with proper formwork	66
Figure 3.14	Masonry prism samples ready for testing	67
Figure 3.15	Full frame for testing with mounted strong beam at top	68
Figure 3.16	Detailed dimensions of strong frame with strong beam	69
Figure 3.17	Arrangement for vertical and lateral load for wall samples	70
Figure 3.18	Jacks for applying vertical and lateral load, (a) Vertical jack (30 Ton), (b) Lateral jack (50 Ton)	71
Figure 3.19	Gauges used in cyclic test, (a) Load gauge, (b) Dial gauge	72
Figure 3.20	Schematic diagram of loading and testing arrangement of masonry walls, (a) Short wall, (b) Long Wall	72
Figure 3.21	Complete test setup of walls, (a) Wall-side, (b) RC overlay-side	73
Figure 3.22	Cyclic loading pattern applied on the wall in reverse cyclic mode	74
Figure 4.1	Failure patterns in short wall-control specimen (SW-C), (a) Cracks at final stage (4 th cycle), (b) Possibility of toe crushing	76
Figure 4.2	Failure patterns in short wall- retrofitted specimen (SW-CR), (a) Unaffected wall sample, (b) Cracks on wall side, (c) Zoomed view	78
Figure 4.3	Cracks at the base of SW-DR in 8 th cycle, (a) Unaffected wall sample (SW-DR), (b) Cracks at bottom of SW-DR	79
Figure 4.4	Details of cracks formation in SW-DR during test, (a) Final cracks at bottom of near end, (b) RC overlay detached from base and wall	79
Figure 4.5	Cracks in LW-C wall specimen	80
Figure 4.6	Generation and propagation of cracks in LW-C sample, a) First crack at 2.34 ton load, (b) Crack propagation through joints and brick	81
Figure 4.7	LW-CR wall sample before testing	82
Figure 4.8	Rocking type of failure in LW-CR sample	83
Figure 4.9	Cracks near toe of LW-CR: (a) On wall, (b) On RC overlay	83
Figure 4.10	Crack developed along the hidden cracks of far side of LW-CR	83
Figure 4.11	Near end of LW-CR wall lifted up from base	84
Figure 4.12	Crushing of top corner of LW-CR wall sample	84
Figure 4.13	Cracks in LW-DR sample: (a) First crack (at base), (b) Final crack	84
Figure 4.14	Visible rebars of LW-DR after test	85
Figure 4.15	Closed view of crack at near end of wall retrofitted directly	85
Figure 4.16	Load - deformation curve for SW-C (Control Specimen)	87
Figure 4.17	Load - deformation curve for SW-CR (Retrofitted)	88
Figure 4.18	Load - deformation curve for SW-DR (Strengthened)	88

Figure 4.19 Load - deformation curve for LW-C (Control).....	89
Figure 4.20 Load - deformation curve for LW-CR (Retrofitted).....	90
Figure 4.21 Load - deformation curve for LW-DR (Strengthened).....	90
Figure 4.22 Envelop curves for short wall specimens	92
Figure 4.23 Envelop curves for long wall specimens	93
Figure 4.24 Comparison between envelop curves for control specimens.....	93
Figure 4.25 Comparison between envelop curves for retrofitted samples.....	93
Figure 4.26 Comparison between envelop curves for strengthened samples	94
Figure 4.27 Cumulative energy dissipation for short wall assembly	95
Figure 4.28 Cumulative energy dissipation for long wall assembly.....	95
Figure 4.29 Hysteresis damping percentage for short wall assemblies	97
Figure 4.30 Hysteresis damping percentage for long wall assemblies	97
Figure 4.31 Stiffness degradation for short wall assemblies	99
Figure 4.32 Stiffness degradation for long wall assemblies	99
Figure 4.33 Comparison between theoretical and experimental load.....	101
Figure 4.34 Comparison of lateral loads of all samples with BNBC 2020.....	101
Figure 4.35 Approximate deflected shape of SW-C sample.....	102
Figure 4.36 Approximate deflected shape of SW-CR sample	103
Figure 4.37 Approximate deflected shape of SW-DR sample.....	103
Figure 4.38 Approximate deflected shape of LW-C sample.....	104
Figure 4.39 Approximate deflected shape of LW-CR sample.....	104
Figure 4.40 Approximate deflected shape of LW-DR sample.....	105
Figure 4.41 Rocking type of failure of URM walls (EIGawady et al., 2007).....	106
Figure 4.42 Failure of wall, (a) Control, (b) Retrofitted (Sergey and Elena, 2011)	106
Figure 4.43 Failure mode of URM walls (Feng et al., 2017).....	107
Figure 4.44 Failure modes of wall samples (Hasnat et al., 2022).....	108
Figure 4.45 Basic URM wall specimens (Yaghoubifar, 2008).....	110
Figure 4.46 Comparison of lateral loads of control specimen	111
Figure 4.47 Comparison of retrofitted samples to walls jacketed on both sides.....	111

LIST OF TABLES

Table No.	Description	Pg. No.
Table 2.1	Factors affecting masonry strength (Hendry et al., 2004).....	11
Table 2.2	Mix proportion and strength of commonly used mortars (BNBC, 2020).	18
Table 3.1	Dimensions and designation of wall specimens	55
Table 3.2	Crushing strength test details of bricks	56
Table 3.3	Water absorption test data of bricks.....	56
Table 3.4	Compressive strength test data for mortar (1:4).....	60
Table 3.5	Test data of prisms	67
Table 3.6	Allowable stress and force of masonry from fm'	68
Table 4.1	Summary of crack formation and failure mode	86
Table 4.2	Summary of data for hysteresis curves (short wall).....	91
Table 4.3	Summary of data for hysteresis curves (long wall).....	92
Table 4.4	Cumulative energy dissipation for each cycle	96
Table 4.5	Hysteresis damping percentage for walls.....	98
Table 4.6	Data of stiffness degradation of walls.....	100
Table 4.7	Predicted and experimental capacity of walls (Yaghoubifar, 2008).....	110
Table A.1	Load-deformation data for specimen SW-C (Control)	120
Table A.2	Load-deformation data for specimen SW-CR.....	121
Table A.3	Load-deformation data for specimen SW-DR	125
Table A.4	Load-deformation data for specimen LW-C (Control)	128
Table A.5	Load-deformation data for specimen LW-CR	130
Table A.6	Load-deformation data for specimen LW-DR	133
Table A.7	Compressive and shear strength of masonry (BNBC 2020)	139
Table A.8	28-days compressive strength data of concrete for base.....	139
Table A.9	Compressive strength test data for concrete of RC overlay.....	140

NOTATION

Symbol	Description
C_0	Uniaxial compressive strength
E	Modulus of elasticity of masonry
E_d	Energy dissipation per cycle
E_s	Elastic strain energy
f'_m	Crushing strength of masonry prism
F_a	Allowable average axial compressive stress for concentrically applied axial load
F_b	Allowable flexural compressive stress if members were carrying a bending load
F_v	Allowable shear stress in masonry
h'	effective height of a wall or column
H	Height of wall
K_{eff}	Effective stiffness
L	Length of wall
M_n	Grade of mortar according to BNBC 2020
T_0	Direct tensile strength
T	Thickness of wall
ζ_{eq}	Hysteresis damping percentage
μ	An apparent coefficient of friction
σ_c	Vertical compressive stress
σ'_c	Crushing strength of the masonry
τ_0	Shear strength at zero precompression

LIST OF ABBREVIATIONS

Symbol	Description
AR	Aspect Ratio
BNBC	Bangladesh National Building Code
CA	Coarse Aggregate
FA	Fine Aggregate
FE	Finite Element
FEMA	Federal Emergency Management Agency
FRP	Fiber Reinforced Polymer
GFRP	Glass Fiber Reinforced Polymer
HCB	Hollow Concrete Block
LW-C	Long Wall Control (Specimen)
LW-CR	Long Wall Control Specimen Retrofitted after Failure
LW-DR	Long Wall Directly Strengthened/ Retrofitted
RC	Reinforced Concrete
SW-C	Short Wall Control (Specimen)
SW-CR	Short Wall Control Specimen Retrofitted after Failure
SW-DR	Short Wall Directly Strengthened/ Retrofitted
URM	Unreinforced Masonry

Chapter 1

INTRODUCTION

1.1 General

Brick masonry is one of the most commonly used structural materials in the construction of low-rise buildings worldwide. It is also one of the oldest construction materials (Moffet, 2016). Prior to the invention of the modern concrete, structural steels and other structural materials, these masonry constructions had shaped the cities and habitats of mankind for centuries. Masonry structures have been a part of us since the earliest days of civilisation. Especially, its impacts are very noteworthy in the historical structures throughout the world. The Shat Gombuj Mosque, the Lalbagh Fort, the Ahsan Manzil are examples of such heritage structures from our country. Similar ancient structures with historical importance can also be seen in other countries such as the Tower of Babylon, Great Wall of China, Pyramids of Egypt, etc. which refers to the sustainability of masonry (Moffet, 2016). Construction of a large number of residential and official buildings using masonry walls is also noteworthy.

Unreinforced masonry (URM) buildings, that represent a large number of buildings around the globe including Bangladesh, is mostly constructed in a non-engineered manner. It has been a very popular form of structural system due to various reasons such as ease in construction, economy, pleasant aesthetics, architectural beauty, fire resistance and effective heat and sound insulation, etc. (Gencel, 2015 and Hendry et al., 2004). In a developing country like ours, URM buildings have been a prevalent form of habitat for a long time and are still being used for low and medium-rise building constructions. However, with the emergence of some advanced construction materials such as concrete and reinforcing steel, and with the development of moment resisting frames like RCC and steel structures the trend of using masonry has fallen and attention shifted to the use of above-mentioned materials and structural forms while masonry is being used as a non-structural element in them. The URM structures, however, are proven to be very vulnerable when subjected to lateral load such as earthquakes and this is the primary disadvantage of this type of

structure. During the last few seismic events occurred globally it is very obvious that these URM buildings cannot take the lateral loads imposed on them by a seismic phenomenon and often fail in brittle manner (Bhattacharya et al., 2014). One of the prime causes of mass casualties in major and moderate earthquakes around the world is the collapse of these non-engineered structures (Macabuag et al., 2012). This is due to the fact the masonry is a heterogeneous material that consists of brick units and joints. Moreover, the tensile strength of URM walls is very poor compared to its compressive strength (Hendry et al., 2004). That is why the URM structures are very vulnerable to earthquakes and their vulnerability is due to the failure caused by the action of in-plane and/or out-of-plane loading. Moreover, most of these buildings do not satisfy the latest code provisions being practiced. Thus, to save these buildings from being collapsed under the action of seismic load strengthening or retrofitting of their constituent elements is required so that their lateral load carrying capacity can be increased and their ductility can be improved as well. This research presents the result of experimental investigation carried out on the strengthening and retrofitting of URM walls with RC overlay on one face under the action of in-plane cyclic load.

1.2 Background of the Research

The construction of low and medium-rise buildings using masonry in a developing country like ours has been practiced since a long time. In Bangladesh, along with many architectural heritage structures, there are a large number of residential and old official buildings as well, which are non-engineered URM structures (CDMP, 2009). In URM, the load bearing walls are the prime component which carry the superimposed gravity load. These walls are constructed using small building blocks such as brick units joined together by mortars of cement and sand, with no reinforcement being provided, which makes it difficult to predict their behaviour. Such structural members are very efficient in resisting gravity loads coming from upper floors if sufficient thickness to the wall is provided. They have some other advantages as well; such as scope of addition and alteration, less and simple formwork, easy method of repairing, inexpensive methods of retrofitting, use of locally available materials, requirement of less skilled labor, less engineering involvement etc. (Sakalle et al., 2018) The URM buildings, however, are barely

reinforced, and due to its low ductility they are more vulnerable to the seismic forces developed during an earthquake (Hasnat et al., 2022). These buildings do not have any lateral load resisting system in them which make them more prone to damage under the action of large lateral force during earthquakes, causing a significant loss of properties and lives as well. In the last century, almost 75% of the fatalities is caused by collapse of buildings during earthquakes. The greatest portion (more than 70%) of this catastrophe is due to collapse of URM buildings (Sar and Sarkar, 2013). A large number of the older buildings in our country are URM buildings that were originally designed for gravity load only. They are weak and prone to failure even under moderate earthquakes. In many cases the buildings have lost major portion of their strength and stiffness. It is due to severe cracks by the repeated seismic events. A study was conducted by Amanat et al. (2007) which recommended that more than 60% of the buildings would be moderately or partially damaged under an earthquake of intensity VIII (MMI) and these buildings need to be retrofitted. Such structures can either be demolished or the preferable option is to find out a favorable technique or solution to increase their lateral stiffness and ductility which will eventually improve their seismic performance. However, it is found from the literature that a remarkable number of research are already conducted on RC structures. Therefore, the understanding of the behaviour of masonry buildings subjected to earthquake induced dynamic loads is a great concern of recent time.

It is, however, essential to understand the seismic behaviour of URM buildings before adopting any strengthening or rehabilitation technique for them. Afterward, an effective and affordable retrofitting scheme can be found out and implemented. A number of retrofitting techniques are available to increase the strength and ductility of URM elements. The addition of structural components such as steel or reinforced concrete frame is one option although it has a main disadvantage of adding significant weight to the building and loss of valuable space in it. Another alternative is related to surface treatment. The possible option could be the use of Fiber Reinforced Polymer (FRP) (ElGawady et al., 2007), grout injection and shotcrete (ElGawady et al., 2006), wiremesh (Ferrocement) (Shah et al., 2017) etc. Numerical studies have also been conducted and validated with the experimental findings

(Gattesco and Boem, 2017 and Ghiassi et al., 2012). A number of numerical studies that involved Finite Element (FE) model to simulate the behaviour of masonry walls strengthened using ferrocement under in-plane loading were undertaken by various researchers (Alam and Amanat, 2004; Khair, 2005).

The use of reinforced concrete (RC) overlay in the seismic strengthening of masonry buildings and its walls have also been investigated by many researchers both experimentally (Mahmoud et al., 2019; Messali et al., 2017) and numerically for instance (Ghiassi et al., 2012). Such studies were conducted with RC jacketing on both sides under cyclic load and on single side under monotonic loading. However, such type of test was not conducted with RC overlay on one face under cyclic loading with some constant gravity load. Therefore, an experimental study is required to know the actual behaviour of URM wall with single layer reinforced jacketing under cyclic loading.

1.3 Core Parameters of the study

URM structures being one of the most common structural forms for ordinary buildings, therefore, it requires special attention while subjected to seismic loads. Specially, their efficient retrofitting technique is a matter of great concern. Use of conventional retrofitting schemes such as grouting, shotcrete, FRP, GFRP, Ferrocement, RC jacketing are studied in a large scale for gravity loads in frame structures. However, less experimental and numerical evidences are available for cyclic loading of URM walls. Hence, it would be interesting to know the actual behaviour of URM for such type of retrofitting techniques. The present research focuses on the use of single layer of reinforced concrete jacketing to study the behaviour of URM wall under cyclic loads with and without retrofitting. In addition, the effects of aspect ratio are also studied for the same.

1.4 Objectives of the Study

This research work focuses on the experiment of unreinforced masonry wall with two different aspect ratios, their direct strengthening and retrofitting after failure with a particular type of RC overlay on one face under the action of cyclic load and respective gravity loads. The main objectives of this research work are:

- i. To investigate the effects of aspect ratio (height to length ratio) in the response of half-scale masonry walls (10 inch wall arrangement – English bond) under the action of cyclic loadings with and without RC overlay.
- ii. To compare the load-deformation relationship of URM walls to that of retrofitted and strengthened walls.
- iii. To evaluate the lateral resistance and energy dissipation of wall in the pseudo-static in-plane wall test.
- iv. To evaluate the effect of single layer RC overlay in strengthening by focusing on stiffness, ductility and hysteretic damping of masonry walls.

1.5 Scope of the Investigation

The primary purpose of the research is to investigate the cyclic load test of URM walls. The effects of aspect ratio and retrofitting technique in terms of RC overlay on single side have been extensively investigated here. The scope of the study can be summarized as follows:

- i. Use of conventional construction materials e.g., bricks, mortar, etc.
- ii. Construction and test of half-scale wall samples of thickness 5 in. with half-scale bricks; prepared in a manner that is used for the construction of a conventional 10 inch load bearing wall with English bond.
- iii. Walls with two aspect ratios namely 1.0 and 0.75.
- iv. Vertical load or gravity load to be encountered (10% of the ultimate compressive strength).
- v. Application of lateral cyclic load at top left corner.
- vi. Strengthening and retrofitting of walls with RC overlay on one face only.
- vii. No opening in the walls.
- viii. Wall type- unreinforced masonry (URM).

1.6 Methodology of the Study

The following methodology has been adopted for this research work:

- i. Four half-scale URM wall samples to replicate a conventional 10 inch wall with English bond were prepared with two aspect ratios (Height/Length) namely, 1.0 and 0.75. There were two wall samples for each aspect ratio.

- ii. The dimensions of the walls (L x H x T) were 1524 mm x 1524 mm x 127 mm for short walls (AR = 1.0) and 2032 mm x 1524 mm x 127 mm for long walls (AR = 0.75).
- iii. Conventional construction materials were used such as half-scale burnt clay bricks of dimension 127 mm x 60 mm x 38 mm and mortar of ratio of 1:4 (by volume).
- iv. Two control specimens (one from each AR) were tested under cyclic static incremental horizontal loads with sustained vertical load on them. Then, these two tested walls were retrofitted with reinforced concrete (RC) overlay on one face and were tested again. Other two walls were directly strengthened using the same RC jacketing and tested in the same manner afterward.
- v. The RC overlay was prepared using a special type of micro-concrete. The mix ratio was 1:1.2:1.7 (cement : sand : stone) by weight with a w/c ratio of 0.50 and the targeted 28 days compressive strength of around 34.5 MPa. To gain this strength and to provide sufficient workability to concrete a water reducing admixture with a dose of 200 ml/bag of cement was used. The thickness of the RC was chosen to be 40 mm for half-scale wall and 6 mm dia. mild steel rod was used as the reinforcing bar at 75 mm (3 in.) c/c in both directions. The bars were anchored to the base (75 mm) with the help of epoxy and the reinforcement mesh was anchored to the wall with a hook that was embedded into the wall to a depth of 50 mm using epoxy.
- vi. Finally, the wall samples were tested under the specified loading and the collected load - displacement data were analyzed to compare the load carrying capacity of the walls.

1.7 Outline of the Thesis

The total thesis report has been divided into five (05) chapters/parts. The first chapter (Chapter-1) introduces the whole thesis work and represents the research background, core parameters to be studied, objectives of the research work and brief methodologies. Apart from this chapter, the rest of the thesis report includes:

Chapter 2 contains “Literature Review” that includes the previous investigations and

experiments on this field and the basics of URM wall behaviour and its mechanical properties.

Chapter 3 includes “Methodologies” of the work. This part represents the details of the experimental works e.g., material collection, material testing, preparation and testing of samples, strengthening and retrofitting details and so on.

The next part, Chapter 4, represents the “Results and Discussion” section in which the total experimental data were summarized and analyzed extensively and a proper discussion section is attached on the basis of the comparison of results.

The last section is Chapter 5 entitled as “Conclusions” and Recommendations which summarizes the overall outcome of the experiment and prospects for future study.

Chapter 2

LITERATURE REVIEW

2.1 Introduction

The structural systems, both masonry structures and moment resisting frames, are designed to withstand the loads imposed on them. Most of the structures constructed during the early phase of construction, were designed to resist the gravity load only. These are the unreinforced masonry structures. A little or no concern was given in the lateral load-resistance. As a result, during any seismic event, a huge loss of assets and lives are caused when these structures experience medium or heavy cyclic load. A vulnerability analysis of the existing masonry buildings on a target area in Basel, Switzerland carried out by Lang (2000) shows that around 45% and 80% of the existing URM buildings will experience heavy damage during an earthquake of intensity VIII (MSK). The condition of URM building is much more severe in Bangladesh, approximately 50% of the private housing units do not have any lateral load resisting system e.g. continuous lintel, in the earthquake prone areas like Chattogram, Sylhet (Ansary, 2003). For the better understanding of the seismic behaviour of these structures there basic properties need to be understood first.

This chapter of the report deals with the embodiment of the theoretical contexts related of this research work. Starting with the review of the basic masonry properties such as its physical and mechanical characteristics e.g., it's compressive and tensile strength, its stress-strain behaviour, types of failure modes, selection criteria for mortar are discussed. After that, a detailed literature review regarding the retrofitting/ repairing/ strengthening techniques of URM walls with proper references are also highlighted here. Finally, a summary on significant findings of previous few research works on retrofitting of URM walls using RC overlay is provided.

2.2 Masonry Structures

Masonry is the oldest and one of the simplest forms of structural system for building construction. The simple construction method of masonry is one of its most important characteristics. The pieces of stone, bricks, or blocks are laid on top of

each other, either with or without cohesion via mortar. It is a simple and adequate process. This technique has been successfully used ever since remote ages. Stone was probably the first material to be used for masonry. In the ancient Near East, evolution of housing was from huts, to apsidal houses and finally to rectangular houses as shown in Figure 2.1 (Lourenco, 2014).

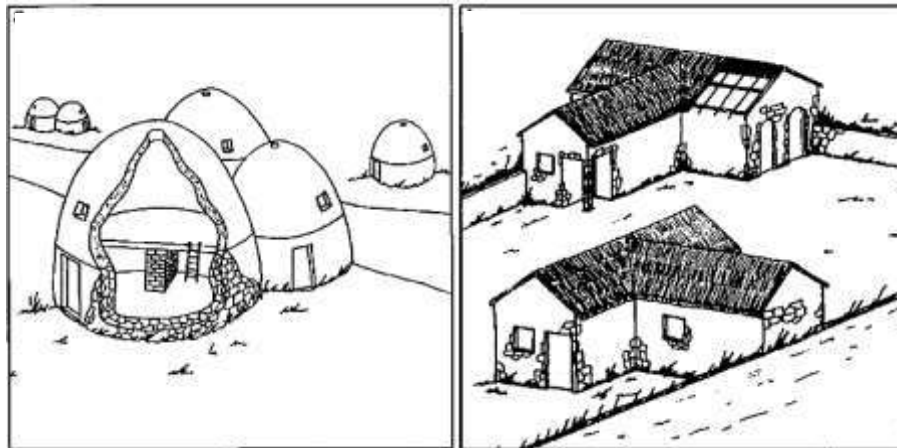


Figure 2.1 Prehistoric architecture of masonry of ancient (Lourenco, 2014)

The huge number of possible combinations generated by the geometry, nature and arrangement of units and the characteristics of mortars raise doubts about the accuracy of the term “masonry” (Lourenco, 2014). A simple classification of stone masonry and brick masonry are shown in Figure 2.2 and 2.3 respectively.

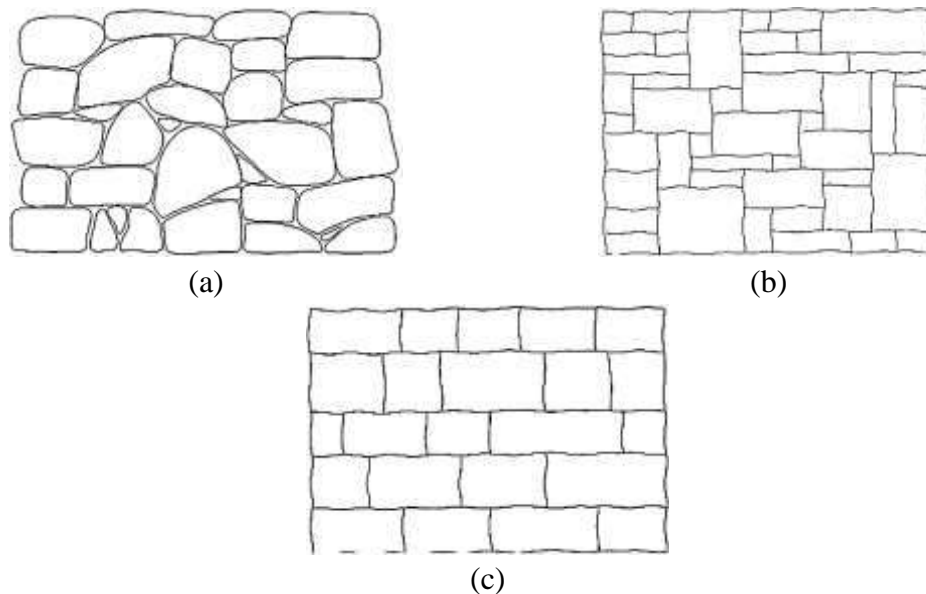


Figure 2.2 Different types of stone masonry, a) Rubble Masonry, b) Ashlar Masonry, c) Course Ashlar Masonry (Lourenco, 2014)

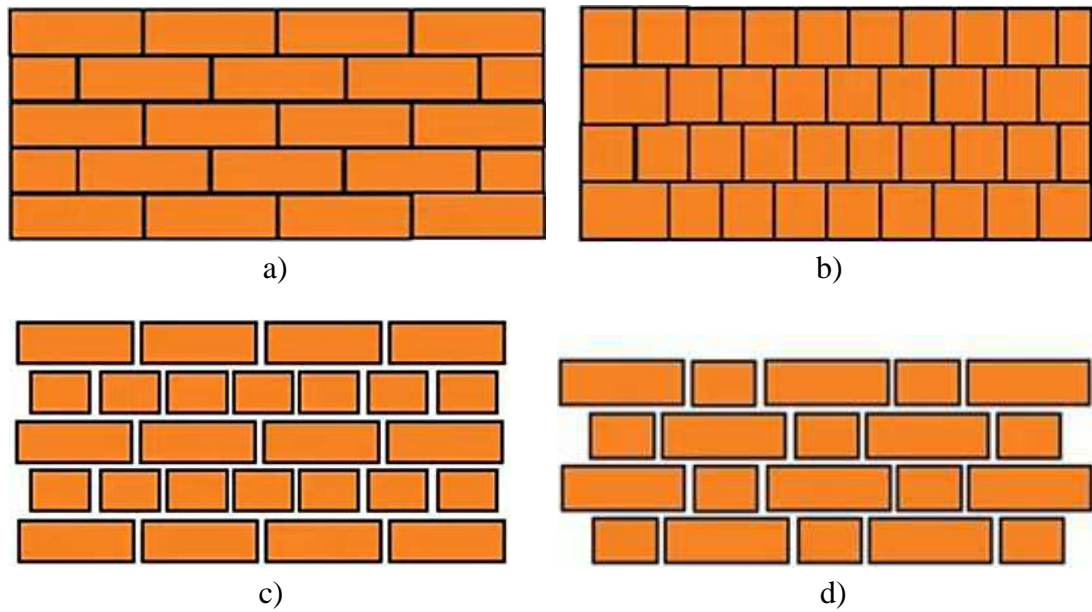


Figure 2.3 Typical bonds in masonry walls, a) Stretcher bond, b) Header bond, c) English bond, d) Flemish bond

2.3 Properties of Masonry

Masonry is typically a heterogeneous and anisotropic material that consists of two different types of elements - brick units and mortar (Elgwady et al., 2002). Brick units can be manufactured from compressed earth, stone or concrete or burnt clay while mortar can be obtained as a mixture of lime or a mixture of cement, lime, sand and water in various proportions. The modeling strategies of masonry are given in Figure 2.4.

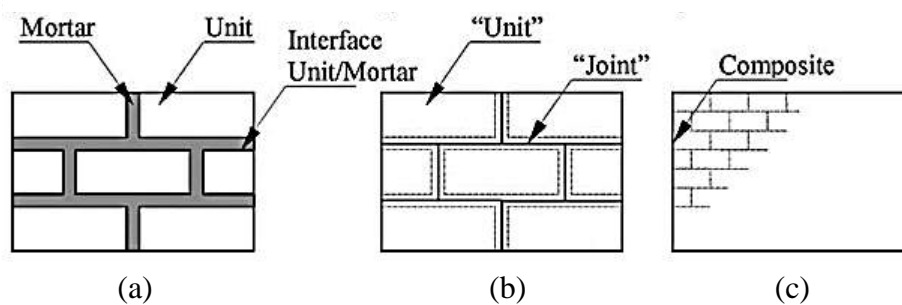


Figure 2.4 Modeling strategies for masonry structures, (a) Detailed micro-modelling, (b) Simplified micro-modeling, (c) Macro-modelling (Lourenco, 2014)

These two materials possess different physical and mechanical properties. Brick are stiffer while mortars are relatively softer and these two finally results in a composite known as masonry. Consequently, depending on the type of brick units and mortar

being used in structures, masonry properties vary from one structure to another as its properties are dependent on that of its constituent elements. Some other factors could also affect the masonry such as the dimension of bricks, mortar joints, arrangement of bed-joints and head-joints, arrangement of brick units and the workmanship as well. While subjected to lateral loadings masonry does not show elastic behaviour even for the range of small displacement. For the design strength of masonry, the current parameters have been derived on an empirical basis from tests on piers, walls and small specimens which has been proven safe for designs, however, at the same time it gives very little knowledge about the behaviour of the material under load. Therefore a more detailed research work and discussion on masonry strength is required and some of those are analyzed and recorded in the following sections.

2.3.1 Compressive Strength of Masonry

The behaviour of masonry under tensile force is very poor as it consists of two different materials that are arranged in regular intervals and the bond between them being very weak. Therefore, the main strength which is supposed to be provided from the side of masonry is its compressive strength and it is expected to resist the compressive forces only. The strength and stiffness characteristics of this masonry are supposed to be influenced by the strength of its constituent elements – bricks and mortar and their arrangement in the masonry (Hendry et al., 2004). The factors given in Table 2.1 are of importance for the determination of compressive strength of masonry (Hendry et al., 2004).

Table 2.1 Factors affecting masonry strength (Hendry et al., 2004)

Unit Characteristics	Mortar Characteristics	Masonry
Strength Type and Geometry: Solid Perforated Hollow Height/Thickness Ratio Absorption Characteristics	Strength: Mix Water/Cement Ratio Water Retentivity Deformation Characteristics Relative to Units	Bond Direction of Stressing Local Stress Raiser

The strength of a unit of particular material increases with decrease in height. It happens due to the restraining effect of the testing machine platens on the lateral

deformation of the unit (Hendry et al., 2004). The units of masonry have to resist the tensile forces as well resulting from restraint of the lateral strains in the mortar. For given materials and joint thickness, the greater the height of the unit the greater the resistance to these forces and the greater the compressive strength of the masonry as illustrated in Figure 2.5 (Hendry et al., 2004).

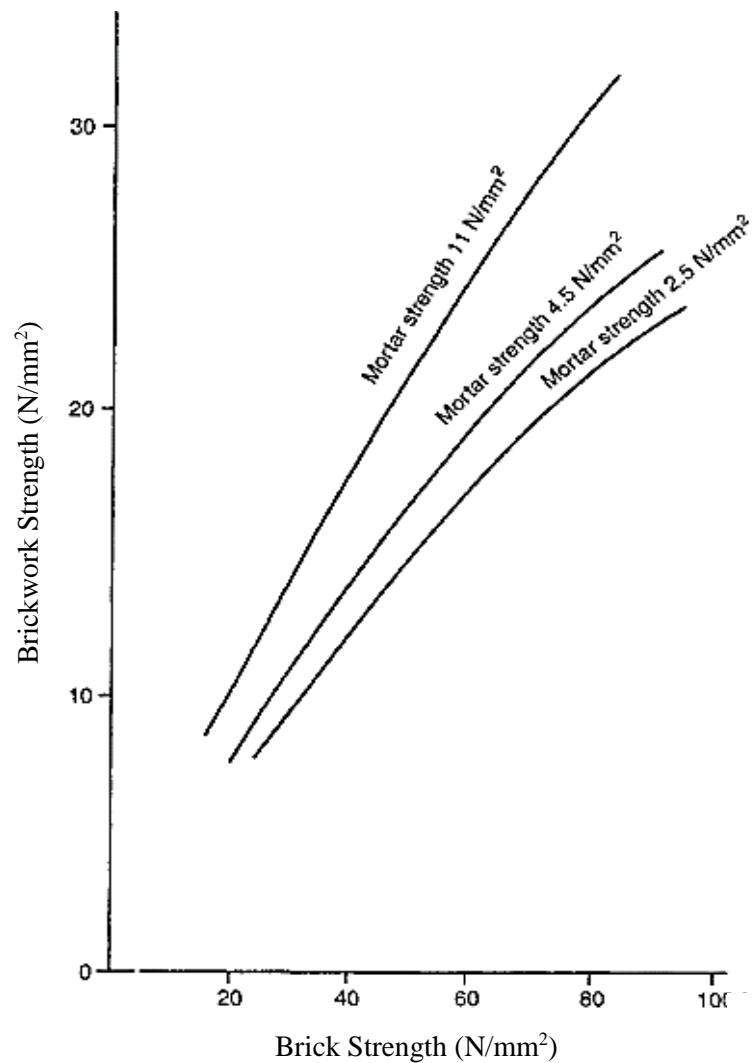


Figure 2.5 Relationship between brick crushing strength and brickwork strength for various mortar strengths (Hendry et al., 2004)

For a particular unit height, increasing the thickness of the mortar joint will decrease the strength of the masonry (Hendry et al., 2004). This is significant for brickwork constructions, as shown in Figure 2.6.

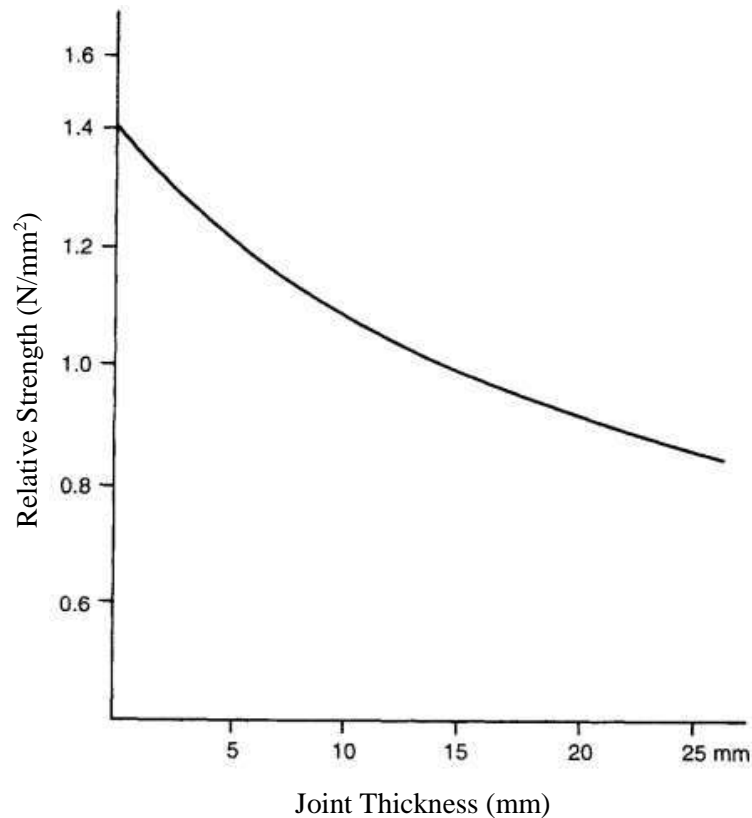


Figure 2.6 Effect of joint thickness on brickwork strength (Hendry et al., 2004)

2.3.2 Tensile Strength of Masonry

The tensile strength of masonry can be classified and illustrated as follows:

2.3.2.1 Direct Tensile Strength

Masonry can be subjected to both in-plane and out-of-plane loading due to the lateral forces being applied on them. The in-plane loading can generate tensile stresses in masonry. These could be due to wind loads, eccentric gravity loads, change in temperature or movement of moisture or due to movement in foundation (Hendry et al., 2004). The tensile resistance of URM, especially across the bed joints, is low and unpredictable and therefore in structural design one cannot generally rely upon this.

The flexural tensile strength developed across the bed joints affect the lateral resistance of a wall supported at its base and top only. If supported on its vertical edges as well, the lateral resistance will depend also on the flexural strength of the masonry in the direction perpendicular to the bed joints. Hendry et al. (2004)

suggested that the strength in this direction is about three times as great as across the bed joints.

2.3.2.2 Flexural Tensile Strength

URM panels used as cladding for buildings have to withstand forces such as lateral wind pressure and suction. The self-weight of a wall might add some stability to it, however, this stability is insignificant in providing the necessary resistance to wind forces. Therefore, one could rely upon the flexural tensile strength of masonry.

In the stronger direction, the flexural tensile strength of clay brickwork varies from 0.8 to 2.0 N/mm², while the strength in bending across the bed joints is about one-third of this (Hendry et al., 2004). In the case of direct tension, the strength is dependent on the absorption characteristics of the bricks and on the type of mortar used as well. Calcium silicate brickwork and concrete blockwork have rather lower flexural tensile strength than clay brickwork, that of concrete blockwork depending on the compressive strength of the unit and the thickness of the wall (Hendry et al., 2004).

2.3.3 Strength of Masonry in Combined Compression and Shear

Buildings subjected to lateral forces experience a combined effect of compressive and shear forces. The strength of masonry under such condition is of importance in relation to the response of the structures. It is experimentally suggested (Hendry et al., 2004) that there lies a Coulomb type of relationship between the shear strength and precompression. There is an initial shear resistance dependent on the adhesion between the units and mortar by a frictional force component proportional to the precompression. This relationship could be expressed as:

$$\tau = \tau_0 + \mu\sigma_c \quad (2.1)$$

Here,

τ_0 = The shear strength at zero precompression,

μ = An apparent frictional coefficient and

σ_c = The vertical compressive stress.

The above mentioned typical relationship is illustrated in the Figure 2.7.

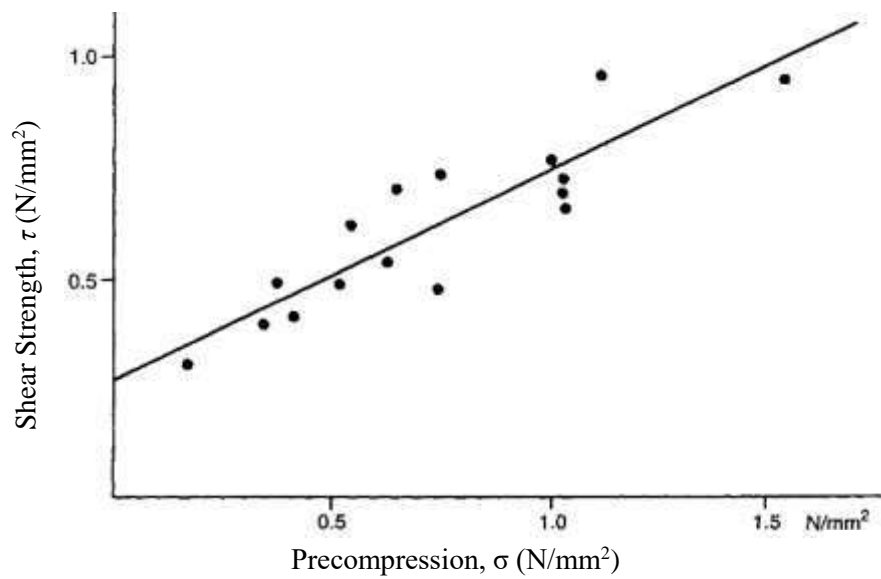


Figure 2.7 Typical relationship between shear strength of brickwork and vertical precompression from test results (Hendry et al., 2004)

2.3.4 Stress-Strain Properties of Masonry

Masonry is generally considered as a linearly elastic material, although tests indicate that the stress-strain relationship is approximately parabolic (Hendry et al., 2004), as shown in Figure 2.8.

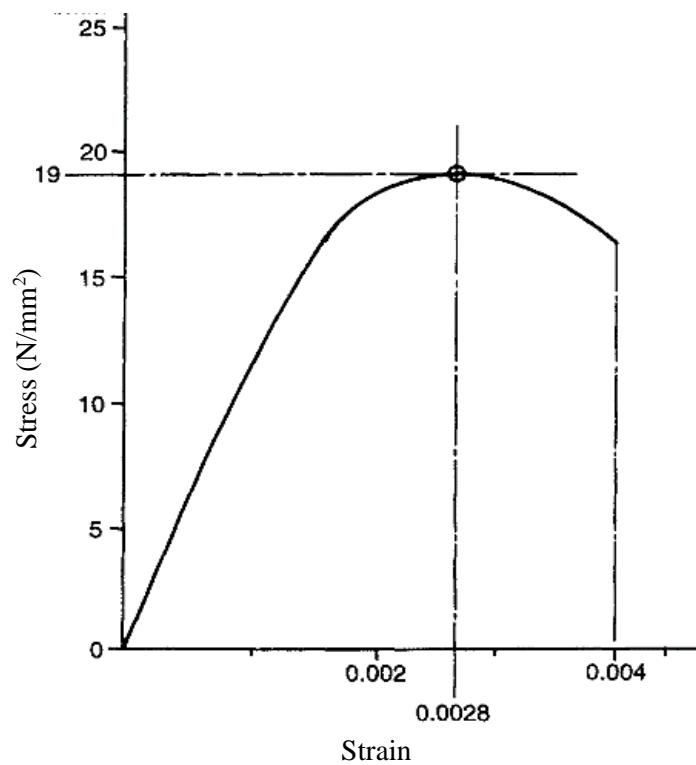


Figure 2.8 Typical stress-strain curve for brick masonry (Hendry et al., 2004)

Practically, masonry is stressed only up to a fraction of its ultimate load, and therefore for the calculation of normal structural deformations the assumption of a linear stress-strain curve is acceptable (Hendry et al., 2004). The Young's modulus could be obtained by various formulae suggested from time to time. However, this parameter is rather variable even in the case of nominally identical samples (Hendry et al., 2004). As an approximation, it may be expressed as

$$E = 700\sigma'_c \quad (2.2)$$

Here,

σ'_c = The crushing strength of the masonry. This value will apply up to about 75% of the ultimate strength.

For the evaluation of long-term deformations, a reduced value of E should be used, in the region of one-half to one-third of that given by equation (2.2).

2.3.5 Yield Criterion for Masonry Units

A yield criterion for uniaxial behaviour of masonry units is illustrated in Figure 2.9 according to Lofti and Shing (1994). Furthermore, mechanical properties of brick units such as clay units are directional in nature due to the extrusion process. Cylinders (0.667-in diameter by 1.3-in height) extracted from three faces of brick units were also tested and it was found that there are variations in compressive strengths. Lofti and Shing (1994) also found that compressive strength of brick units on average is 2 to 3 times larger than the tensile strength. Additionally, uniaxial compression tests of stack bonded masonry prisms show that brick units experience a compression-tension-tension state of stress. Since compressive strength of brick units is much stronger than tensile strength, brick units usually fail in tension. Biaxial compression-tension tests on brick by McNary and Abrams (1985) shows the interaction between compression (C) and tension (T) to fit the following relationship,

$$\frac{C}{C_0} = 1 - \left(\frac{T}{T_0}\right)^{0.58} \quad (2.3)$$

Where,

C_0 = Uniaxial compressive strength and

T_0 = Direct tensile strength.

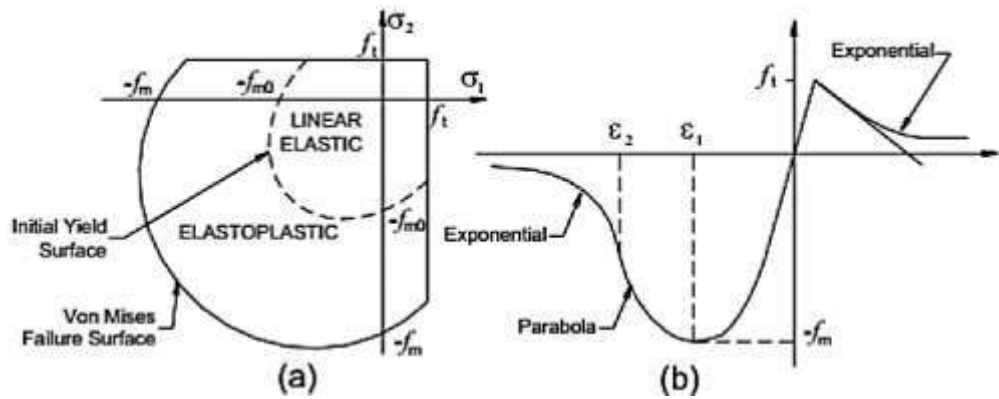


Figure 2.9 Yield Criterion: (a) Typical stress-strain behaviour, (b) For brick unit (Lofti and Shing, 1994)

Khoo and Hendry (1973) also found such interaction between compression and tension in bricks tested under biaxial compression-tension. The concavity in the compression-tension interaction diagram is the indication of the interaction, as illustrated in Figure 2.10.

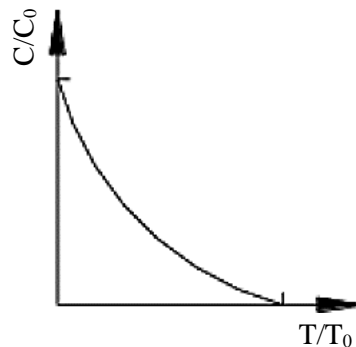


Figure 2.10 Interaction curve for bricks under biaxial compression-tension (Khoo and Hendry, 1973)

2.4 Mortar Types

Mortar consists of three basic components namely, cement, lime and sand. Lime is rarely used in Bangladesh, however, it produces favorable properties when used in a mortar mix. BNBC (2020) defines six basic mortar types, categorized by their compressive strengths. Table 2.2 lists mortar types along with minimum compressive strength and approximate mix proportions needed to meet the strength requirements.

Table 2.2 Mix proportion and strength of commonly used mortars (BNBC, 2020)

Grade of Mortar	Mix Proportion by Volume		Minimum Compressive Strength at 28 days, MPa
	Cement	Sand	
M1	1	3	10
M2		4	7.5
M3		5	5
M4		6	3
M5		7	2
M6		8	1

Depending on the proportions of the above mentioned constituents the properties of mortar vary. For instance, mortar with high water-cement (cementitious materials) ratio has lower compressive strength than low water-cement ratio.

2.5 Lateral Loads on Masonry Buildings

There are two major types of lateral loads that any types of infrastructure including masonry are subjected to – earthquake or seismic load and wind load. The effect of these forces on a masonry are discussed as follows:

2.5.1 Seismic Loads and their Effect on Masonry Buildings

Earthquake possesses the ability to demolish a whole civilization with a single ground motion. It is one of the most terrible natural disasters in the world. Tectonic movements are the main reasons for these dreadful catastrophic events. The ‘continental drift’ was proposed in 1912 to explain this tectonic movement. According to this theory, the continents had been gradually shifting apart ever since they had once nestled together. However, questions aroused about the process of movement of continents. Later, in the year of 1960, evidence of the spreading of the Atlantic Ocean's sea floor was discovered. It was observed that the crust itself is in motion rather than the continents moving over it. The contemporary theory of ‘plate tectonics’ was developed in this way. The Earth's upper mantle and solid crust collectively make up the lithosphere. It glides on the convective, free-flowing, and plastic components of the mantle. The global seismic hazard map representing peak ground acceleration for a probability of exceedance of 10% in 50 years (Silva et al., 2020) is illustrated in Figure 2.11.

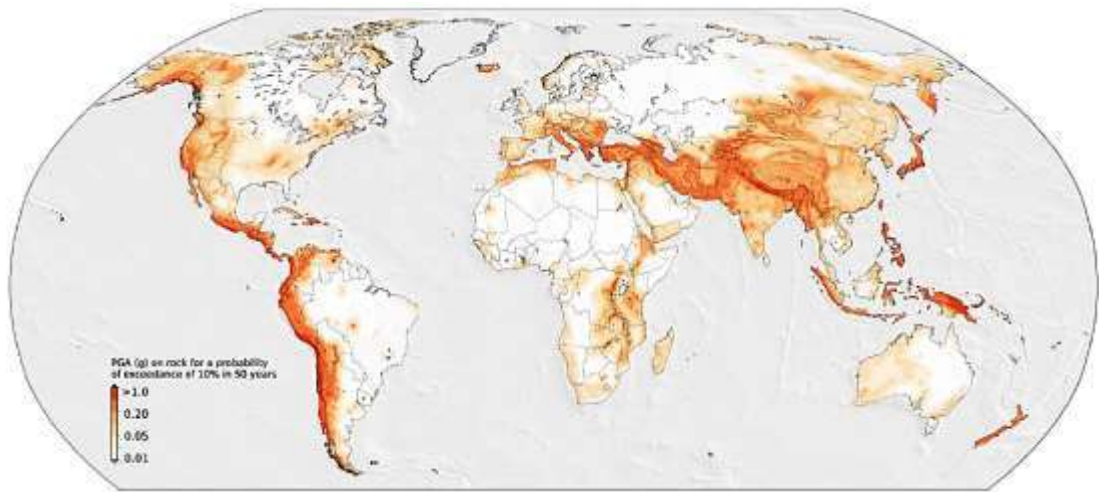


Figure 2.11 Global seismic hazard map showing peak ground acceleration with a probability of exceedance of 10% in 50 years (Silva et al., 2020)

Bangladesh is one of the most natural disaster-prone countries in the world which is affected almost every year by devastating natural disasters. Among them, Earthquakes represent one of the most harmful and fatal one for humans (Rodrigues et al., 2018). The historical record of seismic tremors that occurred in Bangladesh and adjoining areas indicate that the country is at high risk of earthquakes. Mainly, the geological formation, geomorphological landforms, and geophysical environment of this country are responsible for it (Biswas et al., 2018). The dynamic behaviour of the earth's interior plays an important role in the formation of an earthquake (Khan, 2018). Bangladesh sits at the edge of the Indian Plate, the Eurasian Plate, and the Burmese Plate where the Indian Plate is moving north-east and slowly colliding with the Eurasian Plate (Hossain and Hossain, 2020). It makes Bangladesh one of the most tectonically active regions in the world. Moreover, five major faults are significant for the occurrences of devastating earthquakes in this country named Bogra Fault Zone, Tripura Fault Zone, Shilong Plateau, Dauki Fault Zone, and Assam Fault Zone (Al-Zaman and Monira, 2017). Two major active seismic belts, the Arakan system in the east and the Himalayan system in the north, are also accountable for destructive earthquakes in Bangladesh and the surrounding area (Ansary and Arefin, 2020). The tectonic setup of Bangladesh is presented in Figure 2.12.

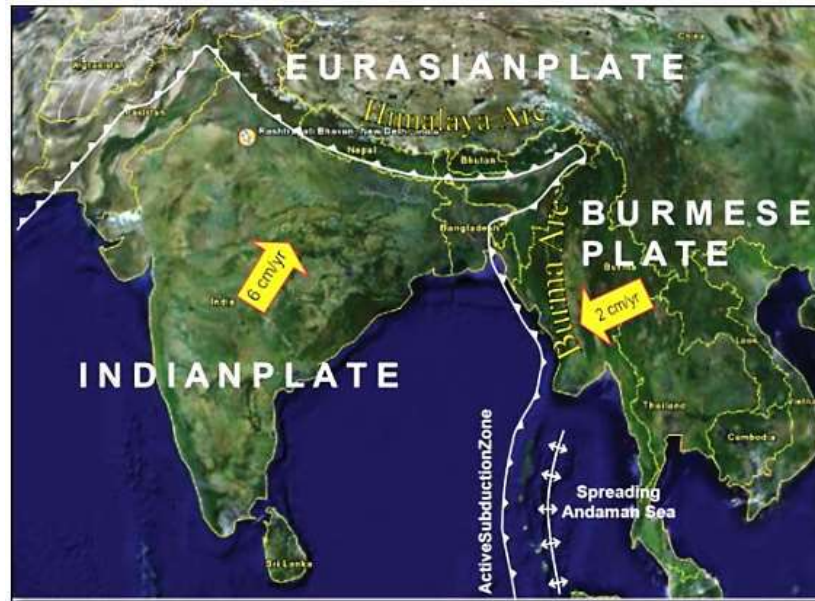


Figure 2.12 Tectonic setup of Bangladesh and plate boundaries (Akhter, 2010)

Previous major earthquakes have resulted in significant structural damages and fatalities in this subcontinent. Total of over 70,000 people were severely affected due to five major earthquakes occurred. Those were Bihar (Magnitude: 8.1, Date: January 15, 1934), Gujarat (Magnitude: 7.7, Date: January 26, 2001), Maharashtra (Magnitude: 6.4, Date: September 30, 1993), Assam (Magnitude: 8.6, Date: August 15, 1950), and Uttarkashi (Magnitude 6.1, Date: October 20, 1991) Earthquakes (Hindustan times, 2015). Bangladesh was adversely influenced by these earthquakes. Due to its location in an earthquake-prone area (Figure 2.13), Bangladesh is at high risk. Long-term historical evidence suggests that Bangladesh experiences earthquakes frequently, with an average Richter scale magnitude of approximately 5. Impairment from these earthquakes includes the collapse of reinforced concrete buildings in the port city of Chattogram (November 1997), serious structural damage to cyclone shelters in the Chattogram neighborhood of Moheshkhali (July 1999), significant cracking in masonry buildings, and malfunction of electric transformers in Chattogram (July 2003), and significant cracks in approximately 25 buildings in Chattogram Division (November 2007), along with other tragedies (Zerin, 2018). In all of these earthquakes, a significant degree of damage was observed in the URM walls.

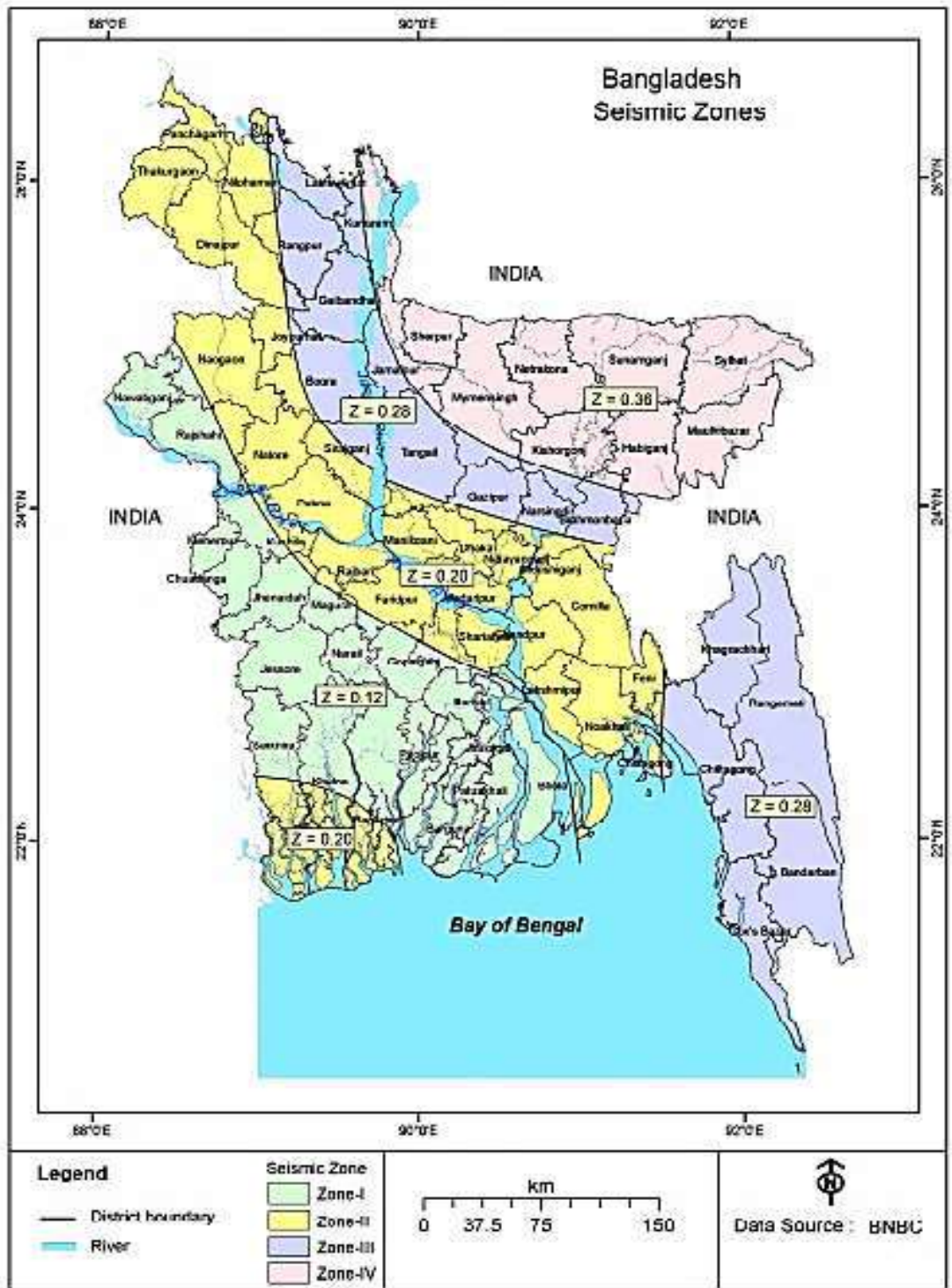


Figure 2.13 Seismic zone map of Bangladesh (BNBC, 2020)

The collapse of URM buildings in the world is not only common in Bangladesh. There are numerous examples of URM buildings from around the globe that are likely to collapse partially or completely during the event of an earthquake as shown in Figures 2.14 to 2.16. These buildings damage residents and people in the surrounding area when they collapse.

The FEMA P-774, 2009 reported that during the Charleston Earthquake (M 7.7), South Carolina in 1886, a significant amount (82 percent) of brick buildings suffered more than minor damage and 7 percent collapsed or were demolished. Forty percent of URM buildings were damaged severely or collapsed at Santa Barbara Earthquake (M 6.2), Southern California in 1925. In the City of Long Beach (near Los Angeles City), 54 percent of unreinforced masonry buildings ended up with damage ranging from major wall destruction to complete collapse at Long Beach Earthquake (M 6.3), Southern California in 1933. In 20 percent of cases, damage fell to over half of the wall area, partial collapse, or complete collapse in either damage category. Out of 37 unreinforced masonry buildings, the core of the business district of Coalinga, only one escaped damage in 1983. About 60% masonry buildings were damaged to the extent that more than half of their walls were ruined during Coalinga Earthquake, Central California. In Loma Prieta Earthquake (M 7.1), Northern California, 374 (16 percent) of the region's a large numbers of (2,400) unreinforced masonry structures suffered serious harm.



Figure 2.14 Izmit earthquake occurred in 1999 (Turkey) (Yolalmis, 1999)



Figure 2.15 Bhuj earthquake occurred in 2001 (India) (NICEE, 2001)



Figure 2.16 Nepal earthquake occurred in 2015 (Nepal)

The records of destruction caused by seismic activities are obviously found in human history. In the year 1751 and 1770, earthquakes destroyed the Port-au-Prince. The building with masonry were forbidden by local authorities as a result of these disasters. The 2010 earthquake caused significant damage to the same and other cities as well. More than 0.2 million structures were damaged or had collapsed. It also included the Presidential Palace and the headquarters of the United Nations Stabilization Mission in Haiti (Nakagawa et al., 2012). These buildings use a confined construction variation consisting of weak hollow concrete blocks (HCBs) with low reinforcement and non-ductile beams and columns (Nakagawa et al., 2012).

Nepal had more than 5,000,000 houses and buildings damaged and about half of those that had collapsed due to the 2015 Gorkha earthquake (Miyamoto and Amir, 2012). Adobe construction, wooden framed houses and rubble stone masonry buildings are more common in Nepal's villages, while most urban and suburban structures make up the bulk of stone or brick masonry structures that make up about 20 percent of reinforced concrete (RC) structures (Miyamoto and Amir, 2012). These masonry structures fail due to the following reasons: lack of anchorage, anchor failure, in-plane failure, out - of-plane failure, in-plane and out-of-plane effects combined with diaphragm failure. Many older URM buildings lack favorable ground and roof anchorage to the URM walls, contributing to sudden failure under seismic excitement.

2.5.2 Wind Loads on Masonry

Cyclones are one of the most destructive natural disasters in the world. The tropical cyclone is the generic scientific word for these events, depending on where they occur. Typhoons, cyclones, severe tropical cyclones, and severe cyclonic storms are some of the other names they are known by. It does not matter what name is given to them; the same forces and conditions are at work creating these massive storms, and every one of them has the potential to cause significant damage or destruction if it moves near populated areas. The formation and pathways of storms over the world are demonstrated in Figure 2.17. The basic wind speed map of Bangladesh is also illustrated in Figure 2.18.

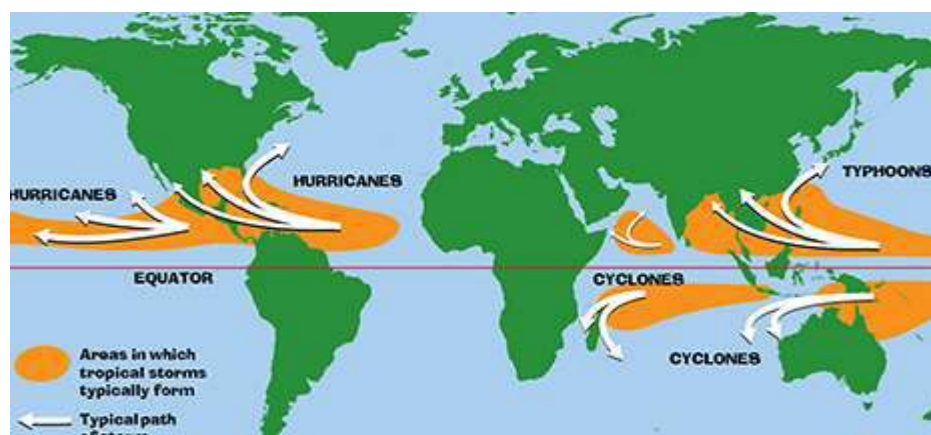


Figure 2.17 Formation and pathways of storms

In past years, cyclones and storms were highly responsible for a lot of deaths and substantial structural damage to infrastructures. Bangladesh is located between two diverse conditions, with the Bay of Bengal to the south and the Himalayas to the north (Rahman and Rahman, 2015). Low and nearly flat topography, an abundance of rivers, and a monsoon climate render the land vulnerable to the severe effects of natural disasters (Islam et al., 2010).

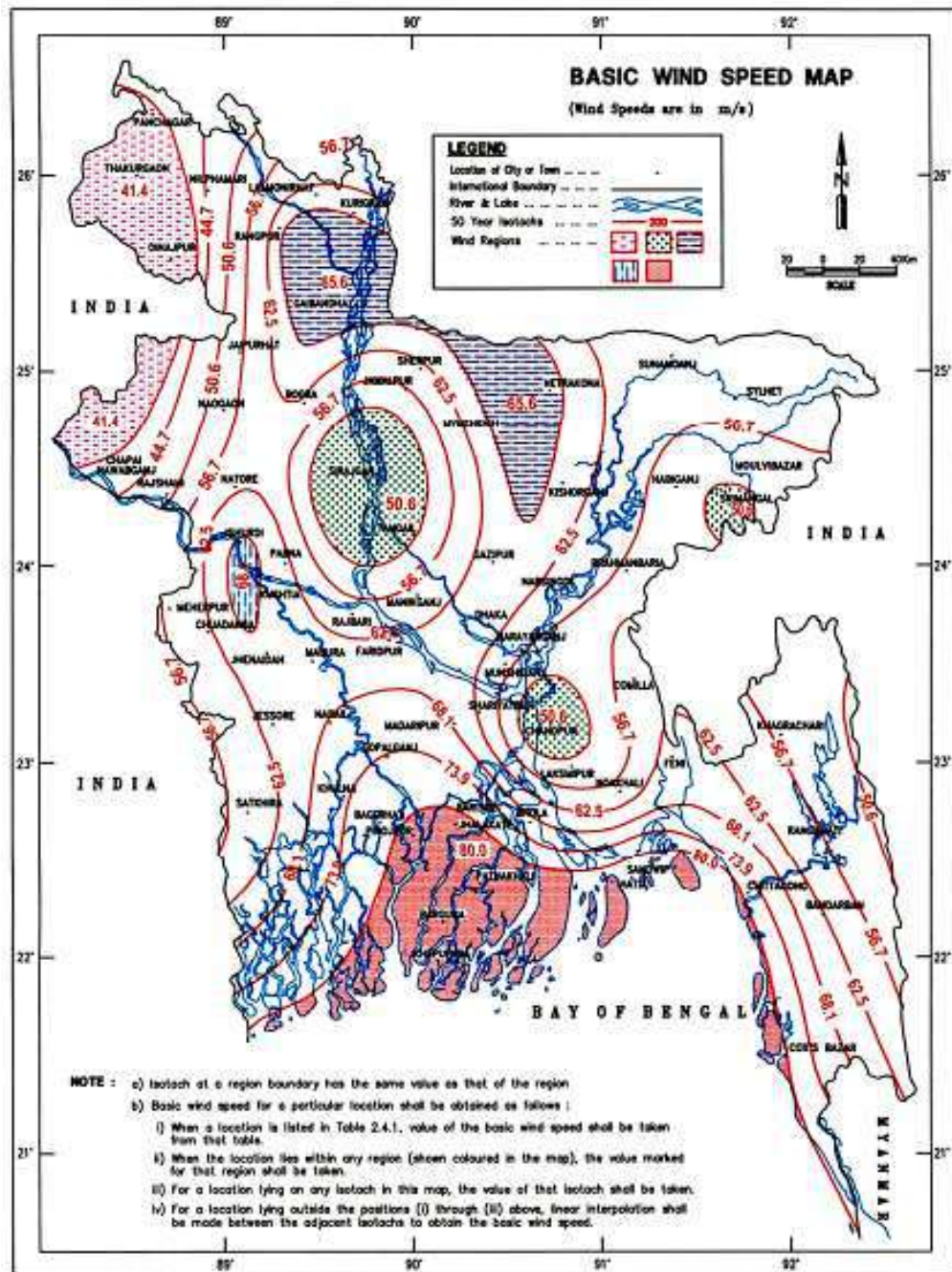


Figure 2.18 Basic wind speed (V , m/s) map of Bangladesh (BNBC, 2020).

In Bangladesh, Bay of Bengal is the primary source of most of the cyclones. Wind and warm water work as the fuel to originate these cyclones. Cyclones in the Bay of Bengal often move first to the northwest before curving eastward. However, this pattern is not uniform, as evidenced by the paths of distinct cyclones. During storm, surges are accompanied by high rainfall and sea swells. If this occurs during high tide, the resulting storm surge can reach heights of up to 12 meters. This destructive wall of water causes the majority of the loss of lives and property (Banglapedia, 2021). Cyclone storm track in Bangladesh is shown in Figure 2.19.

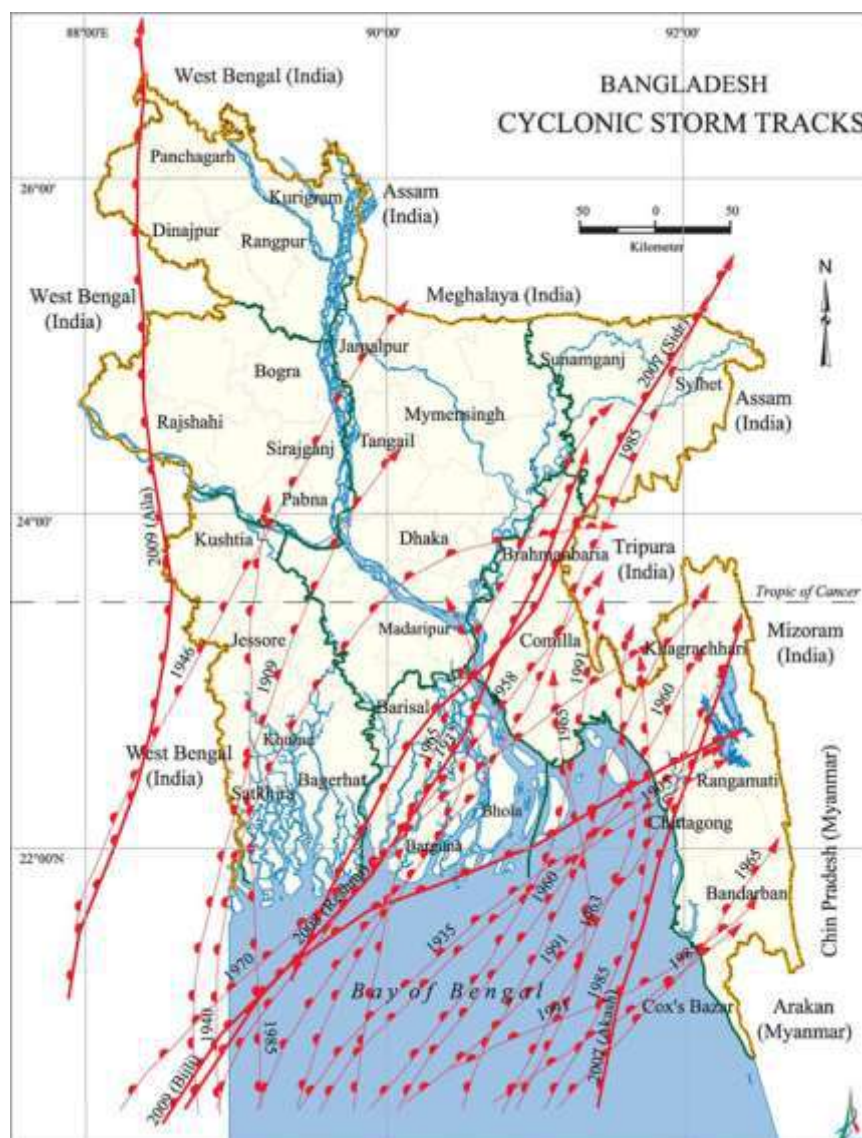


Figure 2.19 Cyclone storm tracks in Bangladesh (Banglapedia, 2021)

In Bangladesh, unreinforced masonry walls used for peripheral and interior partition walls that fit snugly between structural columns and beams are deemed non-structural, despite interacting with the structural parts constraining it. However, in masonry structures these walls serve as load bearing walls and support the loads coming from upper portion of the building. However, these structures behaved profoundly poorly when they were exposed to disasters and experienced cyclic loading. In past, many researches have been conducted regarding masonry structures. Nevertheless, it will be interesting to investigate the behaviour of URM walls built with locally available materials under cyclic loading.

2.6 URM Building Stocks in Bangladesh

The typical and one of the most common types of unreinforced masonry buildings used in our country is made of brick walls as shown in Figure 2.20 (Ansary, 2003). The exterior, and sometimes similar interior walls masonry walls around building, carry the weight or load coming from the upper floor or roof beams. Such walls are called the load bearing walls.



Figure 2.20 Typical Construction of URM Building walls (Ansary, 2003)

Shaw et al. (2013) found that the areas of Dhaka, Chattogram, and Sylhet City Corporation had 326,000, 182,000, and 52,000 houses then. In Dhaka, Chattogram and Sylhet almost all houses are made of brick or mud in the rural region. Sometimes

they use wood, bamboo and tin. Vulnerability assessment were conducted in three major cities e.g. Dhaka, Chattogram and Sylhet by CDMP (2009). According to the report a total of 326825 buildings in Dhaka were surveyed of which 82629 are made of masonry. Among 182277 surveyed buildings in Chattogram, 39447 are URM buildings. Moreover, for Sylhet, it's 23827 out of 52176 surveyed buildings.

2.7 Behaviour of Masonry Walls under Cyclic Loading

The basic resistance mechanisms of structural elements that are subjected to monotonically increasing lateral forces are most easily perceived and developed. When a seismic event occurs, however, buildings sway back and forth and lateral shears and deformations by following many repeated and reversed cycles. Cyclic loading can be classified into two categories namely low-cycle load, or a load history involving few cycles having very large bond stress ranges. This group of loading is very common to seismic and high wind forces. The second group relates to high-cycle or otherwise known as fatigue loading. The load history in this case includes many cycles at a low bond stress range. Bridge members and offshore structures are repeatedly subjected to such kind of seismic and wind load.

Abrams (1992) conducted a series of laboratory experiments on lateral strength and behaviour of URM elements. They revealed that wall or piers need not be considered as brittle. The two test walls were subjected to a simple series of lateral forces using a twin pair of hydraulic actuators. They varied the length to height aspect ratio of the two walls so that they could observe two different behaviour modes such as shear and flexural. In-plane behaviour of the two tested walls suggested that URM walls can be significantly stronger than their strength at initial cracking and possess considerable capacity for inelastic deformations, and need not be limited in strength by forces which include flexural or diagonal tensile cracks as shown in Figures 2.21 and 2.22. It was summarized that tested wall with flexural crack did not tend to reduce the overall shear strength which is why diagonal tension could be reached well after flexural cracks were observed.

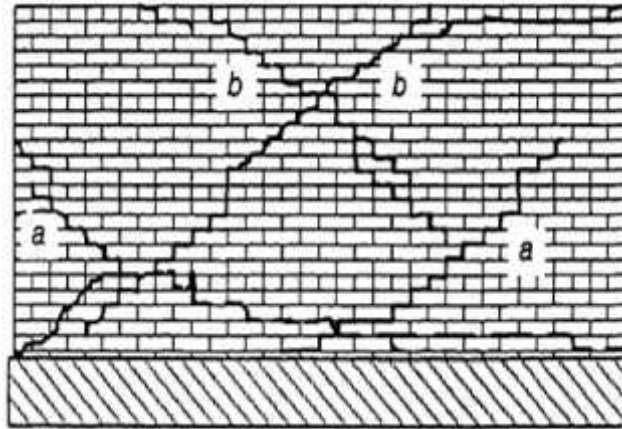


Figure 2.21 Shear Crack Pattern for Tested Wall (Abram, 1992)

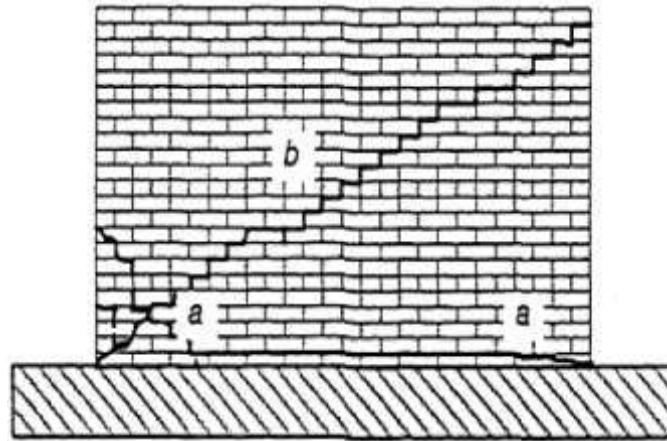


Figure 2.22 Flexure Crack Pattern for Tested Wall (Abram, 1992)

2.8 Response and Failure Modes of Masonry Wall

The response of a masonry wall depends largely on the type and direction of forces the masonry subjected to. The response of masonry walls vary under gravity and lateral loadings. Again the behaviour under the action of lateral load can be classified in two major categories, the in-plane and out-of-plane behaviour as illustrated in the Figures 2.23 and 2.24.

The main concern of our research work is to carry out the in-plane cyclic loading test on URM walls and record the response for the same. The different failure modes of masonry walls under in-plane cyclic loadings are summarized in subsequent sections.

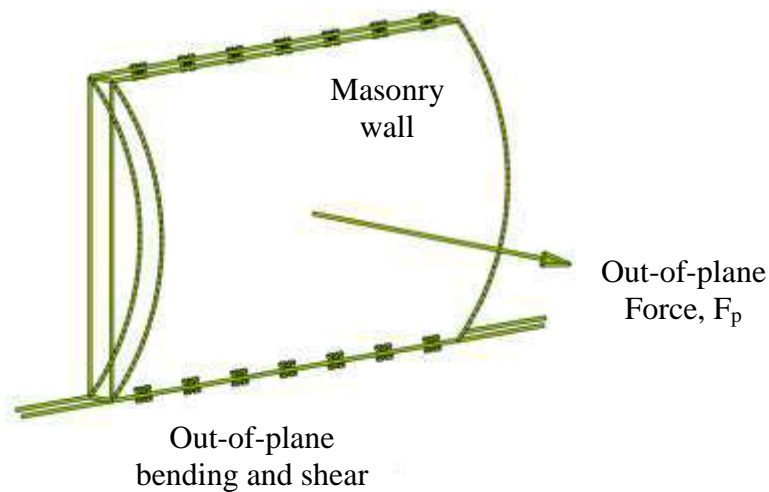


Figure 2.23 Out-of-plane behaviour of URM walls

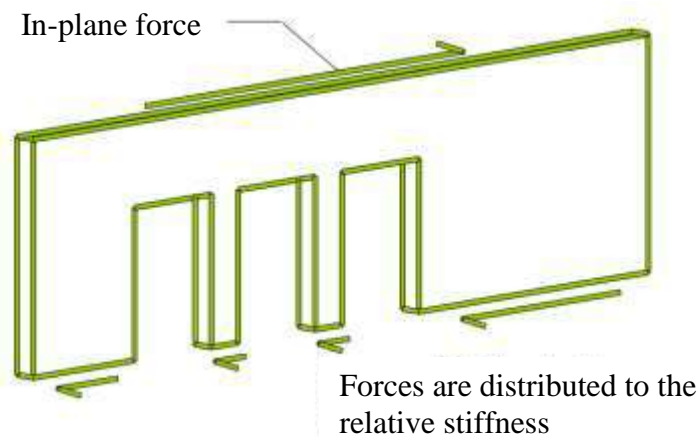


Figure 2.24 Behaviour of URM walls under in-plane loadings

2.8.1 Shear Failure

The shear failure of masonry is related to the principle tensile stress of masonry. Shear failure occurs when this principal tensile stresses, developed in the wall under the combination of the horizontal and vertical loads, exceed the tensile resistance of masonry materials (ElGawady et al., 2006). Walls with low aspect ratios and high axial loads tend to develop a diagonal cracking failure. Diagonal cracks developed in the wall either follow the path of the bed and head joints for relatively strong bricks and weak mortars or may go through the masonry units in case of relatively weak bricks and strong mortars, or both (ElGawady et al., 2007). Diagonal cracks in wall

developed just before the attainment of maximum lateral capacity. These cracks are shown in Figure 2.25 (c) as stair stepped cracks.

2.8.2 Sliding Mode

In case of very low vertical loads and/or low friction coefficient, which may be due to poor quality mortar, horizontal cracks in the bed joints start to form (ElGawady et al., 2006) as a sliding plane extending along the wall length as shown in Figure 2.25 (a). This causes the upper part of the wall to slide on the lower part of the wall.

2.8.3 Rocking Mode

The URM wall may experience rocking motion or toe crushing in case of high moment/shear ratio or improved shear resistance. It depends on the level of the applied normal force. This usually occurs in piers with large aspect ratio and low vertical stress. Final Failure is obtained by overturning of the wall as shown in Figure 2.25 (b) appear in the form of toe crushing due to increased compressive stresses or walking (out-of-plane sliding) (ElGawady et al., 2006).

2.8.4 Flexural Compression Mode

Flexural compression failures are the result of having a wall with higher shear strength than flexural strength. With the improved shear resistance and high moment/shear ratio, crushing of compression zone at the ends of wall usually takes place (Ghiassi et al., 2012). Failure is obtained by crushing one or both top corners as shown in Figure 2.25 (b).

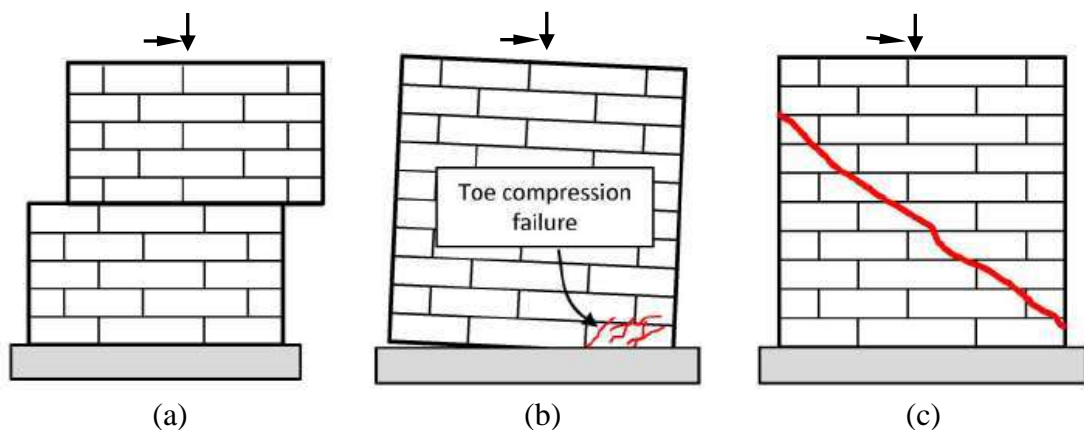


Figure 2.25 Failure mode of URM walls under In-plane load, (a) Sliding failure, (b) Rocking, (c) Diagonal cracking (Ghiassi et al., 2012)

2.9 Allowable Compressive and Shear Stresses in Masonry (BNBC 2020)

The anticipated service loads are determined first to design any engineered masonry structure. The required strength of the masonry can be determined after these loads are established. The specified compressive strength of masonry is designated by f'_m which is used throughout the design and to predict the strength and behaviour of the masonry and thus the size masonry elements are also determined. It is noteworthy that the specified compressive strength of the masonry is related to, however, not equal to the tested compressive strength of the masonry.

To ensure the construction of a safe and functional structure that will meet or exceed the intended service life, measures must be taken to verify that the compressive strength of the assembled materials. The masonry units, mortar and grout if used, must meet or exceed the specified compressive strength of the masonry. The unit strength method or the prism test method is used to verify the compliance with the specified compressive strength. The masonry wall chapter of BNBC 2020 refers the prism test method as a rational procedure for verifying the compressive strength of masonry. ASTM C1314, Standard Test Method for Compressive Strength of masonry prisms, contains provisions for determining the compressive strength of a masonry prism using an assemblage made of representative units, mortar and grout (for grouted masonry construction). The materials being utilized in construction projects are used for prism construction but the prism should not be a reduced-scale masonry component, rather it should represent a quality assurance instrument to demonstrate the function of masonry components. That is why, prisms are typically constructed in stack bond with a full mortar joint. The compressive strength of the prisms obtained from test is corrected to account for different permissible height to thickness ratios of them. This corrected strength must be greater than or equal to the specified compressive strength of masonry f'_m .

a) Axial Compressive Stress

Unreinforced masonry walls, columns and reinforced masonry wall:

$$F_a = \frac{f'_m}{5} \left[1 - \left(\frac{h'}{42t} \right)^3 \right] \quad (2.4)$$

b) Compressive Stress in Flexure

$$F_b = 0.33 f'_m \leq 10 \text{ N/mm}^2 \quad (2.5)$$

c) Shear Stress for Flexural Members, F_v

i) When no shear reinforcement is used

$$F_v = 0.083 \sqrt{f'_m} \leq 0.25 \text{ N/mm}^2 \quad (2.6)$$

ii) When shear reinforcement is designed to take entire shear force

$$F_v = 0.25 \sqrt{f'_m} \leq 0.75 \text{ N/mm}^2 \quad (2.7)$$

d) Shear Stress for Shear Walls, F_v

Unreinforced masonry, clay units:

$$F_v = 0.025 \sqrt{f'_m} \leq 0.40 \text{ N/mm}^2 \quad (2.8)$$

2.10 Damping Ratio and Energy Dissipation of URM under Cyclic Loads

The equivalent viscous damping ratio (ξ_{eq}) and effective stiffness (K_{eff}) of an inelastic bridge system are two of the important design parameters in some of the recent displacement-based bridge design methodologies and procedures. Equivalent viscous damping ratio, ξ_{eq} describes the equivalent viscous hysteretic damping which is a quantitative parameter that can be evaluated at each performance level. Priestley et al. (1996) suggest that ξ_{eq} is obtained based on an equal area approach that represents the same amount of energy loss per cycle. The calculation of ξ_{eq} for cases with symmetric hysteresis loops is shown in Figure 2.26. The area within the inelastic force-displacement response curve, E_d in the Figure 2.27, is a measure of the hysteretic damping or energy-dissipating capacity of the structure. The hatched region in this figure depicts the elastic strain energy stored in an equivalent linear elastic system, E_s . Equation (2.9) represents the equivalent viscous damping ratio, ξ_{eq} . The effective stiffness, K_{eff} , defines the slope of the equivalent linear elastic system represented by E_s , and is also depicted in Figure 2.26. It is the ratio of the force at a given response level to the deformation at that level and is calculated by equation (2.10).

$$\xi_{eq} = \frac{1}{4\pi} \left(\frac{E_d}{E_s} \right) \quad (2.9)$$

$$K_{eff} = \frac{F}{\Delta} \quad (2.10)$$

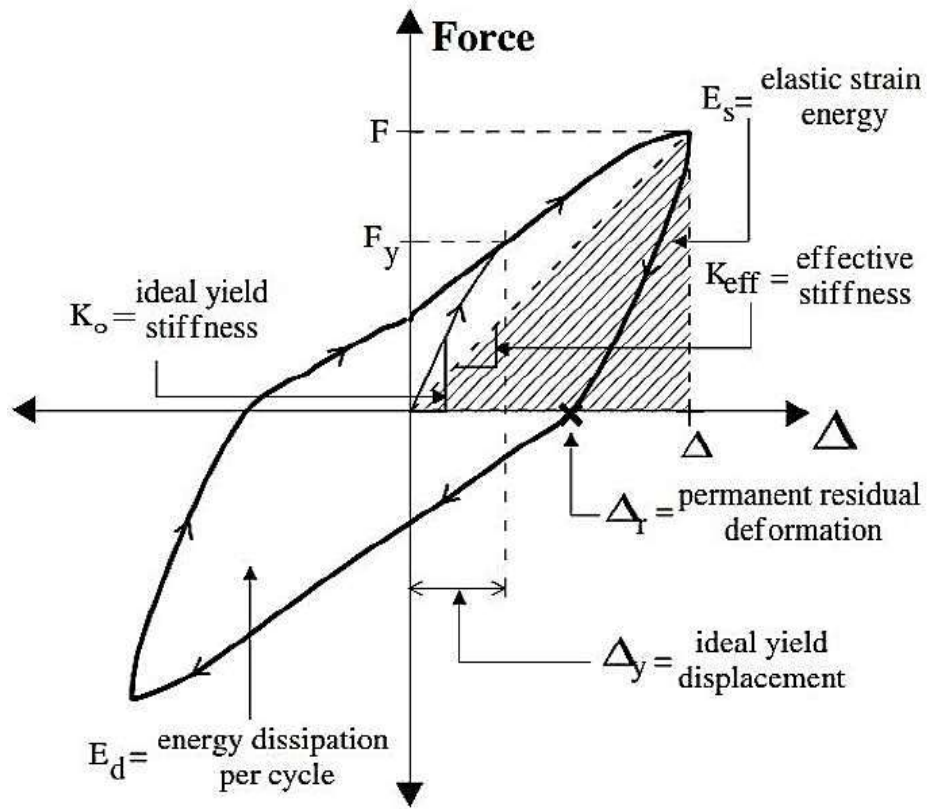


Figure 2.26 Equivalent Viscous Damping Ratio (ξ_{eq}), and Effective Stiffness (K_{eff}) for Symmetric Hysteresis Loops (Hose and Seible, 1999)

In the two loading directions under cyclic loading, some components and systems may experience asymmetric response. The same concept of taking the average of the push and pull responses is applied to determine the equivalent viscous damping ratio (ξ_{eq}) and the equivalent stiffness (K_{eff}). Equation (2.11) derives the equivalent viscous damping ratio for the full asymmetric cycle at a specific force level and it is further defined in Figure 2.27. Hose and Seible (1999) suggested that the energy input or damping energy loss for the push half cycle of the idealized force-displacement loop is represented by area E_{d1} in Figure 2.27. Similarly, the energy loss for the pull half cycle is depicted as area E_{d2} . The hatched regions in Figure 2.27 defines E_{s1} and E_{s2} , which represent the elastic strain energy stored in an equivalent linear elastic system for the push and pull half cycles respectively.

$$\xi_{eq} = \frac{1}{4\pi} \left(\frac{E_{d1}}{E_{s1}} + \frac{E_{d2}}{E_{s2}} \right) \quad (2.11)$$

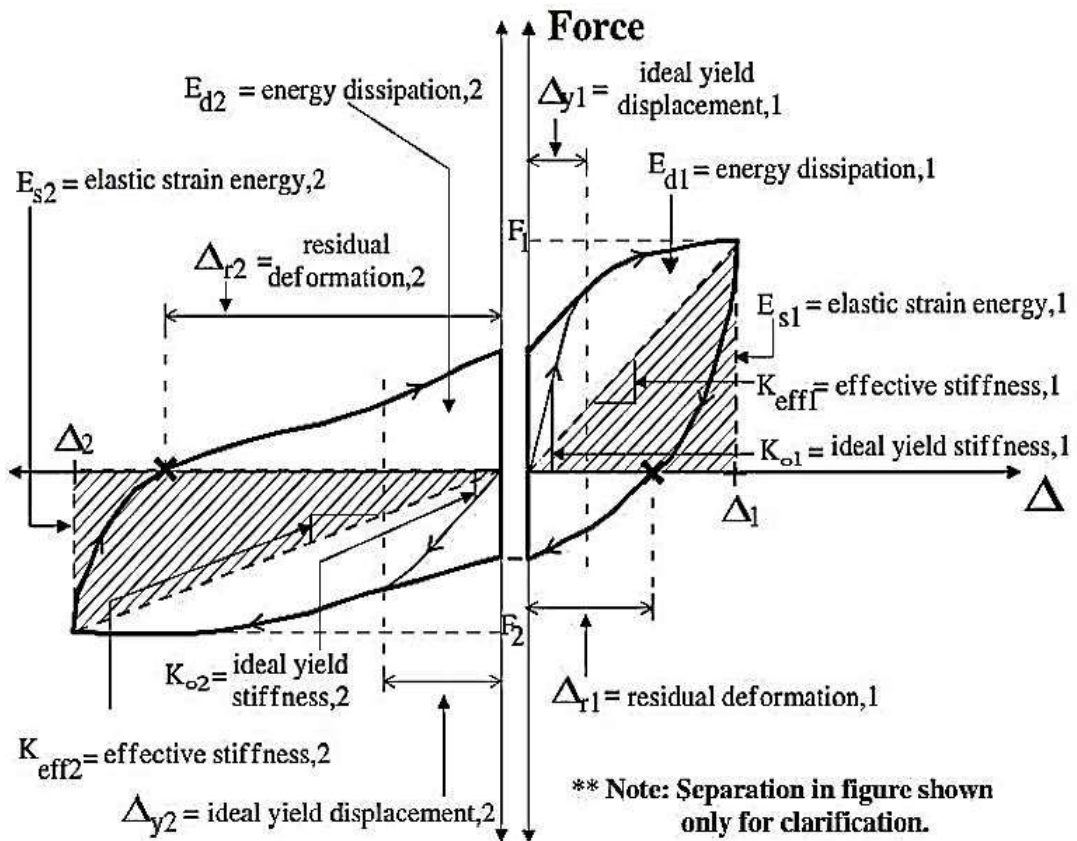


Figure 2.27 Equivalent Viscous Damping Ratio (ξ_{eq}), and Effective Stiffness (K_{eff}) for Asymmetric Hysteresis Loops (Hose and Seible, 1999)

2.11 Strengthening Techniques of URM Walls

The response of URM structures when they are subjected to large ground accelerations during earthquake is very poor. In order to deal with this dangerous situation, effective retrofit strategies must be developed so that the seismic performance of existing URM structures can be increased. Furthermore, reliable methods and tools for analyzing existing URM structures are required to implement efficient retrofit techniques in practice. The possible seismic strengthening and retrofitting techniques for URM walls are enlisted below:

- i. Use of shotcrete
- ii. Use of fiber reinforced polymers (FRP)
- iii. Post-tensioning or prestressing
- iv. Use of thin mortar layer with reinforcement (Ferrocement)
- v. Use of RC jacketing or overlay

- vi. Use of braced frames
- vii. Use of tie rods
- viii. Use of steel strips

The first traditional method that has been used for the seismic strengthening of URM walls involves the removal of one or more wythes of brick and subsequently filling the void with pneumatically applied concrete (shotcrete). Kahn (1984), amongst many, showed that the use of shotcrete is very effective in increasing both the strength and the ductility of URM walls. However, due to the large amount of formwork and surface preparation it required, use of shotcrete becomes very costly.

One of the most promising new methods has been developed for the retrofitting and seismic strengthening of URM walls involves the use of fiber reinforced polymers (FRP). This technique requires a better bonding of FRP overlays to both sides of a URM wall and is typically unobtrusive to the building occupants. This requires very little surface preparation, and as a result it is very economical. Schwegler (1994) conducted full scale tests on URM walls retrofitted with an epoxy-bonded carbon FRP. Results showed that both the in-plane and out-of-plane strength were significantly increased by the use of FRP.

Post-tensioning or prestressing is another fruitful method that has been proposed to increase the strength of URM walls. It has been used extensively to enhance the tensile and flexural capacity of lightly reinforced or unreinforced concrete, which is a brittle material with similar characteristics to URM. For the retrofit of URM structures post-tensioning is applied by core drilling from the top of the masonry walls and vertically prestressing the walls to the foundation. This method is somewhat costly but the advantage of this method is that it does not alter the appearance of the structure which is important for historical structures and that the occupants of the structure need not be disturbed during the application.

The application of thin surface coatings like ferrocement to one or both sides of a URM walls is another strengthening method that has been traditionally used. Ferrocement is an old technique in terms of its application but it is relatively young

in terms of the year devoted to its research for unreinforced masonry buildings. The drawbacks of this method is that it might be labor intensive and can create a great deal of disturbance to the occupants of the structure during retrofit.

Introducing frames to resist shear and moment implemented on URM walls can be another form of strengthening for the same. These frames could be made of different types of materials such as steels, concrete and sometimes timbers.

The use of shear walls increase the strength of existing URM can be done by adding suitable type materials to the wall surface or they are added as new elements. Materials which resist shear loads can be added to the surface of the URM such as gypsum plasterboard, plywood, particle board, or plate steel (Robinson and Bowman, 2000), and are generally fixed to the URM with bolts via a supplementary structure. This means that the surface of the URM is generally covered and may interfere with decorative elements on walls and openings, although this can be worked around with stronger materials such as plate or strap steel. They can add to the thickness of the wall, which is not particularly desirable as it can reduce the scale and area of the interior.

The aim of this research work is to evaluate the performance of reinforced concrete (RC) jacketing over the surface of URM walls against seismic loads in the form of continuously applied cyclic loadings. Figure 2.28 below shows such type of application on the walls of an existing masonry building followed by the analysis and report of BUET-JIDPUS.



Figure 2.28 Application of RC overlay on the face of URM walls (Retrofitting of DoT building at Tejgaon, Dhaka, 2019)

2.12 Experimental Investigations

A large number of laboratory investigations and experiments have been and are being conducted on the strengthening and retrofitting of URM walls to increase both its in-plane and out-of-plane performances under the action of seismic excitation. Some of the remarkable experiment details and their results are summarized below:

2.12.1 Seismic Retrofitting Using FRP and GFRP

Mohamed et al. (2007) conducted a static cyclic loading test on a set of seven half-scale masonry walls before and after retrofitting with FRP. All the specimens were tested under constant gravity load with incrementally increasing in-plane loading cycles. The two effective moment/shear ratio of the tested specimens were 0.5 and 0.7. The key parameter of the test was the amount of FRP axial rigidity: the amount of FRP reinforcement ratio (ρ) times its E modulus (ρE). The FRP was applied on the entire surface of a single-side of each test specimen. Figure 2.29 shows the failure pattern of the wall samples tested.

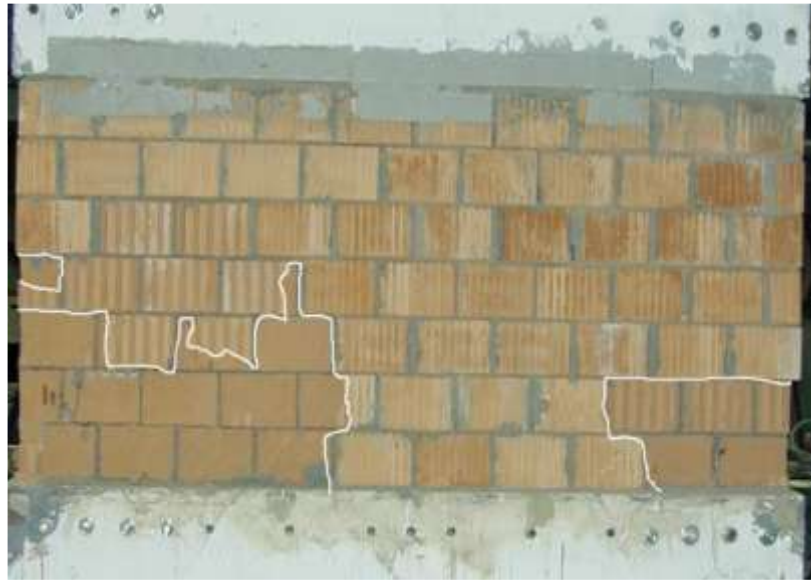


Figure 2.29 Failure mode of samples (Mohamed et al., 2007)

It was found from this research that the lateral resistance was improved by a factor of 1.4–5.9. The increase in the lateral strength was approximately linearly proportional to the amount of FRP axial rigidity. The mode of failure is strongly dependent on the FRP axial rigidity. Higher amounts of FRP axial rigidity led to very brittle failures. The energy dissipation of the retrofitted and upgraded specimens was higher than the reference specimens, however, most of this energy dissipated due to friction in the masonry rather than due to deformations in the FRPs. In no case there was rupture due to anchorage failure. Shear cracks in the form of stair-steps developed through bed and head joints in the URM specimen, however did not produce a brittle failure. The minimum coefficient of friction measured in this investigation for the URM was 0.75.

Saleem et al. (2016) evaluated the seismic performance of FRP retrofitted buildings with openings at different FRP reinforcement levels. Five shake table tests on 1/4-scale models of single-story boxlike masonry buildings were performed. One URM sample and four retrofitted samples with different quantities and layouts of FRP reinforcement were tested. The study parameters were FRP reinforcement ratio (0.4%, 0.24%, 0.12%, 0.06%), strip width, (40 mm and 20 mm), number of strips, and single or double face applications of FRP. Figure 2.30 illustrates the complete experimental set up of this research.



Figure 2.30 Complete experimental setup (Saleem et al., 2016)

Various parameters showed various natures of responses such as the two highest FRP ratios did not show any cracks. The next one gave satisfactory performance compared to the previous ones. For the least FRP content, the performance was found to be very poor, hardly bear even one input motion more than the URM building model. The recommendations were that FRP should be applied at corners and near door and windows openings. Epoxies with higher tensile shear bond strength should be used. Bricks with higher compressive strengths and smaller surface irregularities. Horizontal anchor strips or net types of arrangement can be used. Both in-plane and out-of-plane walls should be retrofitted.

2.12.2 Seismic Retrofitting Using Ferrocement (Wire mesh)

Ashraf et al. (2004) presented the experimental results of quasi-static load test conducted on two full-scale brick masonry walls, one unreinforced and the other confined. The authors investigated the in-plane lateral load behaviour of the walls before and after retrofitting. The walls were constructed closely following the masonry system commonly used in Pakistan and in most South Asian countries. The

walls before retrofitting were tested to their peak resistance. The damaged walls were then retrofitted with grout injection followed by ferrocement overlay and retested to their ultimate failure under the identical conditions. The effectiveness of the proposed confinement and retrofitting scheme was assessed from the damage pattern, energy dissipation, and force-deformation behaviour of the walls tested before and after retrofitting. The test results before retrofitting show that the capacity of confined masonry wall is almost double to that of unreinforced masonry wall. The test results after retrofitting indicate that the applied retrofitting scheme significantly enhanced the lateral load capacity of the unreinforced masonry wall, however it was marginally beneficial in the confined masonry walls. It is concluded that the guidelines provide reasonable estimates of the test observations.

Shah et al. (2017) experimentally investigated the performance of a full-scale single-story confined masonry building by subjecting the samples to quasi static cyclic loading. The retrofitting of the building was done using ferro-cement overlay and cement-based grout injection. The samples are given in Figure 2.31.



Figure 2.31 Specimen before and after retrofitting (Shah et al., 2017)

Damage mechanism and force-deformation behaviour of the retrofitted structure are compared with those of the original structure to quantify the beneficial effects of the retrofitting. Transferred from a mixed compression-flexural-shear mode to a more stable flexural rocking mode. Lateral stiffness, load carrying capacity and deformation capacity were increased by 12%, 4% and 49% respectively. Surprisingly, the ductility decreased by a factor of 8%.

Islam and Ahsan (2019) studied the dynamic behaviour of half-scale unreinforced masonry room in the laboratory of Civil Engineering Department of BUET. The experimental set up is shown in Figure 2.32



Figure 2.32 Complete experimental setup (Islam and Ahsan, 2019)

A half-scale URM room (6' x 5' x 5' and 2.5" wall thickness), was built using M2 type mortar (c:s=1:4) and half-scale brick units. Time history of Imperial Valley Earthquake (5Hz) was chosen as an input motion. The URM model was tested as reference specimen. The reference specimen was then retrofitted on all faces using 18 gauge wire mesh (12 mm x 12 mm i.e., ½ " x ½ " opening).

After test, it was observed for the bare sample that stair-stepped cracks were formed, localized mostly at the corner of the wall. Cracks are mostly generated in the lower 1/3 length of the walls (both in-plane and out of plane wall). Lateral sliding along the bed joints are also visible in the in-plane and out of plane wall. First crack was observed in the out-of-plane wall; Corners are mostly vulnerable in earthquake. Maximum lateral force at the top of the bare model structure is 14.07 kN. For the retrofitted sample, no visible cracks was observed, except a vertical crack in the in-plane wall. The failure was initiated along the intersection of base. Was able to sustain 1.42 times more acceleration than bare model structure. Decreased the

deformation of the structure by around 4.3 to 4.8 times. Both acceleration and lateral force decrease with the increase of frequency (for both model) of the excitation.

Hasnat et al. (2022) conducted an experimental investigation in the laboratory of Civil Engineering department of BUET. The test was conducted on a full scale masonry wall of 125 mm thickness. The sample was tested under quasi-static loading with gravity load imposed as given in Figure 2.33. Then the tested sample was retrofitted using a single layer of ferrocement and tested again. Another sample was directly strengthened using the same mechanism and tested in the similar way.

It was observed from the research that the behaviour of the strengthened walls under a combination of a vertical load and lateral reversed cyclic loading was compared to the control models to observe improvement of lateral load resistance capacity. Ferrocement laminated wall panels showed about 33% increase in lateral load capacity. Strengthening wall panels showed about 78% increase in lateral load capacity, compared to the control. The strengthening also improved the total energy dissipation by a factor ranging from 35.5% to 81% for the walls.



Figure 2.33 Masonry wall sample ready for testing (Hasnat et al., 2022)

Regarding the failure mode, walls, although revealing some arbitrary first cracks at the connecting interface, ultimately exhibited rocking mode of failure at the wall-

baseslab interface and to some extent flexural compression i.e. corner crushing mode.

2.12.3 Seismic Retrofitting PP band and other meshes

Nissanka et al. (2015) worked on mesh type retrofitting for masonry structures to delay or prevent the collapse of buildings. Only the behaviour of in-plane wall was examined using following types of meshes: Steel cage Polymer mesh (Industrial geo-grid and soft polymer) PP-band mesh and Plastic carriage bag mesh (Figure 2.34).



Figure 2.34 Wrapping walls with different mesh, (a) Steel mesh, (b) Soft polymer, (c) Geo-grid, (d) PP-band, (e) Plastic bag (Nissanka et al., 2015)

On the basis of the result data obtained it was concluded that the mesh types can effectively increase the residual seismic capacity of URM walls. When selecting the particular mesh type, in addition to structural performance following characteristics should be considered: Available in local or in the market - Low-cost when compared with others, meshes should be non-corrodible, mesh roughness, to provide a good grip, thickness of the mesh, without making the plaster difficult to apply and flexible material, which can provide easy installation.

Nayak and Dutta (2016) studied the effects of openings in walls that influence the crack and damage propagation leading to failure. This study was to explore the effectiveness of low cost and easily implementable strengthening techniques such as tying up the masonry walls by PP bands, wrapping the walls using steel wire mesh, and horizontal L-shaped reinforcing bars for URM structures. Application of PP bands are illustrated in Figure 2.35. Free-standing walls with PP bands strength goes

up to 1.36 times. Diagonal shear cracking and their propagation at corners of openings were observed. For door in one out-of-plane walls and windows in other sides, strength went up to 2.21 times whereas for door in in-plane walls and windows in other sides strength was 2.08 times.



Figure 2.35 Application of PP bands on room (Nayak and Dutta, 2016)

Jamshid et al. (2018) conducted an experimental work on URMs to evaluate the performance of the retrofitting technique using polypropylene (PP) band. The displacement-controlled lateral deformation has been investigated experimentally. The monotonic load-displacement behaviours of a URM wall and the wall retrofitted with PP band were compared. At the same time, the performance of a PP band-retrofitted building during a real earthquake was also observed.

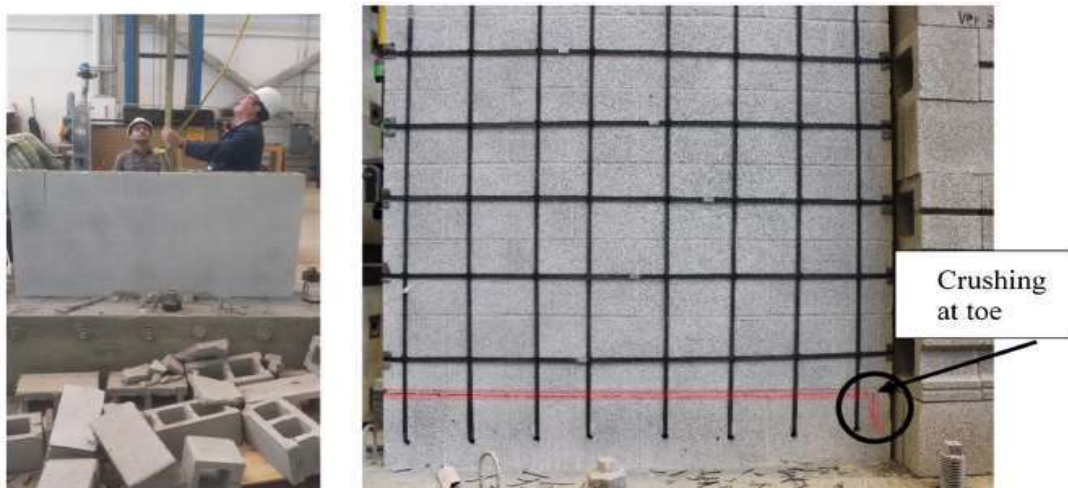


Figure 2.36 After test condition of wall specimen (Jamshid et al., 2018)

It was observed from the test that the energy absorption capacity was increased by two times. The ductility capacity increased by three times. The load carrying capacity was increased by 22%. After test condition of the wall specimen is illustrated in Figure 2.36.

2.12.4 Seismic Retrofitting Using RC Overlay

Sergey and Elena (2011) conducted a series of cyclic loading test on URM walls and presented the results for the same to evaluate in-plane shear behaviour and identify shear strength, stiffness and energy dissipation.



Figure 2.37 Application of RC jacket on both sides of the wall (Sergey and Elena, 2011)

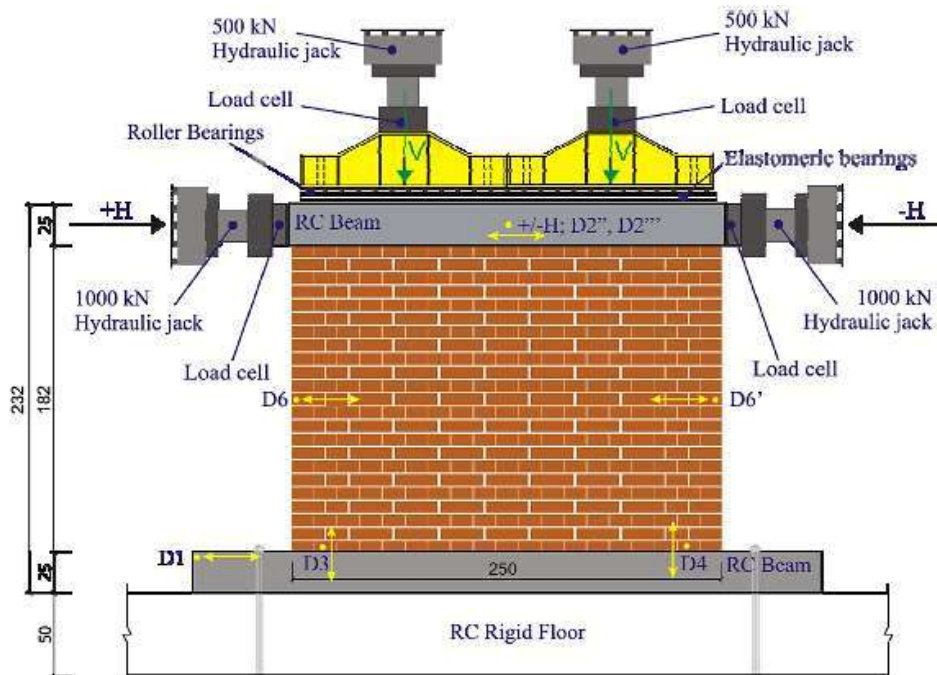


Figure 2.38 Full setup of masonry wall for cyclic test (Sergey and Elena, 2011)

Eight walls in two series were assembled in laboratory. The first series contains four unreinforced masonry walls build from solid clay bricks and lime mortar. The walls from second series are strengthened and have the same material, geometry properties and vertical load levels as the first one. The traditional strengthening method by application of RC coating (jacket) on both sides was used. The main goal of the tests was to compare the behaviour of unreinforced and strengthened walls under horizontal loading. The results from the tests showed that the strengthening method leads to significant improvement in the shear resistance of the strengthened walls. The application of RC jacket and the loading arrangement are given in Figure 2.37 and 2.38 respectively.

Ghiassi et al. (2012) intended to develop a rational method for design and seismic evaluation of unreinforced masonry walls strengthened with reinforced concrete layers as given in Figure 2.39. Four failure modes are considered for the walls, and the strength relations and acceptance criteria for each of them are provided in accordance with FEMA 356 and ASCE 41 relations for reinforced concrete and masonry walls. The accuracy of the proposed method in predicting the nonlinear behaviour and governing failure modes of the strengthened walls is validated by comparing the results with available experimental and performed numerical results.

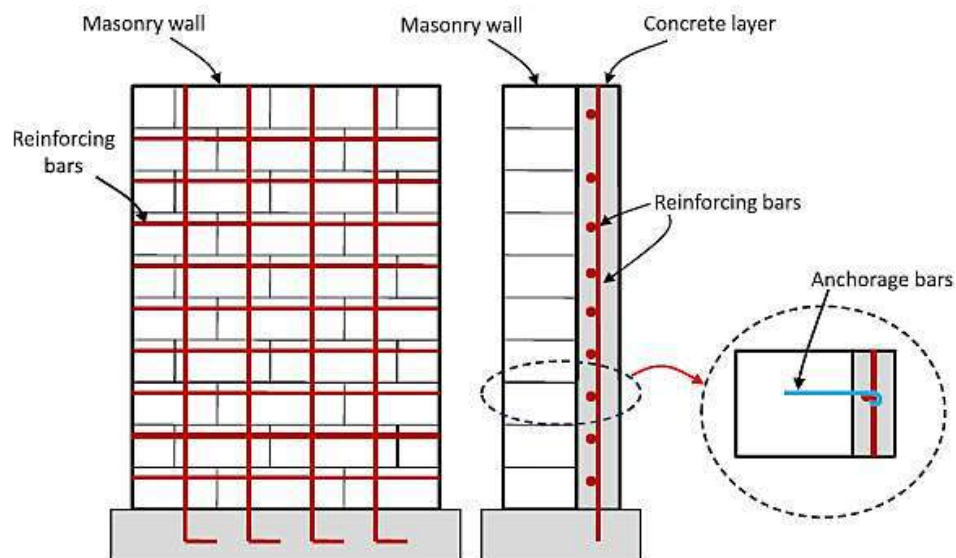


Figure 2.39 Typical detail of masonry wall strengthening with reinforced concrete layer (Ghiassi et al., 2012)

Khajeheian and Maheri (2017) reported on the experimental and numerical investigations of the seismic behaviour of unreinforced concrete block masonry (URCBM) structural walls. The samples were externally retrofitted on one, or both sides, by reinforced concrete (RC) layers. The behaviour factor (R) components are extracted from nonlinear static pushover analyses of full-scale masonry walls having different aspect ratios. It is found from the research that R-value of masonry shear wall increases with an increase in the aspect ratio of the wall. Also, application of RC layers influenced the behaviour factor, as it directly affects both ductility and ultimate capacity of the wall. Finally, based on findings presented, R-values of 2.0, 2.5 and 3.0 are proposed for URCBM, one-sided and two-sided retrofitted concrete block masonry shear wall construction, respectively.

Many masonry buildings in Europe were built after the Second World War during a booming economy when seismic risk was not properly considered and, as a consequence, seismic codes were not available yet. Several of these buildings are quite small since they are used by one or two families. Because of the huge developments in the knowledge on seismic actions, there is now a major concern for the vulnerability of these buildings under possible earthquakes. Messali et al. (2017) conducted experimental work focusing on the seismic strengthening of a masonry typology widely used for social housing. It is based on hollow masonry bricks with horizontal holes and poor cementitious mortar.

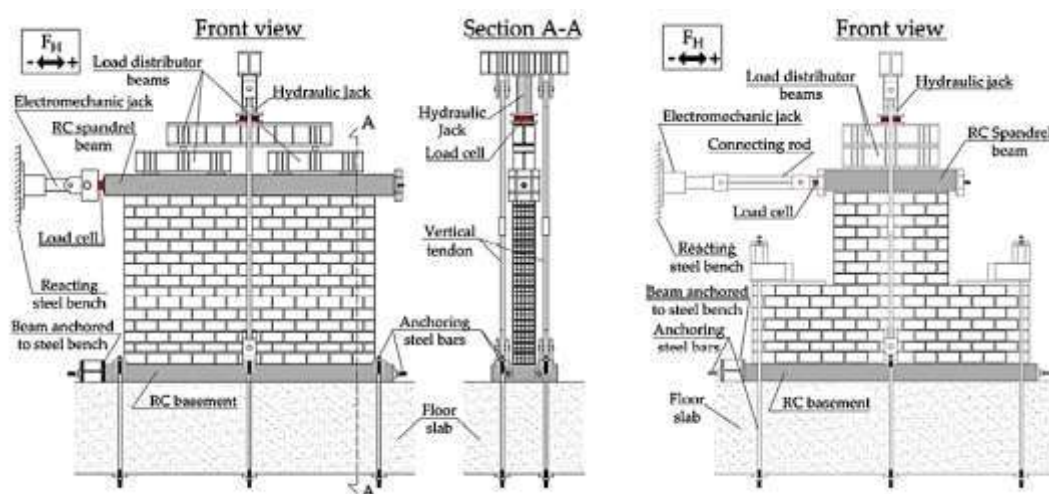


Figure 2.40 Test setup for the shear walls (Messali et al., 2017)

The test set up is given in Figure 2.40. Results of quasi-static cyclic tests carried out on full-scale unreinforced masonry walls with different geometries, representing either a shear wall or a pier-spandrel assembly, are presented. The specimens were repaired or strengthened with a thin layer of high-performance mortar reinforced with light steel-mesh. The test results show the effectiveness of the proposed technique since it provides a remarkable enhancement of both lateral strength and displacement capacity.

Mustafa et al. (2018) carried out in-plane tests at the laboratory of the Faculty of Civil Engineering in Sarajevo to study the seismic resistance of URM walls. The samples were categorized in two groups - four full-scale (233 x 241 x 25 cm) and nine reduced-size specimens (100 x 100 x 25 cm) made of solid clay brick and lime-cement mortar were subjected to cyclic shear and monotonic pushover loading program under constant vertical pressure. One-sided or two-sided reinforced concrete or mortar jacketing was applied to improve lateral resistance and displacement capacity. Figure 2.41 and 2.42 illustrate the cracks in wall samples before and after retrofitting.

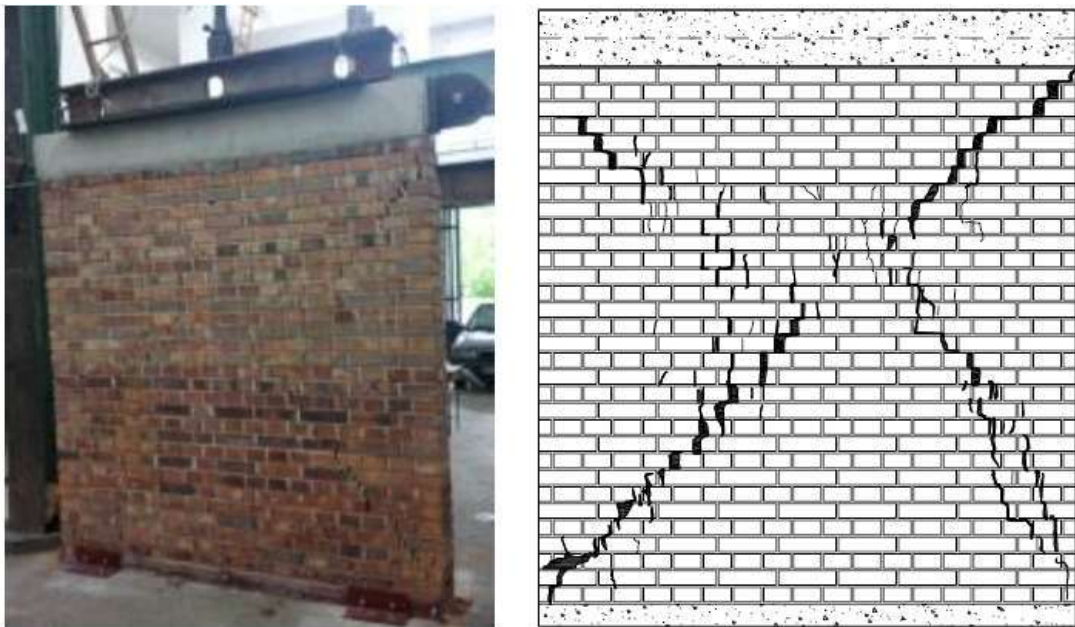


Figure 2.41 Crack patterns and crack width of URM walls (Mustafa et al., 2018)



Figure 2.42 Failure mode of strengthened samples (Mustafa et al., 2018)

The positions of the reinforcing mesh were changed - one way of strengthening was with the orthogonal position of reinforcement mesh Q196 and “new” type of connectors made of shaped $\text{Ø}5$ reinforcing bars. The connectors were placed vertically (9 pieces/m²) and horizontally (4 pieces/m²) in joints and grouted with high strength quick-hardening mortar. In the second type of strengthening, the mesh Q196 was inclined to 45° (135°) in order to follow the principal stress trajectories. Plain walls fail in shear with a typical cross-diagonal crack pattern. Jacketed walls exhibit rocking and significantly larger ductility compared to plain walls. Wallets were tested for compressive strength and elastic modulus of masonry and the results show significant variations.

Mahmoud et al. (2019) presented the results of numerical studies of full-scale unreinforced concrete block masonry walls, externally retrofitted by reinforced concrete layers focusing on the in-plane shear capacity. At first, small-scale masonry walls were tested and their results were used to develop and calibrate numerical micro models for full-scale walls. Nonlinear pushover analyses are conducted to investigate the effects of a number of problem variables on the performance of the retrofitted walls. Numerical results reveal that wall boundary conditions affect its response considerably. Also, a significant enhancement in wall capacity and ductility is observed due to the application of the reinforced concrete layers. The monotonic loading set up for the wall samples conducted by the authors is illustrated in Figure 2.43.

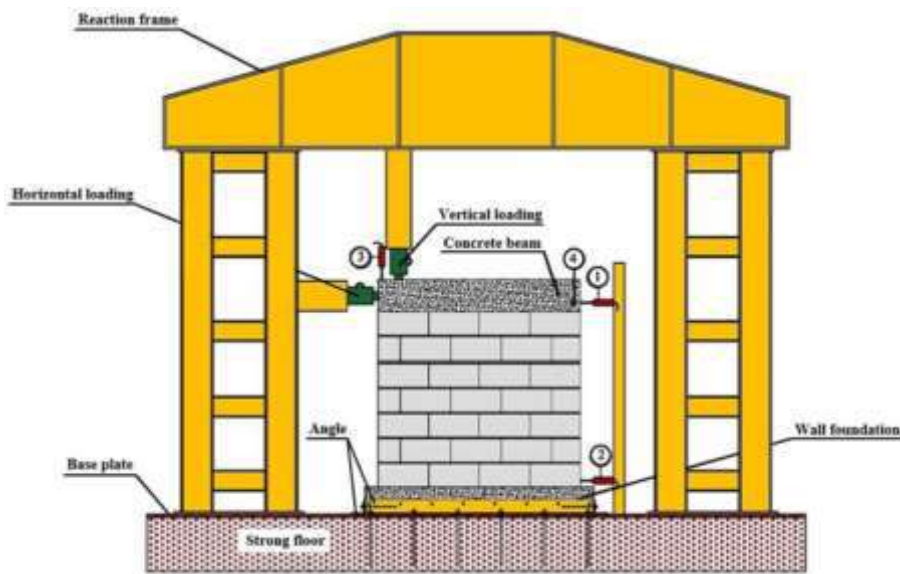


Figure 2.43 Setup for monotonic loading on wall samples (Mahmoud et al., 2019)

2.13 Summary

The performance of URM walls under seismic events has become a great concern. For that the lateral cyclic loading tests were conducted on the wall samples by different researchers. The experimental details mentioned in Section 2.12 are examples of such research. Specially, the retrofitting of URM walls with RC overlay is the field we need to look into with details. The research papers show that a number of experimental works have already been done on the effect of RC jacket on both sides of masonry, which has been a common retrofitting technique. However, in some cases, the application of RC jackets on both sides of walls becomes impossible due to some obvious reasons. The prominent one in this category is unavailability of enough space inside the rooms of the URM buildings for providing the shoring works necessary for the formwork of the RC casting. Again, the RC jacket on both sides reduces the valuable usable space inside the building. In this case, a feasible solution could be the application of RC overlay on the exterior side of the wall only, thus saving more interior space and making the retrofitting work much easier for the workers and engineering team as well. Thus the actual behaviour of these wall samples in this condition need to be evaluated and validated. However, no remarkable experimental details have been found on the seismic retrofitting of URM

walls with reinforced concrete jacketing on one side only. Therefore, this research work focuses on the application of the same on some half-scale URM walls before and after testing under lateral cyclic loadings to know the actual response of the walls for the stated retrofitting scheme. With the evaluation of some important parameters such as lateral load carrying capacity, lateral displacement, ductility, energy dissipation, stiffness degradation, the effect of aspect ratio (i.e., height to length ratio) will also be evaluated in this research.

Chapter 3

METHODOLOGY

3.1 Introduction

This chapter comprises of the detailed experimental program to investigate the effectiveness of reinforced concrete overlay as externally bonded upgrading materials on one face for the in-plane retrofitting of URM walls. The experimental program includes the followings:

- i. Determination of material properties
- ii. Walls and samples preparation
- iii. Preparation of test set up
- iv. Test of control specimens
- v. Retrofitting and strengthening of walls followed by cyclic test
- vi. Collection of test data

3.2 Geometry and Physical Properties of Test Specimens

Four half-scale masonry wall specimens were prepared with two aspect ratios (Height/Length) namely, 1.0 and 0.75. The samples were prepared with half-scale burnt clay bricks of dimension 127 mm x 60 mm x 38 mm. The walls were prepared using English bond to replicate a conventionally used full scale 10 inch wall. There were two samples for each aspect ratio. The dimensions of the walls (L x H x T) were 1524 mm x 1524 mm x 127 mm (5 ft. x 5 ft. x 5 in.) with AR = 1.0 and 2032 mm x 1524 mm x 127 mm (6 ft. 8 in. x 5 ft. x 5 in.) with AR = 0.75. These two walls are designated as short wall and long wall respectively. The details of dimensions and geometry of the wall specimens are given in Figure 3.1 and Figure 3.2.

One sample from each group was treated as control specimen and tested under the action of cyclic loading with a certain amount (10 % of compressive strength capacity of the wall) of gravity loads imposed on them with the help of rollers and joist. The sample was then retrofitted with the specified retrofitting scheme and tested in the same manner again up to failure. The other sample from each group was

directly strengthened following the same procedure and technique and tested to get their capacity under specified loading condition.

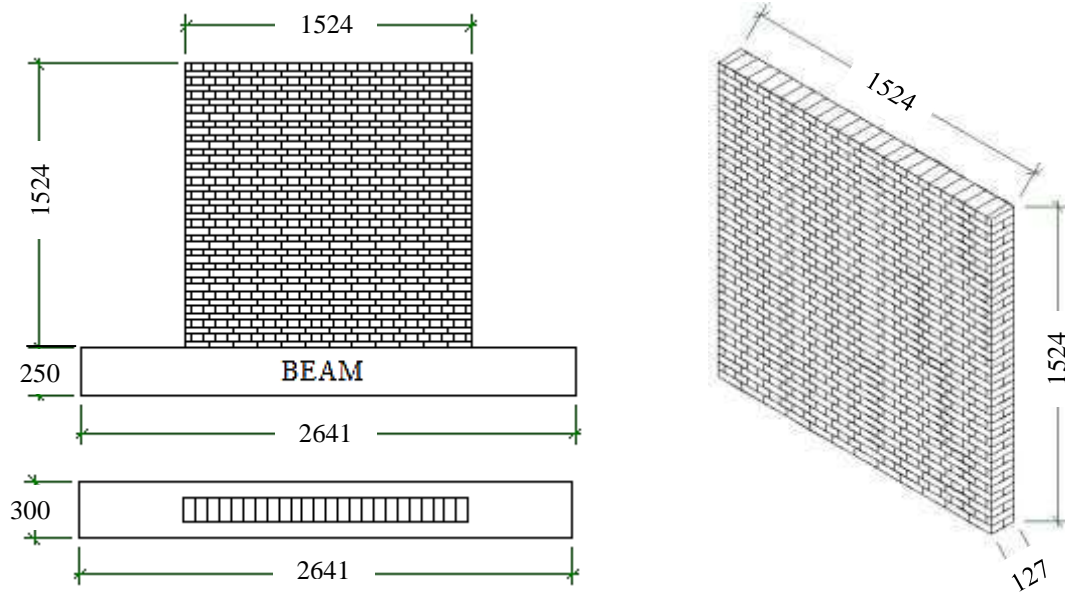


Figure 3.1 Detailed dimensions (in mm) of a typical wall sample (short wall)

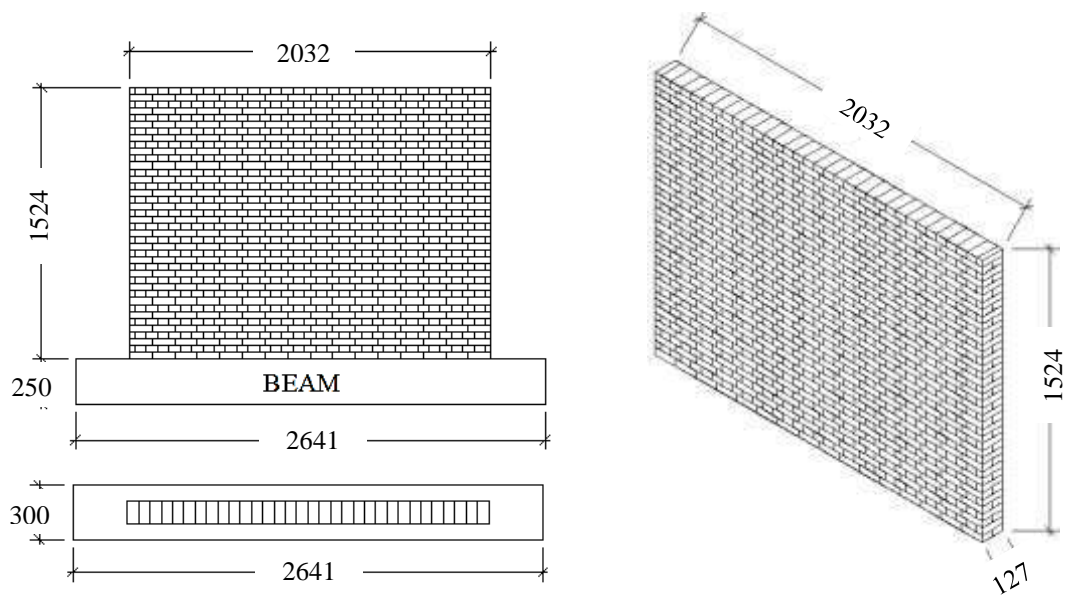


Figure 3.2 Detailed dimensions (in mm) of a typical wall sample (long wall)

The summary of wall identities; their groups and designation, state of retrofitting (i.e., retrofitted or not), allowable gravity loads and their retrofitting details are given in Table 3.1.

Table 3.1 Dimensions and designation of wall specimens

Wall Type	Wall ID	Wall Designation	Dimension (mm)	Retrofitting Configuration	Gravity Load (Ton)
Short Wall (2 types of samples)	SW-C	Short Wall - Control Specimen	1524 x 1524 x 127	Un-retrofitted	4.1
	SW-CR	Short Wall - Control Specimen Retrofitted after failure	1524 x 1524 x 167	6 mm dia. bar @ 75 mm c/c in both direction within 40 mm thick RC on one side	4.1
	SW-DR	Short Wall - Directly Strengthened	1524 x 1524 x 167		4.1
Long Wall (2 types of samples)	LW-C	Long Wall - Control Specimen	2032 x 1524 x 127	Un-retrofitted	5.5
	LW-CR	Long Wall - Control Specimen Retrofitted after failure	2032 x 1524 x 167	6 mm dia. bar @ 75 mm c/c in both direction within 40 mm thick RC on one side	5.5
	LW-DR	Long Wall - Directly Strengthened	2032 x 1524 x 167		5.5

3.3 Material Properties

The materials used for the preparation of wall specimens, their retrofitting and strengthening to complete the research work are enlisted below:

1. Bricks
2. Sand (Sylhet sand and Local sand)
3. Cement
4. Water
5. Stone Chips
6. Admixture
7. Micro-concrete
8. Mild steel rod as reinforcement
9. Steel plates

The physical and mechanical properties of materials were determined in the Concrete Lab and Strength of Materials Labs of the Civil Engineering Department of BUET.

3.3.1 Properties of Bricks

Half-scale burnt clay bricks were used for the construction of the masonry walls. The bricks were arranged in the wall following the English bond system to replicate the arrangement of a full scale 10 inch wall conventionally used in the construction of masonry buildings. The average dimensions of the bricks were 127 mm x 60 mm x 38 mm (Length x Width x Height).

The compressive strength of the brick samples were determined in the laboratory. Bricks were immersed in water at room temperature for 24 hours. Then both sides of the bricks were flushed with silicate materials. Then the brick samples were kept under wet jute bags for 3 days. Finally, brick samples were ready for testing. The water absorption value was also determined after 24 hours of immersion in water followed by the oven drying. The result of tests are summarized in Table 3.2 and 3.3.

Table 3.2 Crushing strength test details of bricks

Sl.	Length (mm)	Width (mm)	Observed Load (kN)	Actual Load (kN)	Area (mm ²)	Strength (MPa)	Average Strength (MPa)
1	125.00	60.00	142	137.48	7500.0	18.33	12.5
2	126.33	60.67	74	72.55	7664.2	9.47	
3	127.00	61.33	118	114.56	7789.3	14.71	
4	125.33	59.67	92	89.74	7478.2	12.00	
5	128.83	61.67	64	63.00	7944.7	7.93	

Table 3.3 Water absorption test data of bricks

Sl.	OD* Weight (gm)	SSD** Weight (gm)	Water Absorbed (gm)	Water Absorption (%)	Average (%)
1	437	539	102	23.34	21.3
2	467	556	89	19.06	
3	475	561	86	18.11	
4	444	557	113	25.45	
5	454	547	93	20.48	

* OD => Oven-dried

** SSD => Saturated surface dried

The dimension comparison of half-scale brick samples and a full-scale brick are illustrated in Figure 3.3 and 3.4.

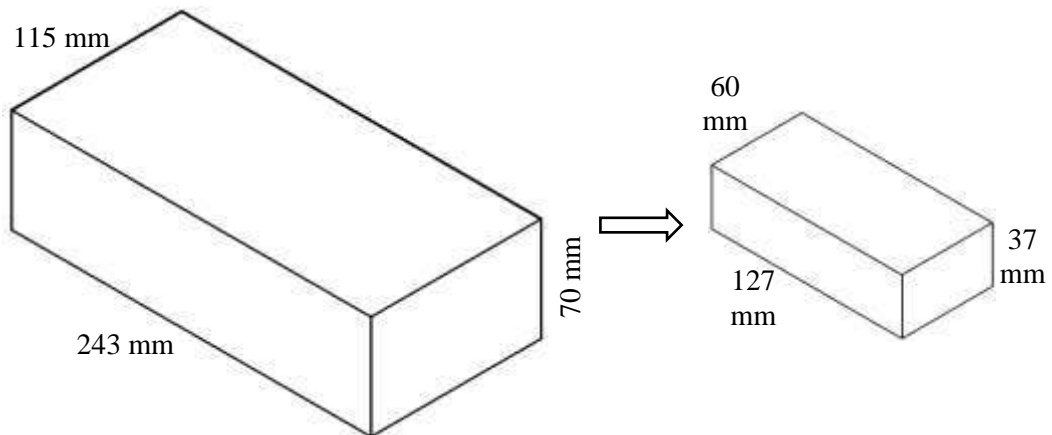


Figure 3.3 Dimensions of reduced scale brick compared to a full size brick unit

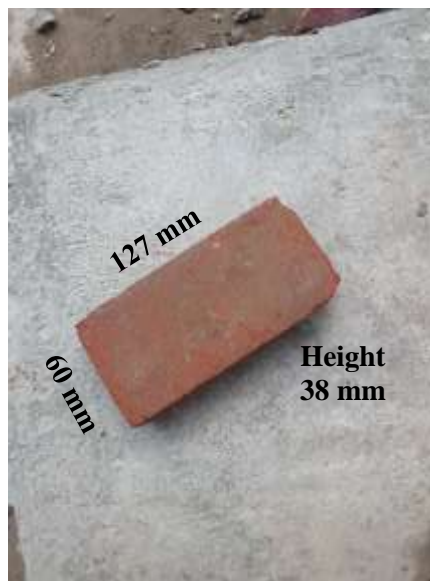


Figure 3.4 Half-scale brick unit with side dimensions

3.3.2 Properties of Cement

Cement was used as a binding agent to set and harden the aggregates together. The most important uses of cement are as a component in the production of mortar in masonry, and of concrete, a combination of cement and an aggregate to form a strong building material. The research work was conducted using Fresh cement (CEM I, Type A).

3.3.3 Properties of Fine Aggregates (Sands)

Two different types of sands were used in the lab work. Local sand has been used for masonry wall constructions and Sylhet sand has been used for base and RC overlay casting. Figure 3.5 shows the gradation curve of local sand and Sylhet sand respectively. The Fineness Modulus (FM) value for Sylhet sand and local sand were found to be 3.25 and 1.08 respectively.

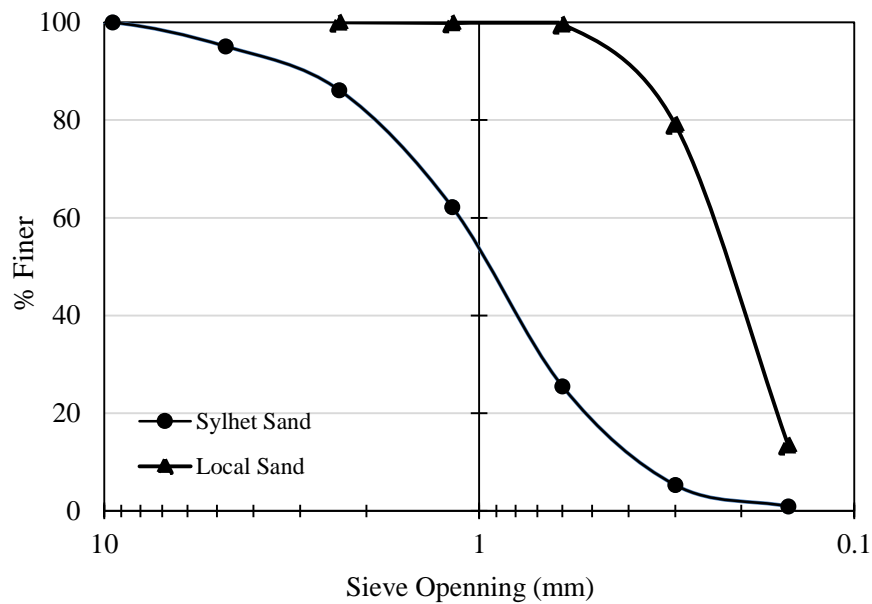


Figure 3.5 Gradation curve for Sylhet sand and local sand

3.3.4 Properties of Coarse Aggregate

Coarse aggregate provides strength and volume to the concrete. The durability of concrete depend on the type, quality and size of the aggregates being used. Usually, 19 mm downgrade stone chips were used for concrete casting. Two types of coarse aggregates were used in this research work. First one was 19 mm downgrade stone chips used for the construction of the strong base for wall samples.

Another type of coarse aggregate was used for the RC jacketing. Its gradation curve is given in Figure 3.6. It was a 5 mm downgrade stone chips that was used to produce micro concrete for casting the thin layer of concrete with reinforcement anchored into the wall. It was also helpful in gaining high compressive strength after 28 days

of curing. The targeted strength was 34.5 MPa in a project of retrofitting using the same type of materials at a building of the Department of Telecommunications.

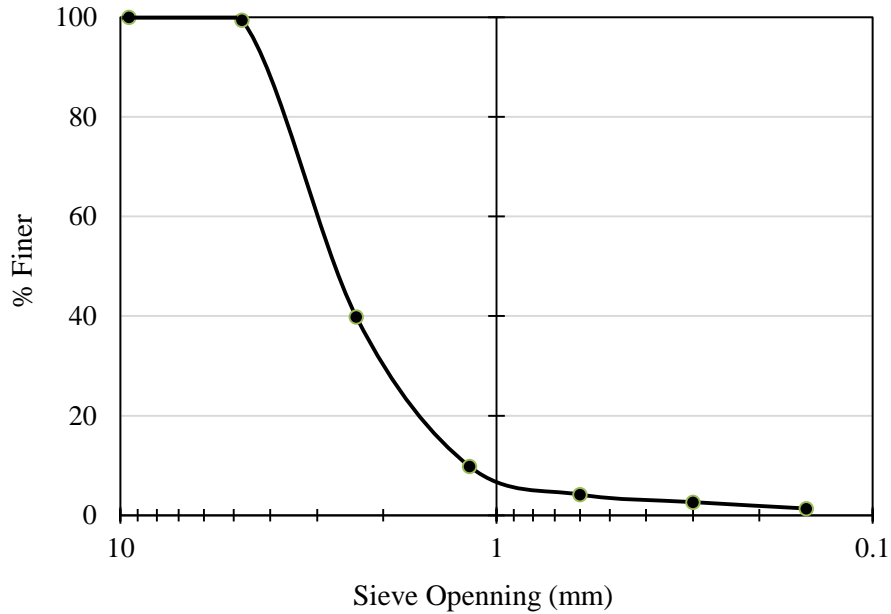


Figure 3.6 Gradation curve for 5 mm downgrade coarse aggregate used for RC overlay

3.3.5 Properties of Mortar

According to the BNBC 2020, Type-M2 mortar with cement:sand (1:4) proportions were used in the construction of the samples. This type of mortar is used in the local construction practice in Bangladesh with a minimum compressive strength of 7.5 MPa after 28 days of curing.

Compressive strength of mortar was determined in the concrete laboratory of Civil Engineering department, BUET. 50mm x 50mm x 50mm (2" x 2" x 2") cubes were made for this testing purpose. After curing in water for 7 days and 28 days the samples were tested under compressive load. The average value of compressive strength of mortar after 28 days of curing was obtained as 12.0 MPa, 11.3 MPa, 12.3 MPa and 10.0 MPa for SW-C, SW-DR, LW-C and LW-DR samples respectively. The strength of samples after 7 days of curing were also determined in the lab. Table 3.4 summarizes the details of compressive strength test data of mortar.

Table 3.4 Compressive strength test data for mortar (1:4)

Wall Type	Days	Sample No.	Area (mm ²)	Actual Load (kN)	Compressive Strength (MPa)	Average Strength (MPa)
SW-C	7 days	1	2580.64	11.68	4.53	4.4
		2	2580.64	10.82	4.19	
		3	2580.64	11.48	4.45	
	28 days	1	2580.64	32.75	12.69	12.0
		2	2580.64	27.97	10.84	
		3	2580.64	32.06	12.42	
SW-DR	7 days	1	2580.64	16.60	6.43	6.5
		2	2580.64	20.57	7.97	
		3	2580.64	13.42	5.20	
	28 days	1	2580.64	27.74	10.75	11.3
		2	2580.64	32.70	12.67	
		3	2580.64	26.71	10.35	
LW-C	7 days	1	2580.64	15.33	5.94	6.2
		2	2580.64	16.14	6.25	
		3	2580.64	16.57	6.42	
	28 days	1	2580.64	34.05	13.19	12.3
		2	2580.64	27.38	10.61	
		3	2580.64	33.41	12.95	
LW-DR	7 days	1	2580.64	10.88	4.22	5.3
		2	2580.64	14.05	5.45	
		3	2580.64	16.04	6.22	
	28 days	1	2580.64	22.31	8.65	10.0
		2	2580.64	30.40	11.78	
		3	2580.64	24.52	9.50	

3.3.6 Properties of Reinforcing Bars

Mild steel rods were used as reinforcement in the base for wall construction and in the RC overlay. 500W steel bars of diameter 16 mm was used as longitudinal bars in base and 8 mm dia. bars were used as stirrups. For RC on the face of URM walls 6 mm dia. bars of same strength was used. The surface of the rods were cleaned up and made free of any type of rust before using.

3.3.7 Admixture

To gain high strength of concrete for RC overlay a high range water reducing admixture named Master Glenium was used during the mixing of concrete. This helped the concrete to gain early high strength. The dose was 200 mL/bag of cement. It also increased the workability of the concrete which made it flow easily and fill up every corners within the formwork.

3.3.8 Timber for Formworks

The casting of base and the RC overlay was done in the formwork made of stout timbers. The thickness of the timber used for the construction of formworks was 25 mm (1 inch) or larger. The inner surface of the formwork was made smooth for base construction and thin sheets of plywood was used on the inner surface of the formwork for RC casting. The formworks were properly attached and anchored with the wall and its base.

3.4 Construction of URM Wall Specimens and their Retrofitting

URM wall specimens were prepared in two distinct steps following the usual construction practice. This section describes the systematic process of sample preparation followed by the step by step pictorial descriptions of specimen formation.

3.4.1 Base Preparation for URM Walls

Total four wall samples were prepared on individual bases. According to the dimension and length of the walls, one single type of base was chosen to be fit for all type of samples. The longest wall sample had a length of 2032 mm (6 ft. 8 in.). Keeping this in mind the length of the base was chosen to be 2640 mm (8 ft. 8 in. i.e., 1 feet excess on both sides). The space of the strong frame in the lab where the walls were to be tested also played a role in choosing the base dimension. The cross-sectional dimension of the beam was 300 mm (12 in.) wide and 250 mm (10 in.) deep. It was prepared using 19 mm downgrade stone chips as CA, Sylhet sand as FA and cement as binder in the ratio 1:1.25:2.5. Each beam was reinforced with 10 – 16 mm dia. bars and 8 mm dia. rods were used as shear reinforcement with rings of two sizes as illustrated in Figure 3.7 and 3.8. The strength of the concrete used in base

after 28 days of curing was found to be 37.2 MPa. The values of 28 days strength are given in Table A.8 of Appendix.

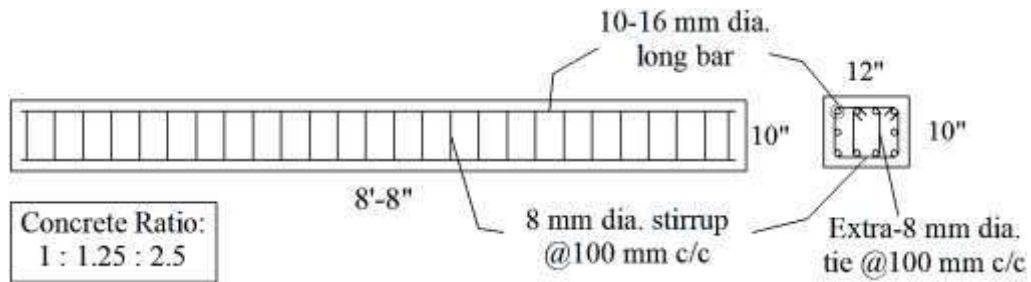


Figure 3.7 Dimension and reinforcement detailing of the RCC base



Figure 3.8 Construction of RCC base for masonry wall

3.4.2 Masonry Wall Construction

The URM walls were constructed on the centrally marked place on beams top surface after 28 days of curing of the base. Holes were drilled in the base at proper locations to insert the reinforcing bars at 75 mm c/c to embed into the base.

The walls had a height of 1524 mm (5 ft.). That is why they were constructed in two stages. Approximately half of the wall was prepared on first day and the rest was on the following day. The English bond for masonry wall was used with one layer of stretcher and another layer of header and so on. To replicate a full-scale 10 in. wall being used in conventional construction work, the whole sample was reduced to half-scale including the mortar thickness. The thickness of the mortar was maintained to

be around 8 -10 mm throughout each joints. The cement sand mortar specimens were prepared for each walls at the time of their construction. Finally, the walls were wrapped with thick clothes and curing was done by pouring water on them on regular basis. Some of the pictorial representations of the masonry wall construction are illustrated in Figure 3.9.



Figure 3.9 Construction of walls, (a) Construction in progress, (b) Fully prepared URM walls

3.4.3 Retrofitting Work

One URM sample from each group was tested as control specimen and then retrofitted with predefined retrofitting scheme. Another two samples were directly strengthened following the same technique. The retrofitting started with the preparation of surface where the RC overlay was supposed to be applied. The reinforcing bars in the form of 6 mm dia. MS rods were inserted into the wholes that were drilled into the base. The anchoring between bars and base was done using epoxy. The holes were first blown to clear all type of debris and dust from them. Then epoxy was poured into the holes and the rods were inserted into them vertically. Eventually the chemical helped the bars to get adhered to the base strongly. After that the casing of rod was completed by providing horizontal bars in between the vertical rods and the wall surface, thus the vertical bars were at the outer side of the jacket. Both the bars were placed at 75 mm (3 in.) c/c. The cage was attached with the surface of the wall using anchors bent at more than 90 degree. One

part of it was inserted into the mortar joints of brick layers by an amount not more than 50 mm (2 in.) and the other limb held the adjacent rod (approx. length 40 mm) in the form of a hook.



(a)



(b)

(c)

(d)

Figure 3.10 Application of epoxy for anchoring rebar with base, (a) Holes in the base, (b) Marks @75 mm, (c) Applying epoxy, (d) Inserting bars



Figure 3.11 The 90-degree hook used for the anchoring of rebars with wall

For short wall (5 ft. x 5 ft.) total 9 hooks (in 3 rows x 3 columns) were used in a uniformly spaced square grid system. In case of long wall (6 ft. 8 in. by 5 ft.), the length being greater, total number of hooks was 12 (in 3 rows x 4 columns) Care was taken during this anchoring not to disturb the integrity of the masonry at all. The details of hooks and anchoring are given in Figure 3.10 to 3.12 showing the length of the hook and its attachment with the wall as well.

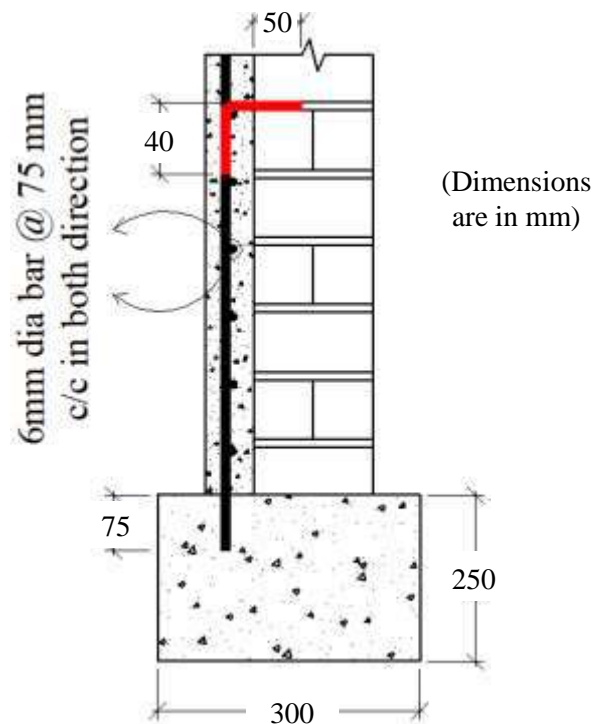


Figure 3.12 Schematic detailing of reinforcement and its anchoring

After that the formwork was attached properly with the cage anchored to the base and the wall itself. Sufficient rigidity and stiffness was provided to the formwork by adding temporary shoring to prevent any type of unwanted catastrophe during the casting of concrete into it. The concrete was then mixed in a ratio of 1:1.2:1.7 (Cement: Sand: Stone) by weight with a w/c (water/ cement) ratio of 0.50. Admixture was also provided at a dose of 200 mL/bag of cement to provide adequate amount of workability and gain early strength. Figure 3.13 shows the fully prepared wall samples ready with formwork for the casting of concrete.



Figure 3.13 Wall sample fully prepared for casting with proper formwork

Finally, the casting was done very carefully and slowly to avoid any type of failure. The clear cover of 15 mm was maintained properly and the top surface was levelled with the wall-top surface to provide a plain horizontal platform during test.

Concrete cylinders were also prepared at the time of casting. Three samples for 7 days and 3 for 28 days test. After 24 hours of casting the formworks were removed very carefully and sample was set to curing for a period of 28 days. The retrofitting and strengthening was done following these procedure with the exception that during retrofitting, the wall already had cracked in several locations. Therefore, special care was taken during those operations. The average compressive strength of the concrete of RC overlay after 28 days of curing was found to be 37.1 MPa, 37.2 MPa, 33.2 MPa and 35.7MPa for LW-DR, SW-DR, LW-CR and SW-CR samples respectively. The data of compressive test of concrete cylinders are given in Table A.9 of Appendix.

3.5 Test of Wall Specimens

Prior to the cyclic test, the vertical and lateral load carrying capacity of the bare masonry sample were estimated using the mechanical properties obtained from prism test. Then the proper test procedure was followed to conduct the experiment. The following sub-sections describe the whole testing process and its supportive arrangements.

3.5.1 Prism Test and Estimation of the Capacity of Masonry

Prism tests were conducted using the representative samples of the masonry walls units. Total three prism samples were prepared using five stacks of bricks placed in the same manner as was used for wall construction i.e., English bond. The thickness and ratio of mortar was also the same. Following the ASTM C1314 for prism test of masonry, the samples were prepared during the construction of walls and cured under water for 28 days and finally tested under gradually increasing gravity load to get the value of the compressive strength of masonry i.e., f'_m . Using this value and following the BNBC 2020 code provision for the allowable stress determination of masonry structures (Part VI, Chapter 7: Masonry Structures, Article 7.3 – 7.5) the vertical and shear stress carrying capacity of each wall were determined. These values were helpful in the test of masonry. The pictorial representation of prism test and its data are illustrated in Figure 3.14 and Table 3.5 and Table 3.6.



Figure 3.14 Masonry prism samples ready for testing

Table 3.5 Test data of prisms

Sl.	Height (mm)	Length (mm)	Width (mm)	Area (mm ²)	Load (N)	Strength (MPa)	Average Strength, f'_m (MPa)
1	190	150	150	22500	255930	11.375	11.1
2	190	150	150	22500	239892	10.662	
3	190	150	150	22500	245257	10.900	
4	190	150	150	22500	258080	11.470	

Table 3.6 Allowable stress and force of masonry from f'_m

Wall Type	f'_m (MPa)	Area (mm ²)	Allowable Stress (MPa)		Allowable Force (Ton)	
			Compr., F_a	Shear, F_v	Compr., P_a	Shear, P_v
Short Wall	11.1	187500	2.17	0.08	41.1	1.6
Long Wall	11.1	250000	2.17	0.08	55	2.1

3.5.2 Experimental Setup

The main theme of the test was to apply a cyclic load at the top of walls using hydraulic jack while the wall is subjected to a certain amount of gravity load (a percentage of its axial load carrying capacity) to prevent compression failure. It also depicts the actual scenario of a masonry building while it simultaneously experiences seismic excitation from the quaking of ground and the stress due to the gravity load coming from vertical direction. This type of test has been conducted in the Concrete Laboratory of the CE department of BUET where there is a strong symmetric frame system to apply lateral loads to any specimen of a limited dimension and scale. The laterally braced strong column of that frame as shown in Figure 3.15 and 3.16 are capable of applying a good amount of lateral load to the walls.



Figure 3.15 Full frame for testing with mounted strong beam at top

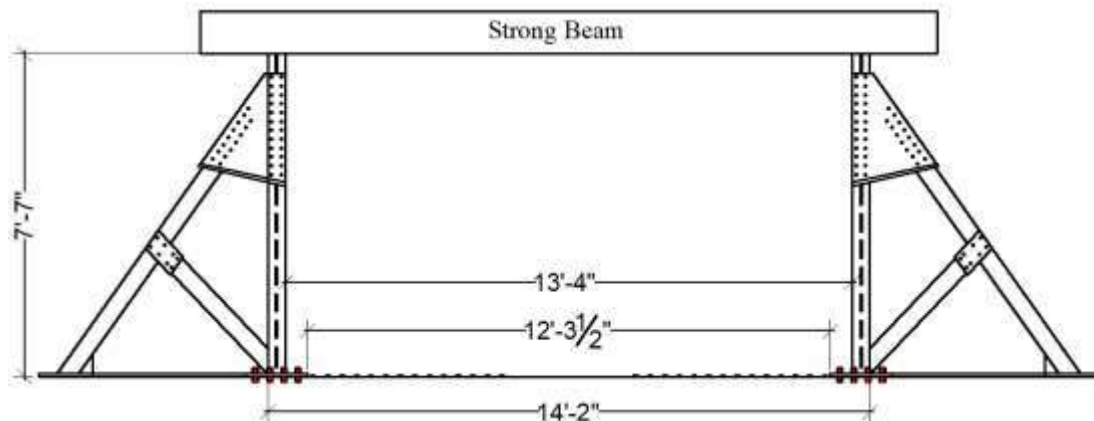


Figure 3.16 Detailed dimensions of strong frame with strong beam

The supporting arrangement and setups for the smooth conduction of the cyclic loading test of URM and retrofitted walls are as follows:

- i. Anchors for fixing base to the floor of lab.
- ii. Top steel plate to be placed on the top surface of the wall.
- iii. Four rollers to distribute the gravity load evenly on the wall.
- iv. Joist or beam over rollers to transfer the gravity load.
- v. Hydraulic jack for gravity load.
- vi. A very strong beam or joist to take the reactive force from vertical jack.
- vii. Anchoring of vertical jack to the strong beam at the top and joist below.
- viii. Hydraulic jack of sufficient capacity (50 Ton) to apply lateral loads.
- ix. Anchoring of lateral jack to the strong column.
- x. Set up for applying cyclic load directly at the top of wall.

Prior to bringing the samples to the testing frame, the smooth surface of the wall was colored evenly with white lime for easy observation of cracks. Then the colored samples were brought to the testing frame by using a chain and pulley system and/or using roller beneath the base of walls. A large number of labors were involved in it to ensure that the walls experience no harm or damage during this shifting operation. The base of the wall (RCC beam) was anchored to the floor of the lab with the help of long bolts inserted into the pre-existing holes on the floor and making them tight enough using nuts and steel plates (where necessary) to prevent any slightest movement of base. The base was also anchored to the adjacent columns of the strong frame on either side using MS plates and rods.

To distribute the gravity load uniformly over the wall an MS steel plate of relevant size (for short wall – 72 in. x 11 in. x 1 in. and for long wall – 80 in. x 11 in. x 1 in.) was used over the top surface of the wall. The top plates were so prepared that they can apply both push and pull type of forces on the wall and for that a MS plate of sufficient dimension at the far end was attached to hold that portion of wall during time of pull. At the jack end there was a U-shaped section or C-section welded to the near end of the top plate. This C-section also had arrangement for the head of the lateral jack to be attached with the use of nut and bolt (double shear). Both the plates (at near and far end) were firmly attached to the top plate to prevent any type of buckling or failure at the time of testing. Again, to ensure the uniformity of gravity load a double-layered geotextiles was placed in between the top plate and the wall surface. At the same time the top surface of the top plate was provided with chambers for 4 cylindrical rollers to be fit in and move freely during test. Above the 4 rollers there was another beam (box section) of sufficient length on which the gravity load was applied using a 30 Ton jack. This beam also had chamber beneath the surface to hold the rollers. A thick MS plate was placed in between box section and vertical jack to prevent any type of local failure in the beam. To support the vertical load from jack a very strong beam from the lab was raised above the existing frame and kept on it spanning between the two columns. MS plates were used in between the beam and columns which was welded to both members. The strong beam was anchored with the columns very firmly to take the upward load reaction and counter balance the negative moment.



Figure 3.17 Arrangement for vertical and lateral load for wall samples

The lateral jack was attached to the strong column with the help of MS plates of sufficient thickness, nut bolts and welding. Only one jack was used from the left side for both pushing and pulling the wall specimen. The anchorage for lateral jack was designed for the both cases (compressive and tensile reaction). Figure 3.17 and 3.18 show the arrangement of vertical and lateral load for walls and the jacks to be used for testing.

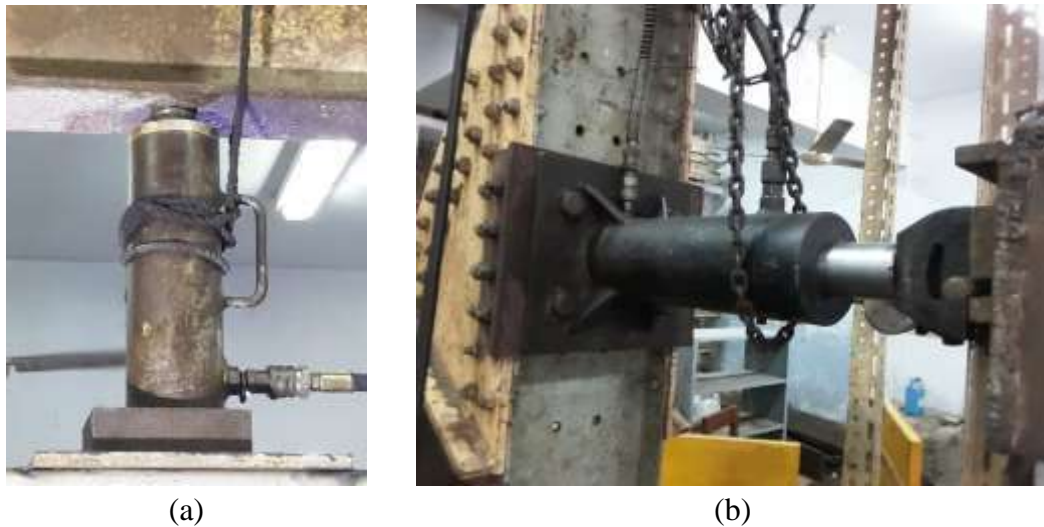


Figure 3.18 Jacks for applying vertical and lateral load, (a) Vertical jack (30 Ton), (b) Lateral jack (50 Ton)

3.5.3 Instrumentation

The lateral loads were recorded from a load gauge having a capacity of measuring load up to 50 tons as shown in Figure 3.19(a). For vertical load that was kept constant, there was another load gauge. To measure the deformation total four dial gauges were used – one at the near end or jack end (50 mm range), one at the far end (50 mm range), the other one at the mid-point of the total height of far end (25 mm range) and the last one at the base to record the movement (if any) of base. The first two dial gauges were used to average the values obtained from them and to calculate the top displacement. The gauge at the mid was used to get the profile of lateral deformation with the incremental reverse cyclic loading. The dial gauges had a factor of 1:100 i.e., a full revolution of 100 units would give the value of 1 mm of deformation. The dial gauges were attached to the respective points on the wall using two mounting frames. Sufficient amount of dead load was put on the base of the frame to prevent any type of movement in it. The position of one deformation gauge

is shown in Figure 3.19(b). A schematic diagram of the full arrangement of the short and long walls are given in Figure 3.20(a) and 3.20(b). Figure 3.21 shows the fully prepared wall sample ready for testing.

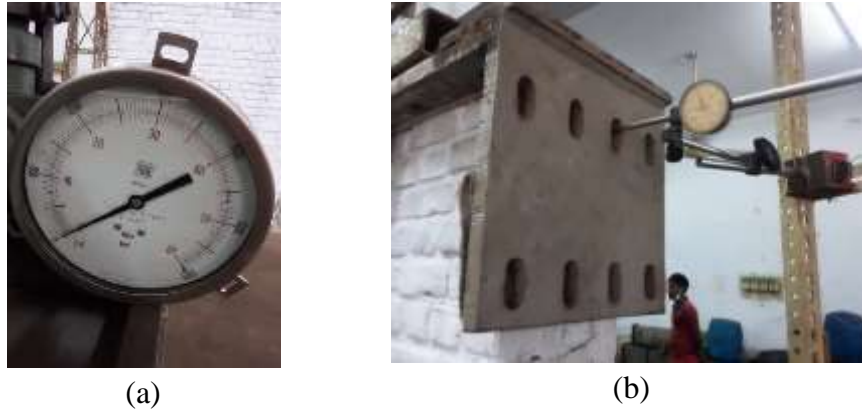


Figure 3.19 Gauges used in cyclic test, (a) Load gauge, (b) Dial gauge

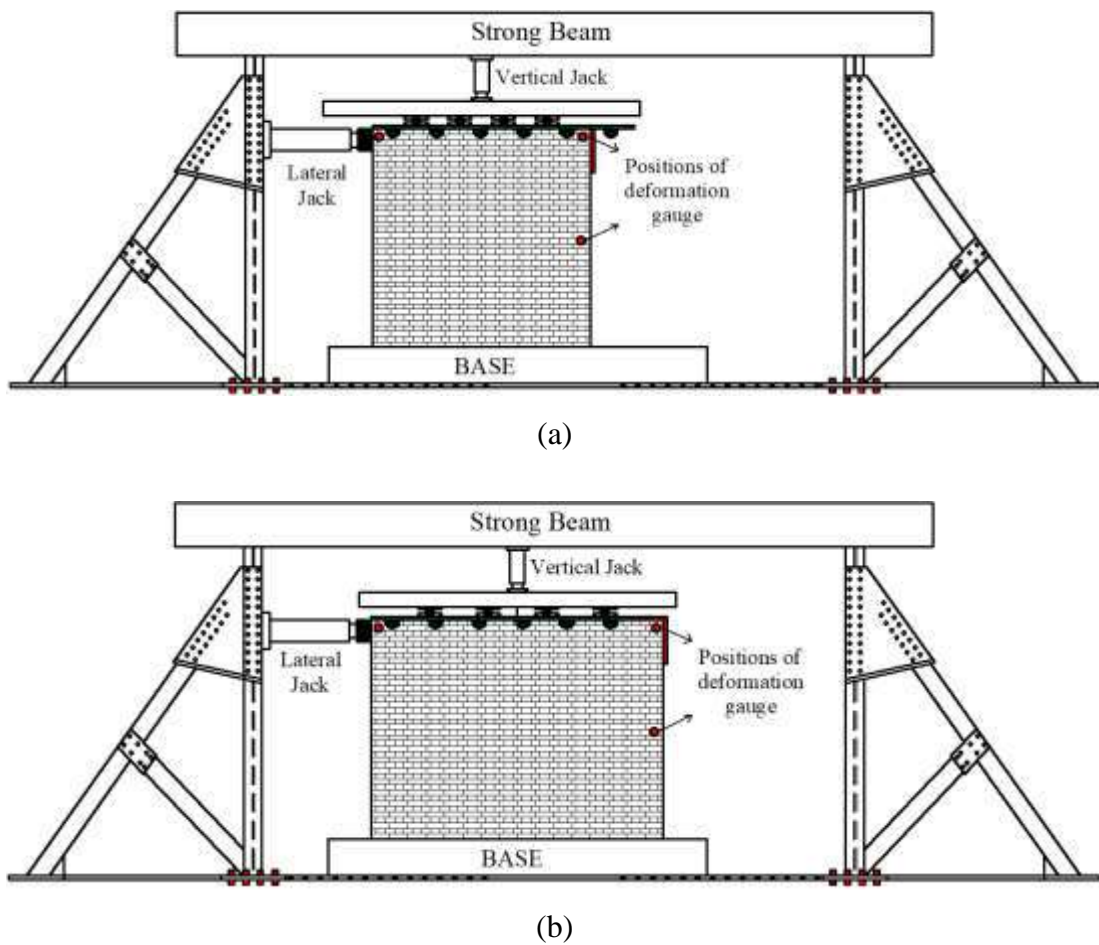


Figure 3.20 Schematic diagram of loading and testing arrangement of masonry walls, (a) Short wall, (b) Long Wall



(a)



(b)

Figure 3.21 Complete test setup of walls, (a) Wall-side, (b) RC overlay-side

3.5.4 Loading Scheme

The loading pattern used in the test was very much similar to the loading scheme shown in Figure 3.22. The test was conducted as a load-controlled test scheme. The intervals of loadings were chosen based on the minimum reading the load gauge could provide us (which was 5 bars = 1 unit). The gravity load was applied with a jack in vertical direction and it was kept and maintained constant during the test. The value was 4.1 ton (9000 lb.) for short wall and 5.5 ton (12000 lb.) for long wall.

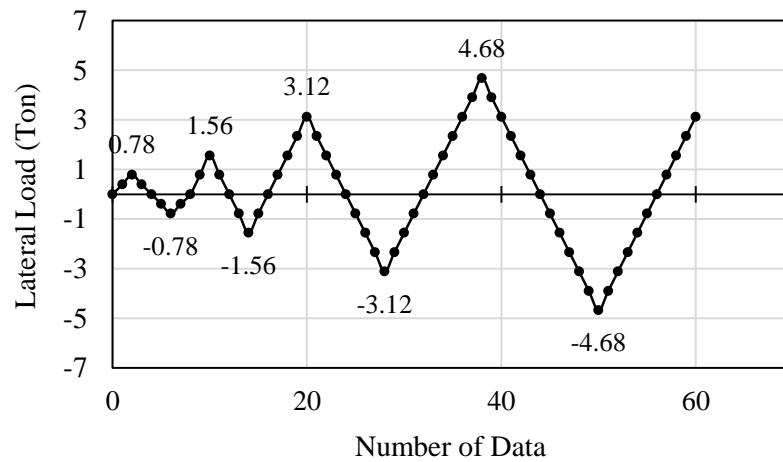


Figure 3.22 Cyclic loading pattern applied on the wall in reverse cyclic mode

Chapter 4

RESULTS AND DISCUSSION

4.1 Introduction

The lateral cyclic loading tests were conducted on each wall sample for each case as discussed in the previous chapter and the data were collected to analyze and observe the behaviour and response of wall samples. This chapter summarizes those data and also presents the total analysis of this research work. Both the qualitative and quantitative results are incorporated in this section. The qualitative results include the photographs that depicts the actual response of the test specimens under the applied loadings and the crack patterns as well. The quantitative results are comprised of the numeric values obtained after analyzing the test data of load and displacement. The values are plotted in graphs to know the actual scenario with the evaluation of the relevant parameters such as energy dissipation, ductility, stiffness degradation, hysteresis percentage damping, envelop curve, the deflection profile of the wall end etc. and these parameters from each samples are compared to finally conclude the findings.

4.2 Analysis of Test Results

The test was conducted in the lab accordingly and the response of the walls were observed and analyzed in terms of formation of first cracks, crack patterns, failure modes, ultimate load and corresponding displacement. There were two sets of samples including two specimens each and the number of tests conducted was six (06) in total. The samples showed different types of failure modes like shear failure for control specimen of short wall to rocking type of failure for retrofitted samples. Also the crushing of corners were observed. The results are illustrated in the following sections.

4.2.1 Failure Modes of Short Wall Assemblies

The formation of cracks and failure modes of the samples from the short wall assembly are discussed here.

4.2.1.1 Control specimen (SW-C)

The control specimen of short walls (with aspect ratio 1.0) experienced the crack formation at near end while lateral load reached up to 3.12 ton in first push of 3rd cycle. The crack propagated to the bottom corner of far end in the next (4th) cycle. Crack was generated in the same layer of reverse loading and met the previous downward propagating cracks. The ultimate lateral load reached up to 3.9 ton in reverse direction and no further loading was applied due to the possibility of total collapse of the wall assembly with the load arrangement. The maximum lateral displacement at top was recorded to be 6.15 mm at that load. There was a possibility of toe crushing if the push load was further increased as the crack started to propagate to the bottom far end diagonally. It is noteworthy that the gravity load at this instance was increased to a value of 13300 lb. from 9000 lb. The failure mode of the wall is given in Figure 4.1.



Figure 4.1 Failure patterns in short wall-control specimen (SW-C), (a) Cracks at final stage (4th cycle), (b) Possibility of toe crushing

4.2.1.2 Specimen Retrofitted After Failure (SW-CR)

The retrofitted sample already had cracks in the wall as illustrated in Figure 4.1 above. The failure mode of SW-CR followed the trace of that existing cracks of the control specimen. Wherein the bare wall experienced first crack in 3rd cycle, the retrofitted one got its first crack in 5th cycle and load was 6.24 ton push. The crack was initiated from the pre-existing crack as expected. However, no trace of cracks were found when the load was reversed except that the previous cracks sealed only. Even when load reached at peak of next cycle (6th) at 9.36 ton, only the previous cracks expanded a little bit; no new cracks were found on the surface of the wall,

same was the scenario in case of reverse loading of this cycle. However, the wall started to experience the formation of cracks that might cause toe crushing at the highest loading of 7th cycle (12.48 ton). Cracks were also observed at the base and beam interface at this stage causing the wall to tilt a little bit and eventually the gravity load increased to 5 ton.

In the reverse loading of the same cycle (at 9.36 ton pull) cracks appeared in between the 1st and 2nd layer of masonry of far end corner side. And at 12.48 ton, the wall was detached from the base as before. The thickness of these two cracks were 0.35 mm and 0.55 mm respectively.

When load was applied for 8th cycle, we could not proceed beyond 11.70 ton of first push and numerous types of cracks were formed at this stage as discussed below:

- i. Crack was found at 9th joint measured from bottom and the width of that crack was 0.30 mm.
- ii. Diagonal shear cracks were formed in the wall side.
- iii. The whole wall assembly was detached from base in alternate push and pull respectively i.e., the anchoring between the concrete base and reinforcing bars failed.
- iv. No remarkable crack was observed on the RC overlay except a thin crack at the bottom far end.
- v. There was a chance of toe crushing at that region during push.
- vi. Flexural compression type of failure occurred at top near end where lateral jack was applying force.
- vii. The crack was formed in square pattern extended in 3 layers of bricks from top surface.

The failure mode and crack patterns of the short wall sample retrofitted after failure (SW-CR) are illustrated in Figure 4.2. It shows the propagation of step-like cracks with their zoomed view as well.

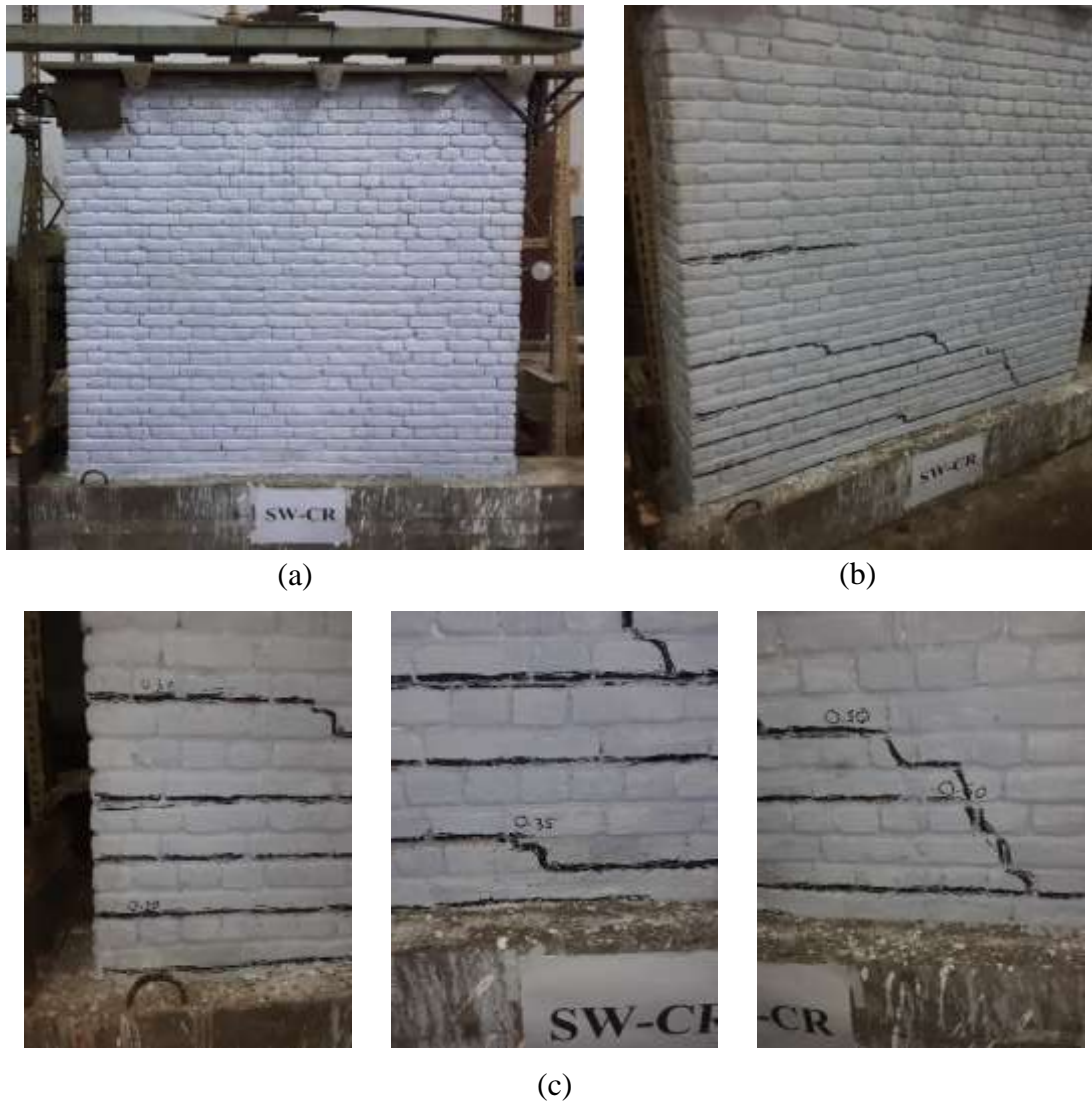
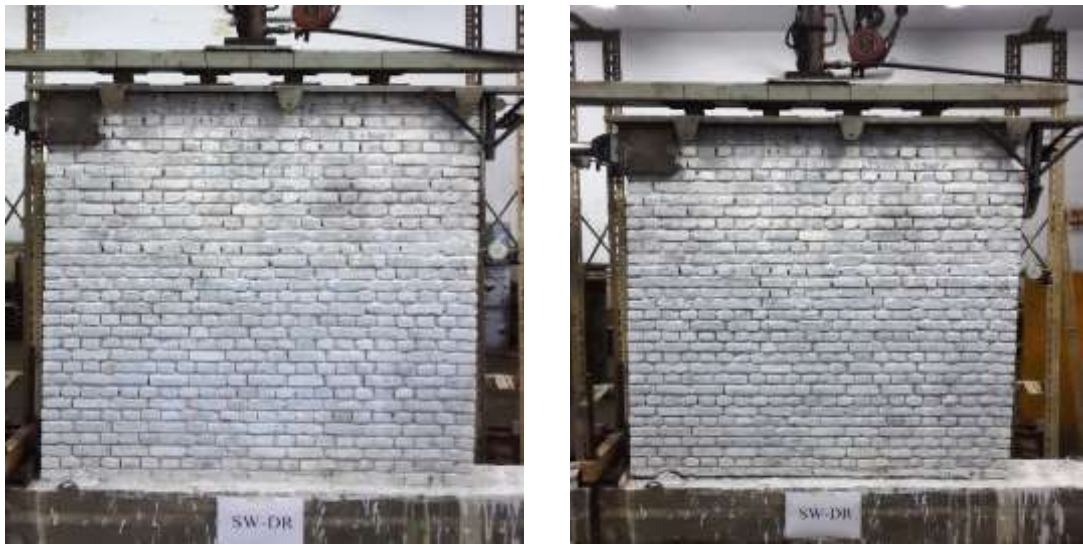


Figure 4.2 Failure patterns in short wall- retrofitted specimen (SW-CR), (a) Unaffected wall sample, (b) Cracks on wall side, (c) Zoomed view

4.2.1.3 Directly Strengthened Specimen (SW-DR)

The strengthened sample from short wall assembly when subjected to lateral loading did not show any type of cracks in wall. Rather, it suffered the rocking type of failure as the bottom of far end side was detached from base while push was applied in 6th cycle. It was the first crack observed at 9.36 ton. When reversed 9.36 ton of load was applied in the same cycle, visible cracks were seen in the far bottom side of wall only, no cracks were observed in the RC overlay in this state. However, the sample was still about to take a considerable amount of cyclic load.



(a)

(b)

Figure 4.3 Cracks at the base of SW-DR in 8th cycle, (a) Unaffected wall sample (SW-DR), (b) Cracks at bottom of SW-DR



(a)



(b)

Figure 4.4 Details of cracks formation in SW-DR during test, (a) Final cracks at bottom of near end, (b) RC overlay detached from base and wall

In the first push of 7th cycle (maximum load 12.48 ton), no remarkable change was noticed. In the pull state, however, the previous cracks opened up much more and the anchorage failure was clearly visible. This cycle was completed without any collapse until the last cycle was reached. In the last cycle (8th cycle), only push of amount 10.14 ton was applied for safety reason. At this state, the anchorage failures were observed very clearly as shown in Figure 4.3 and Figure 4.4. The crack width was about 9 mm at the end. The bottom end of far side also experienced crack formation due to the action of rocking and stress concentration at that region and the RC overlay at top of near side (i.e., below the jack end) showed a tendency of delamination. Due to the action of flexural compression, the top end also suffered the crack formation. The gravity load was increased up to 18000 lb.

4.2.2 Failure Modes of Long Wall Assemblies

The crack formation and failure modes of the samples from the long wall assembly are discussed and illustrated in following sub-sections.

4.2.2.1 Control Specimen (LW-C)

The control specimen of long wall with aspect ratio of 0.75 experienced the crack formation as shown in Figure 4.5 and 4.6.

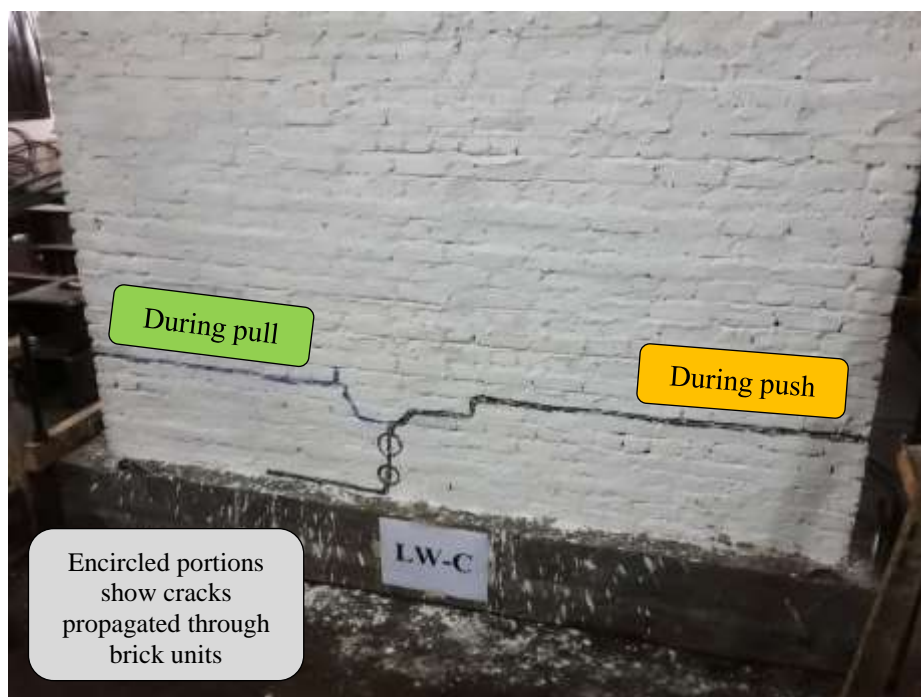


Figure 4.5 Cracks in LW-C wall specimen

Observations made during the time of the test of this sample are-

- i. First crack was formed during the first push of 4th cycle at 2.34 ton in the mortar joint between the 7th and 8th layer of brick units on the near end side of the wall.
- ii. Final cracks were formed when 5.46 ton load was reached and the vertical load reached the value of 6.13 ton.
- iii. The width of crack was 4.95 mm.
- iv. The ultimate displacement was 7.72 mm at 5.46 ton of lateral load.

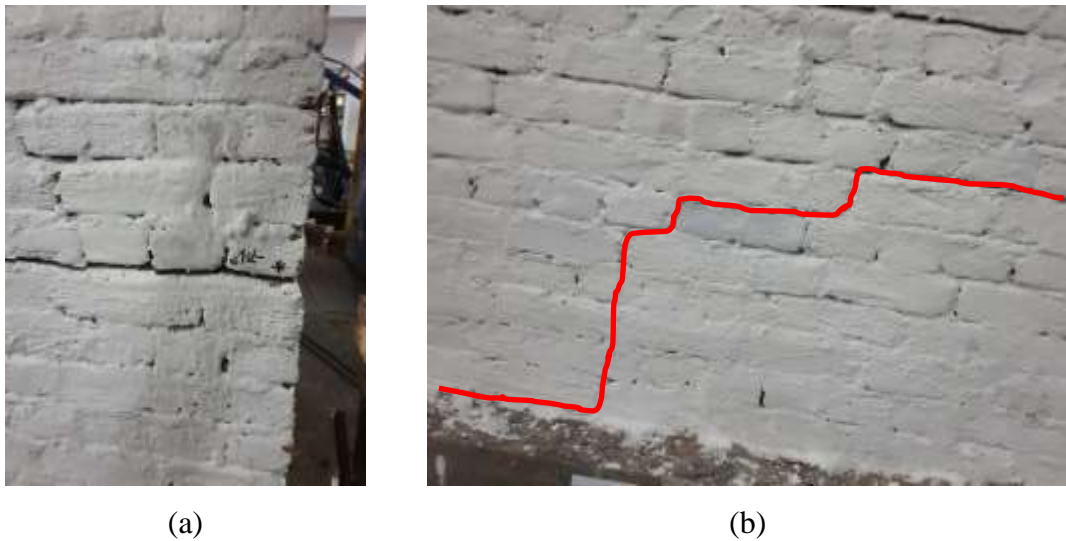


Figure 4.6 Generation and propagation of cracks in LW-C sample, a) First crack at 2.34 ton load, (b) Crack propagation through joints and brick

4.2.2.2 Specimen Retrofitted After Failure (LW-CR)

The retrofitted sample already had cracks in the wall as illustrated in Figure 4.6 above. The failure mode was found to be rocking and flexural compression type of failure. The illustration of the wall specimen before and after testing are given in Figures 4.7 to 4.12:

The observations made on the response and failure mode of this wall are -

- i. Despite the presence of cracks in wall, the sample showed up its first crack at a load of 10.92 ton push of 7th cycle while the ultimate load of control specimen was 5.46 ton.
- ii. First crack was formed at the junction of wall and base of near end.

- iii. When reverse loading was applied, the sample had crack (at -12.48 ton) being visible at the same location of that observed in LW-C in reverse loading.
- iv. In 8th cycle, the maximum push was 15.6 ton when the cracks seemed to be in very critical condition that is why no further application of load was made.
- v. The width of crack at this time was found to be 7.7 mm.
- vi. There was a possibility of toe crushing if load was further increased.
- vii. The RC overlay showed a sign of delamination from the wall near the toe.
- viii. The reverse loading was also applied gradually, however, no readings were taken and only the failure and crack formations were observed. It was found that at a pull of 15.6 ton, the cracks from LW-C test began to appear and widen gradually, most interestingly, the RC overlay behind those cracks also got some cracks as well.
- ix. During the last cycle cracks were formed at the top of far end due to flexural compression. The stress concentration at that region was so high that even the RC portion was crushed and the rebars were exposed. Cracks were also visible in wall.



Figure 4.7 LW-CR wall sample before testing



Figure 4.8 Rocking type of failure in LW-CR sample

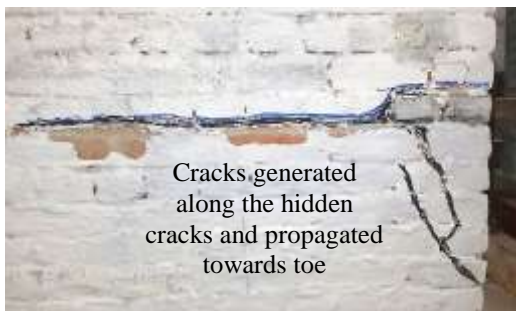


(a)

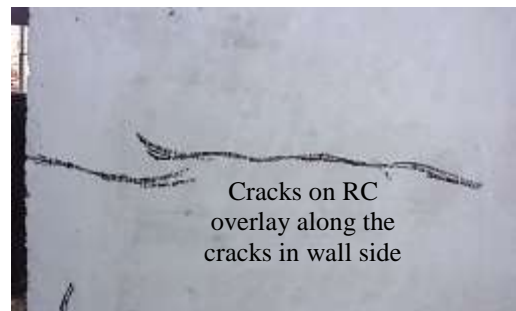


(c)

Figure 4.9 Cracks near toe of LW-CR: (a) On wall, (b) On RC overlay



Cracks generated along the hidden cracks and propagated towards toe



Cracks on RC overlay along the cracks in wall side

Figure 4.10 Crack developed along the hidden cracks of far side of LW-CR



Figure 4.11 Near end of LW-CR wall lifted up from base



Figure 4.12 Crushing of top corner of LW-CR wall sample

4.2.2.3 *Directly Strengthened Specimen (LW-DR)*

The strengthened sample from long wall assembly went through a remarkable range of lateral load. The observations are illustrated in Figures 4.13 to 4.15.



Figure 4.13 Cracks in LW-DR sample: (a) First crack (at base), (b) Final crack



Figure 4.14 Visible rebars of LW-DR after test



Figure 4.15 Closed view of crack at near end of wall retrofitted directly

The observations made during the test of LW-DR specimen are:

- i. The first crack was observed at 14.04 ton of push in 8th cycle and the location was at the wall-base-interface of near end.
- ii. The ultimate lateral load was 18.72 ton (final load of the 8th cycle) and the displacement at this load was 18.35 mm at top and 11.08 mm at mid of wall.
- iii. No trace of crack was found either on the face of wall or on RC overlay.
- iv. The crack propagated towards the toe of the wall creating the possibility of crushing at that region. But the load was reversed to avoid total collapse.
- v. The failure mode was rocking type of failure.
- vi. The rebars were detached from the holes and were clearly visible due to the widening of cracks and the crack width was found to be around 15 mm.
- vii. While reverse loading (pull) was applied previous crack began to seal itself but no crack was found on the other side of the wall.

- viii. Due to the possibility of total collapse of the whole wall assembly and load set up the test was stopped in the second pull and load reached to 12.48 ton with a top displacement of 2.97 mm in opposite direction.

The summary of the above mentioned discussions are given in the Table 4.1 below:

Table 4.1 Summary of crack formation and failure mode

Parameter	Wall ID	Cycle and Load Type**	Gravity Load* (Ton)	Lateral Load (Ton)	Displacement at Top (mm)	Max. Crack Width (mm)	Failure Mode
First crack	SW-C	3 rd (Push-1)	4.1	3.12	4.17	-	-
	SW-CR	5 th (Push-1)	4.1	6.24	2.28	-	-
	SW-DR	6 th (Push-1)	4.1	9.36	3.08	-	-
	LW-C	4 th (Push-1)	5.5	3.12	0.93	-	-
	LW-CR	7 th (Push-1)	5.5	10.92	2.51	-	-
	LW-DR	8 ^h (Push-1)	5.5	14.04	2.93	-	-
Final crack	SW-C	4 th (Push-1)	5.7	3.90	6.15	3.95	Rocking and Toe crushing
	SW-CR	8 th (Push-1)	5.0	12.48	11.3	1.11	Diagonal shear
	SW-DR	7 th (Push-1)	7.7	12.48	8.23	-	Rocking and diagonal shear
		8 th (Push-1)	8.2	10.14	13.43	9.0	
	LW-C	5 th (Push-1)	6.1	5.46	6.72	4.95	Rocking
	LW-CR	8 ^h (Push-1)	9.1	15.60	11.0	7.7	Rocking and diagonal shear
LW-DR	8 ^h (Push-1)	8.8	18.72	18.36	15	Rocking and Toe crushing	

* Gravity load increased with the increase in lateral force

** Load type:

Push-1: Load from 0 to (+ve)_{max}

Pull-1: Load from (+ve)_{max} to 0 (Release)

Pull-2: Load from 0 to (-ve)_{max}

Push-2: Load from (-ve)_{max} to 0 (Release)

4.3 Analysis of Test Data and Graphical Representations

The test data were analyzed for finding the required parameters for the fulfilment of the objectives of the thesis works. The parameters are presented and discussed in the following sections:

4.3.1 Load-Deformation Response (Hysteresis Curves)

The load-deformation curve from the deformation data recorded at top of short wall assembly are illustrated in Figures 4.16 to 4.18. The control specimen (SW-C) underwent only four (04) complete cycles with a maximum lateral load of 3.90 tons and top displacement of 6.15 mm (Figure 4.16). The next cycle was initiated, however, the wall could not take any load beyond 3.12 ton. The loops were found to be closely spaced as expected.

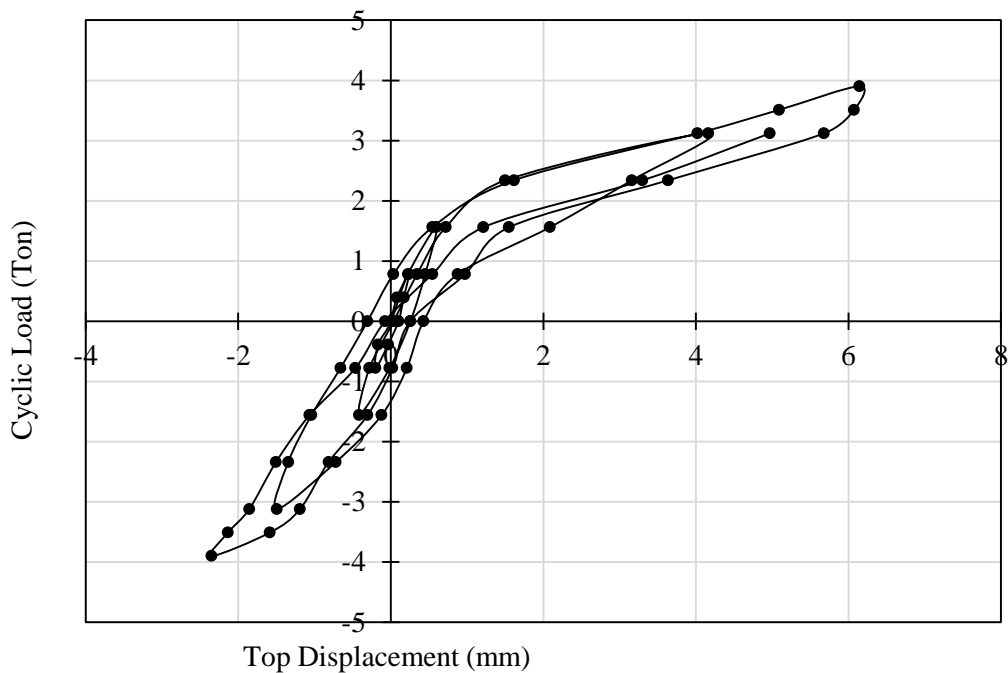


Figure 4.16 Load - deformation curve for SW-C (Control Specimen)

The control specimen of short wall retrofitted after failure went through total 7 cycles of lateral load with a maximum of 12.48 ton. The 8th cycle was continued up to 11.7 ton only. The displacement was maximum at this time which was 11.3 mm. The load-deformation behaviour is illustrated in Figure 4.17.

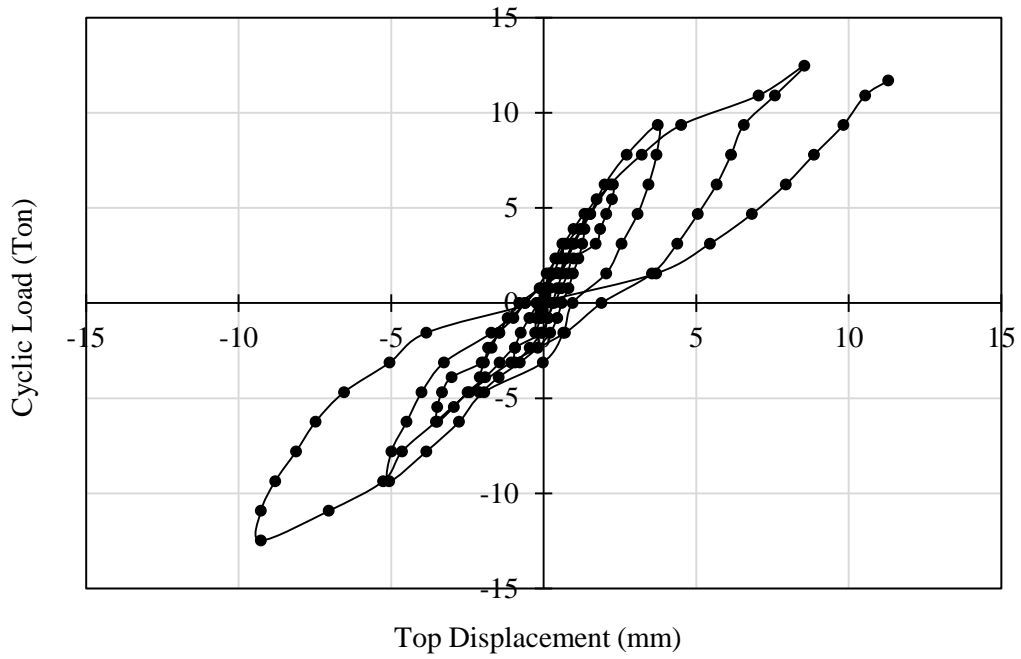


Figure 4.17 Load - deformation curve for SW-CR (Retrofitted)

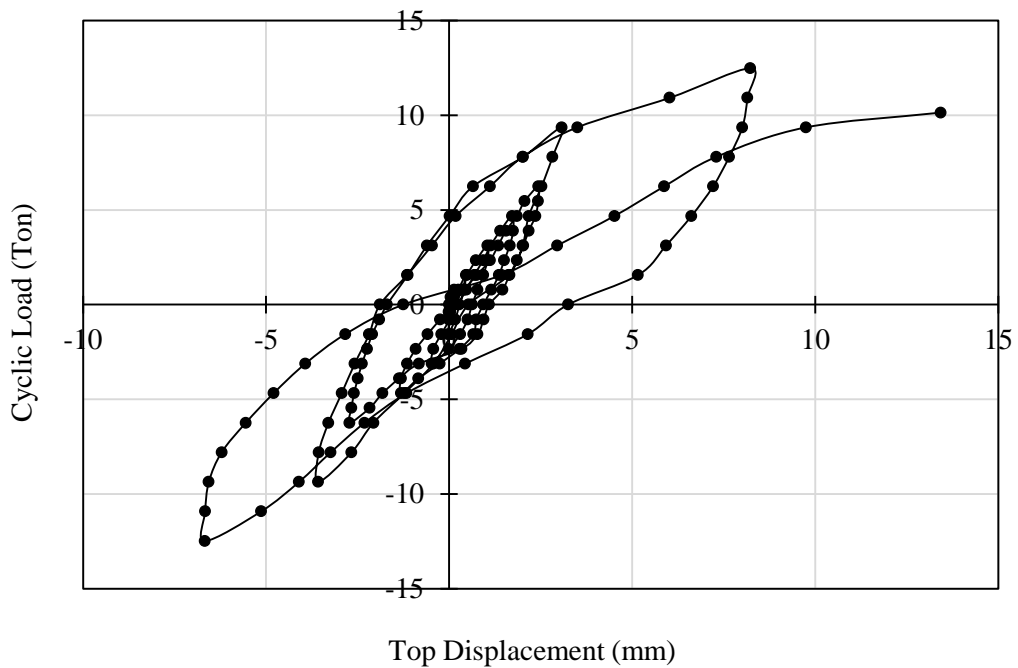


Figure 4.18 Load - deformation curve for SW-DR (Strengthened)

The last sample of short wall assembly was directly strengthened and tested. The curves are plotted in Figure 4.18. The maximum load was 12.48 ton in 7th cycle and

maximum deflection was observed in 8th cycle which was 13.43 mm at 10.14 ton of lateral load.

The data of load and deformation recorded at top of long wall assembly were also plotted to create the same graph as illustrated in Figure 4.19 to 4.21. The control specimen (LW-C) underwent 4 complete cycles and 75% load of the 5th cycle. Maximum lateral load was 5.46 ton and top displacement was 6.72 mm as shown in Figure 4.19. The loops were found to be closely spaced.

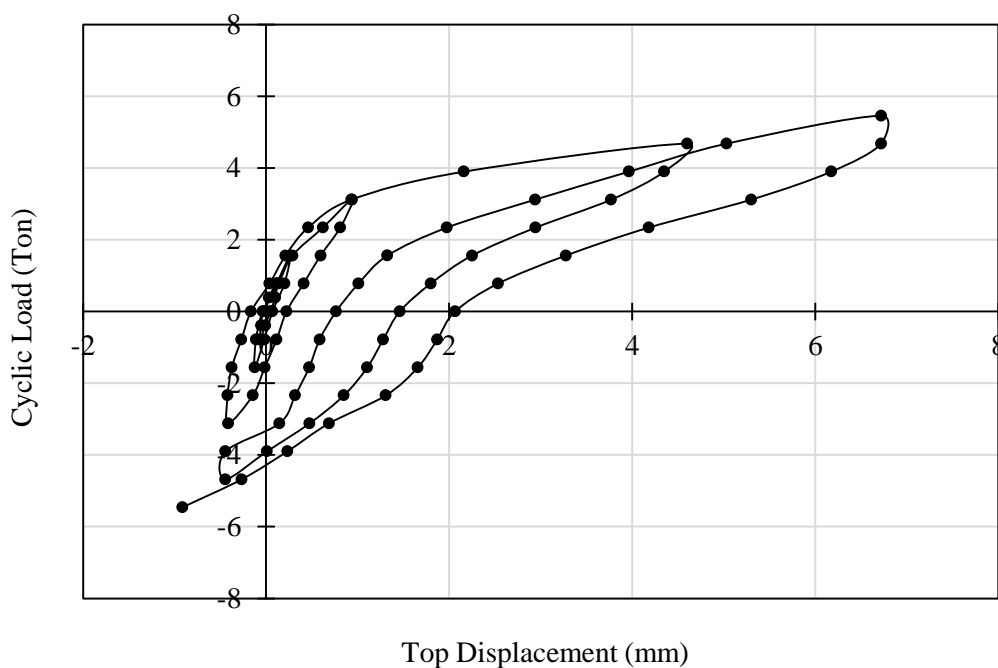


Figure 4.19 Load - deformation curve for LW-C (Control)

Similar to that of SW-CR, the control specimen of long wall assembly was also retrofitted and tested again and this time the total number of full cycles were 7 with maximum load of 12.48 ton. The 8th cycle was continued up to 15.6 ton only, however, the displacement was maximum at this time which was 11 mm. The curve is plotted in Figure 4.20.

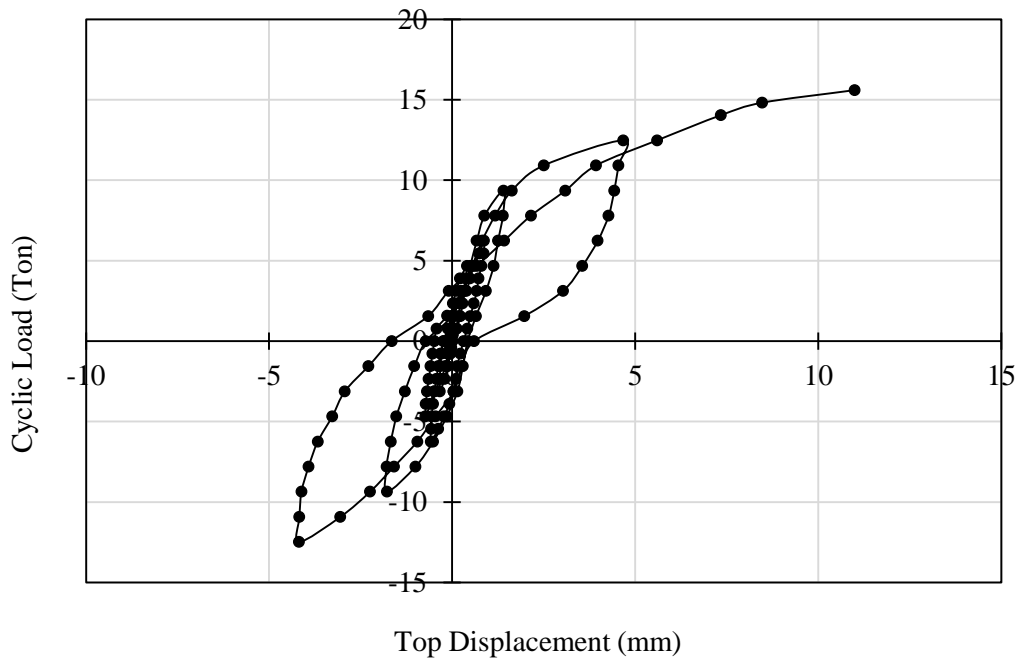


Figure 4.20 Load - deformation curve for LW-CR (Retrofitted)

The last sample of long wall assembly was directly strengthened and tested. The maximum load was 18.72 ton in 8th cycle and maximum deflection of 18.36 mm was observed in this cycle as illustrated in Figure 4.21.

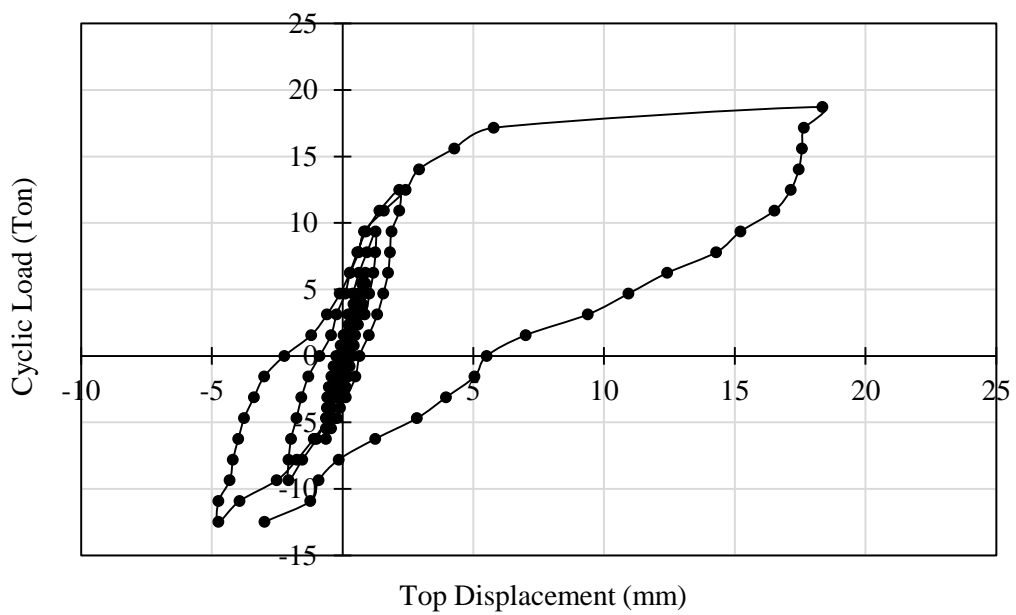


Figure 4.21 Load - deformation curve for LW-DR (Strengthened)

The test data of wall samples were analyzed to find out the ductility of the specimens and to illustrate a clear comparison among them. From the data analysis and the study of hysteresis curves it was found that the ductility of wall samples were highly influenced by the incorporation of RC overlay on one side. The summary of the data of hysteresis curves are given in Table 4.2 and 4.3 for short walls and long walls respectively. The control specimen of short wall has a ductility of 26.15 wherein for retrofitted and strengthened samples it is around 4.3 times and 7.5 times higher respectively. The ductility of the control specimen of long walls is 58.43 which is around 2.2 times higher than the control specimen of short wall. After retrofitting, its ductility was increased by 3.4 times and when the long wall sample was strengthened directly the ductility value was influenced remarkably with a factor of 9 as compared to the control specimen. The envelop curves are given in Figure 4.22 to 4.26.

Table 4.2 Summary of data for hysteresis curves (short wall)

Wall ID	Cycle	Max. Lateral Load (Ton)	Max. Top Deflection (mm)	Ductility	Remarks
SW-C	1	0.78	0.24	26.2	
	2	1.56	0.60		
	3	3.12	4.17		
	4	3.90	6.15		
SW-CR	1	0.78	0.10	113.0	
	2	1.56	0.28		
	3	3.12	0.94		
	4	4.68	2.10		
	5	6.24	3.49		
	6	9.36	5.06		
	7	12.48	9.27		Max. load
	8	11.70	11.30		Max. Def.
SW-DR	1	0.78	0.14	195.3	
	2	1.56	0.46		
	3	3.12	1.05		
	4	4.68	1.72		
	5	6.24	2.72		
	6	9.36	3.58		
	7	12.48	8.23		Max. load
	8	10.14	13.43		Max. Def.

Table 4.3 Summary of data for hysteresis curves (long wall)

Wall ID	Cycle	Max. Lateral Load (Ton)	Max. Top Deflection (mm)	Ductility	Remarks
LW-C	1	0.78	0.12	58.4	
	2	1.56	0.26		
	3	3.12	0.94		
	4	4.68	4.6		
	5	5.46	6.72		
LW-CR	1	0.78	0.06	200.0	
	2	1.56	0.13		
	3	3.12	0.34		
	4	4.68	0.73		
	5	6.24	0.87		
	6	9.36	1.78		
	7	12.48	4.68		
	8	15.60	11.0		
LW-DR	1	0.78	0.04	524.4	
	2	1.56	0.18		
	3	3.12	0.41		
	4	4.68	0.63		
	5	6.24	0.88		
	6	9.36	2.06		
	7	12.48	4.74		
	8	18.72	18.36		

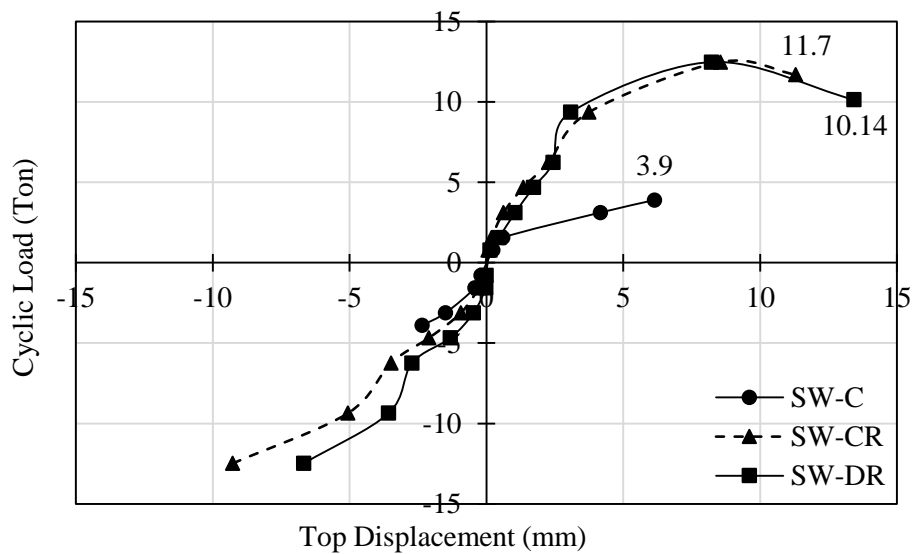


Figure 4.22 Envelop curves for short wall specimens

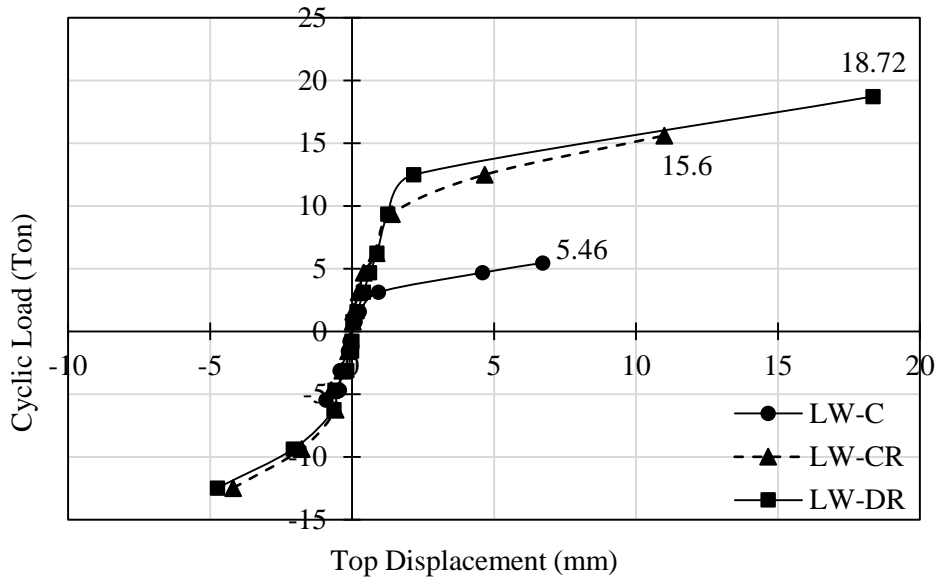


Figure 4.23 Envelop curves for long wall specimens

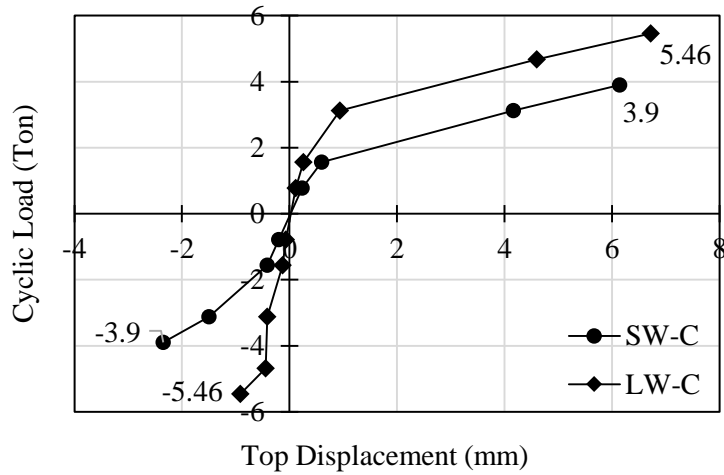


Figure 4.24 Comparison between envelop curves for control specimens

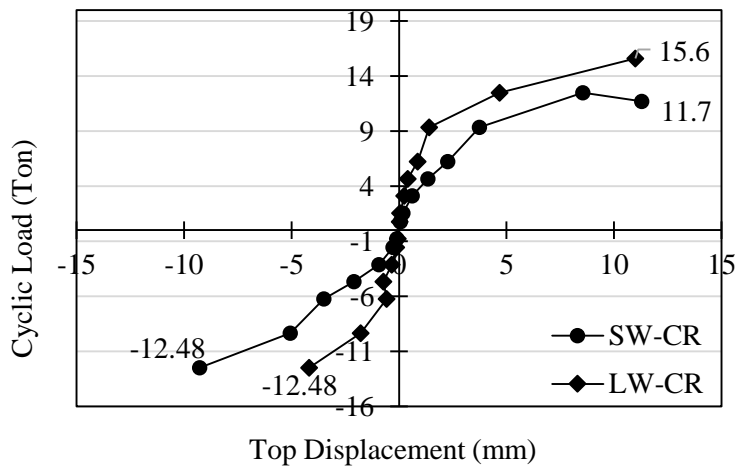


Figure 4.25 Comparison between envelop curves for retrofitted samples

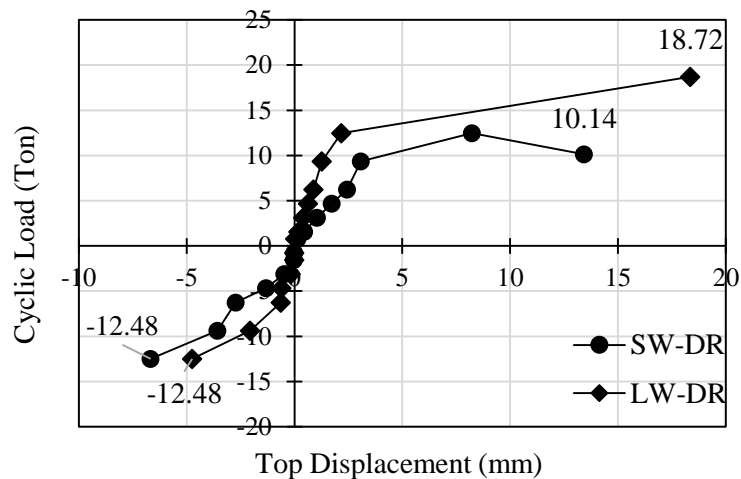


Figure 4.26 Comparison between envelop curves for strengthened samples

The Figures 4.22 to 4.26 above illustrate that the samples with RC overlay of each aspect ratio shows almost same pattern in the response behaviour under cyclic loading. When it comes to the type of sample (e.g., control specimen, retrofitted sample or strengthened sample) from each aspect ratio, results show that samples with $AR = 0.75$ are stiffer compared to that with $AR = 1.0$. Long wall samples experience less deformation. At the same time, they can sustain more lateral forces compared to short walls, as expected from the code provision. The ductility of the long wall samples are also much greater than short wall samples.

4.3.2 Energy Dissipation

The energy with which a structure is hit is dissipated through each cycle to lessen the effect of that energy on the structure. It denotes the strength of the materials of the structure. Energy dissipation (E_d) through hysteresis damping plays an important role in the seismic design. As suggested by Hose and Seible (1999), E_d has been represented by area enclosed within the load-displacement curve at each displacement level. This refers to the total area under the loop shown in Figure 2.27 and 2.28. The elastic strain energy (E_s) stored in an equivalent linear elastic system is represented by the area hatched under the triangular region in the same figure.

The average cumulative energy dissipation at different displacement levels of short wall assemblies are presented in Figure 4.27. The figure showed that the wall-strengthened directly with RC overlay on one side (SW-DR) achieved maximum

improvement in total energy dissipation (about 11.56 times corresponding to the control specimen SW-C and 1.27 times corresponding to the retrofitted specimen after testing i.e., SW-CR). The cumulative energy per cycle was also shown in Figure 4.27 and as expected SW-DR showed maximum cumulative energy dissipation among three specimens tested. For long wall samples, same pattern was followed. The directly strengthened achieved maximum improvement in total energy dissipation. The cumulative energy dissipated for LW-DR was almost 12.33 time corresponds to the control specimen and 4.2 times compared to the retrofitted sample as shown in Figure 4.28. The summary of the data for energy dissipation for each cycle of wall sample are given in Table 4.4.

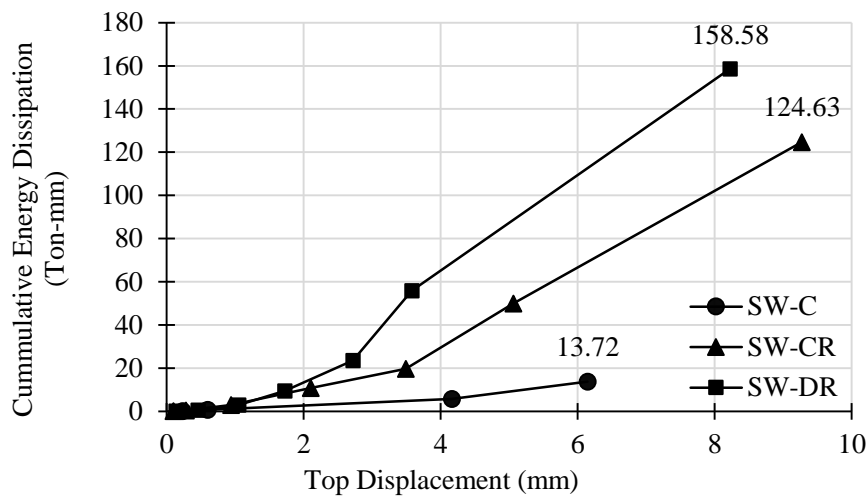


Figure 4.27 Cumulative energy dissipation for short wall assembly

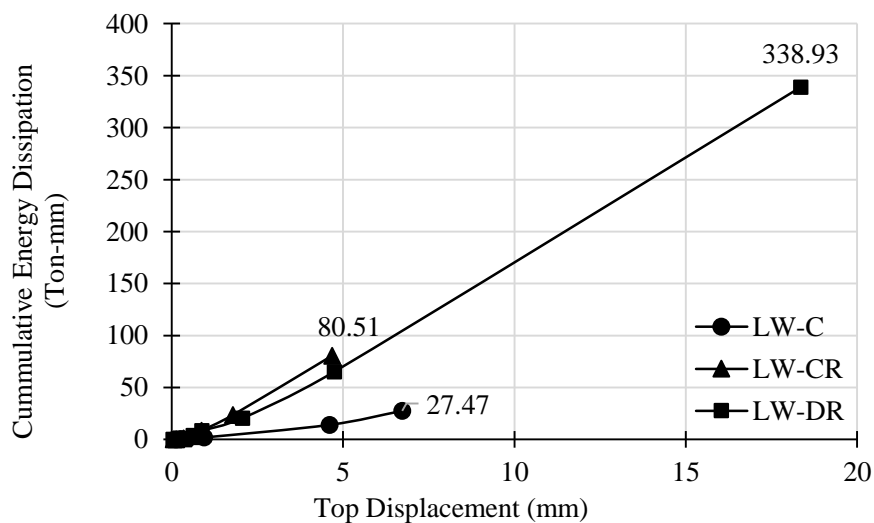


Figure 4.28 Cumulative energy dissipation for long wall assembly

Table 4.4 Cumulative energy dissipation for each cycle

Wall ID	Cycle	E_d (Ton-mm)	Cumulative E_d (Ton-mm)	Remarks
SW-C	1	0.13	0.13	Control specimen
	2	0.58	0.71	
	3	4.96	5.67	
	4	8.05	13.72	
SW-CR	1	0.0546	0.05	9.1 times higher than control specimen
	2	0.367	0.42	
	3	2.4674	2.89	
	4	7.877	10.77	
	5	8.964	19.73	
	6	30.14	49.87	
	7	74.76	124.63	
SW-DR	1	0.07	0.07	11.56 times higher than control specimen
	2	0.42	0.49	
	3	2.4	2.89	
	4	6.482	9.37	
	5	14.14	23.51	
	6	32.34	55.85	
	7	102.73	158.58	
LW-C	1	0.0624	0.06	Control specimen
	2	0.215	0.28	
	3	1.6	1.88	
	4	12.16	14.04	
	5	13.43	27.47	
LW-CR	1	0.0263	0.03	2.93 times higher than control specimen
	2	0.117	0.15	
	3	0.876	1.03	
	4	2.223	3.25	
	5	5.13	8.38	
	6	15.1	23.48	
	7	57.03	80.51	
LW-DR	1	0.0312	0.03	12.34 times higher than control specimen
	2	0.2	0.23	
	3	0.913	1.14	
	4	2.714	3.85	
	5	4.47	8.32	
	6	12.2	20.52	
	7	44.62	65.14	
	8	273.79	338.93	

4.3.3 Hysteresis Percentage Damping

The hysteretic damping plotted against lateral top displacement for short walls are shown in Figure 4.29. For short wall retrofitted after failure (SW-CR), the hysteretic damping ranges from 7.85% to 16.61%. For the long wall control specimen (LW-C), the hysteretic damping ranges from 5% to 13.7%. The values for other samples are illustrated in Figure 4.29 and 4.30 and in Table 4.5.

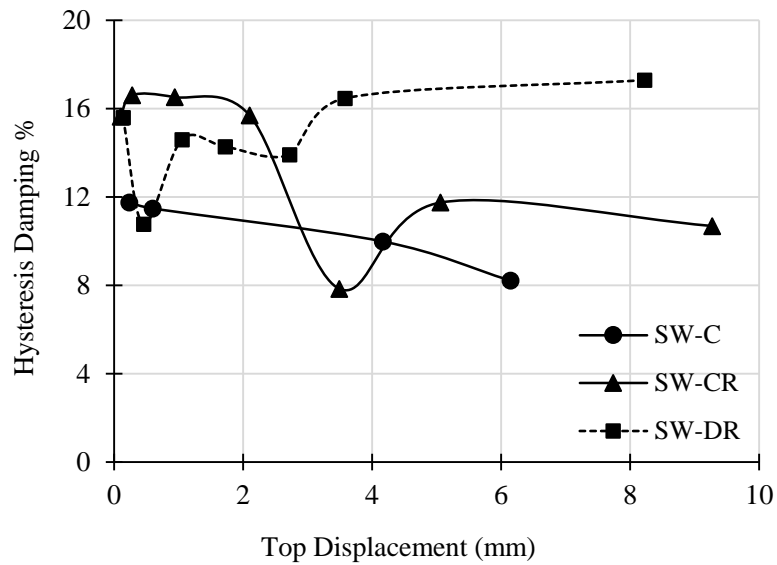


Figure 4.29 Hysteresis damping percentage for short wall assemblies

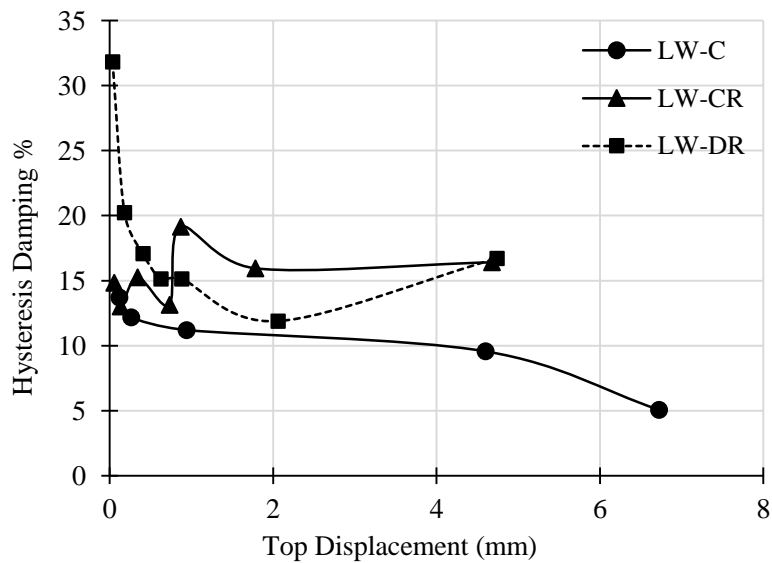


Figure 4.30 Hysteresis damping percentage for long wall assemblies

Table 4.5 Hysteresis damping percentage for walls

Wall ID	Cycle	E _{s1}	E _{s2}	E _{d1}	E _{d2}	Damping %	Remarks
SW-C	1	0.09	0.08	0.07	0.06	11.75	8.22% - 11.75%
	2	0.47	0.32	0.37	0.21	11.48	
	3	6.5	2.33	3.17	1.79	9.99	
	4	11.98	4.58	5.38	2.67	8.22	
SW-CR	1	0.02	0.04	0.02	0.031	15.64	7.85% - 16.61%
	2	0.15	0.21	0.18	0.19	16.61	
	3	0.97	1.46	1.12	1.35	16.52	
	4	3.15	4.91	3.24	4.64	15.7	
	5	7.1	10.88	3.32	5.64	7.85	
	6	17.53	23.68	13.74	16.4	11.75	
	7	53.35	57.81	34.39	40.37	10.69	
	8	66.11	-	-	-	-	
SW-DR	1	0.05	0.01	0.068	0.01	15.6	10.77% - 17.29%
	2	0.36	0.02	0.415	0.004	10.77	
	3	1.64	0.74	1.9	0.5	14.6	
	4	4.03	3.08	4.05	2.43	14.28	
	5	7.61	8.49	6.13	8.01	13.92	
	6	14.39	16.73	14.12	18.22	16.47	
	7	51.32	41.62	64.95	37.78	17.29	
	8	68.06	-	-	-	-	
LW-C	1	0.04	0.03	0.04	0.02	13.7	5.07% - 13.7%
	2	0.2	0.1	0.12	0.091	12.18	
	3	3.03	0.65	0.87	0.728	11.2	
	4	13.1	1.04	11.85	0.309	9.56	
	5	21.08	2.5	13.43	-	5.07	
LW-CR	1	0.01	0.02	0.01	0.02	14.84	13.01% - 19.16%
	2	0.04	0.1	0.03	0.09	13.01	
	3	0.37	0.52	0.30	0.58	15.27	
	4	0.97	1.7	0.78	1.44	13.15	
	5	2.71	1.81	2.32	2.81	19.16	
	6	6.58	8.31	5.91	9.19	15.95	
	7	29.17	26.08	30.79	26.24	16.41	
	8	85.8	-	-	-	-	
LW-DR	1	0.01	0.002	0.03	0.002	31.83	11.89% - 31.83%
	2	0.14	0.01	0.19	0.012	20.24	
	3	0.63	0.28	0.56	0.352	17.09	
	4	1.46	1.4	1.22	1.49	15.14	
	5	2.75	1.98	2.52	1.95	15.13	
	6	5.92	9.64	3.5	8.7	11.89	
	7	13.54	29.58	14.8	29.82	16.72	
	8	171.8	18.56	-	-	-	

4.3.4 Stiffness Degradation

The secant stiffness is defined as the ratio between the lateral resistance and the corresponding top lateral wall displacement. It was used to assess the variation in stiffness of walls with incremental lateral loading and top displacement. The stiffness of the specimen at a certain displacement level of a cycle was considered as the average of stiffness in the positive and negative loading directions (El-Diasity et al., 2015). Figure 4.31 and 4.32 and Table 4.6 show the stiffness degradation with top displacement for short and long walls, respectively.

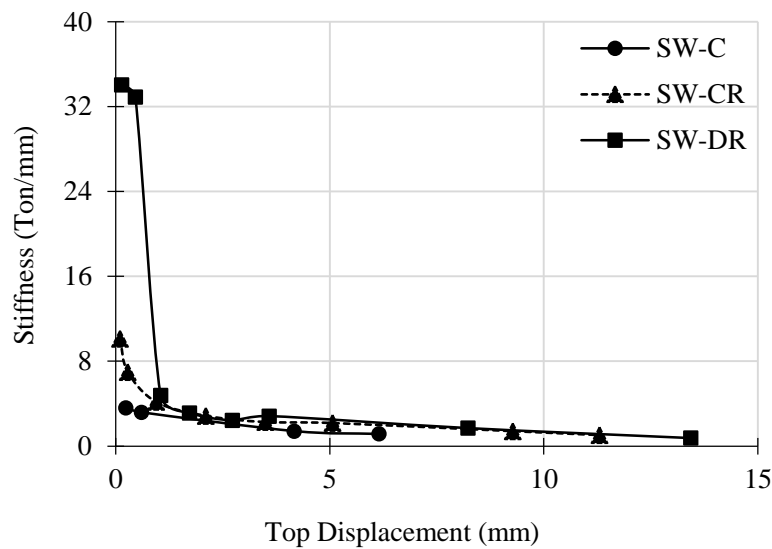


Figure 4.31 Stiffness degradation for short wall assemblies

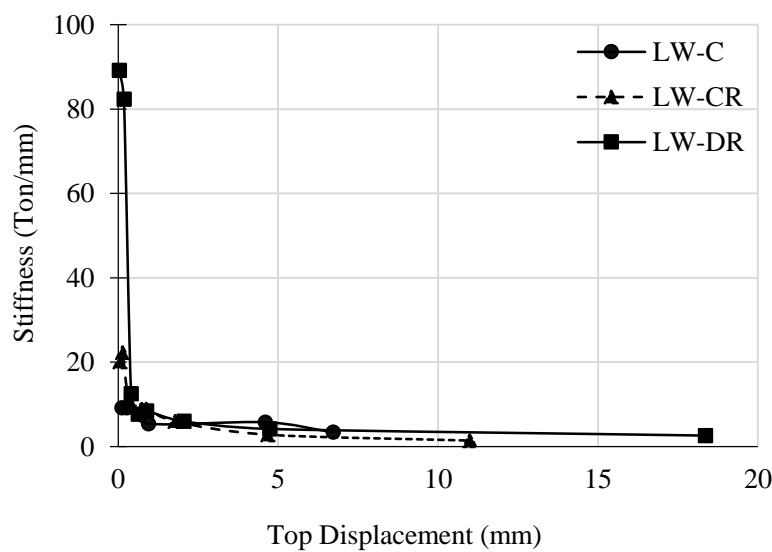


Figure 4.32 Stiffness degradation for long wall assemblies

Table 4.6 Data of stiffness degradation of walls

Wall ID	Cycle	$K_{\text{eff-1}}$ (Ton/mm)	$K_{\text{eff-2}}$ (Ton/mm)	K_{avrg} (Ton/mm)	Remarks
SW-C	1	3.32	3.9	3.61	3.61 to 1.15
	2	2.61	3.76	3.19	
	3	0.75	2.09	1.42	
	4	0.63	1.66	1.15	
SW-CR	1	12.48	7.8	10.14	10.14 to 1.04
	2	8.32	5.67	7	
	3	5.01	3.34	4.18	
	4	3.48	2.23	2.86	
	5	2.74	1.79	2.27	
	6	2.5	1.85	2.18	
	7	1.46	1.35	1.41	
	8	1.04	-	1.04	
SW-DR	1	5.67	62.4	34.04	34.04 to 0.76
	2	3.41	62.4	32.91	
	3	2.97	6.6	4.79	
	4	2.72	3.56	3.14	
	5	2.56	2.29	2.43	
	6	3.04	2.62	2.83	
	7	1.52	1.87	1.7	
	8	0.76	-	0.76	
LW-C	1	6.78	11.56	9.17	9.17 to 3.39
	2	5.94	12.48	9.21	
	3	3.32	7.52	5.42	
	4	1.02	10.52	5.77	
	5	0.81	5.97	3.39	
LW-CR	1	26	14.18	20.09	20.09 to 1.42
	2	32.84	11.77	22.31	
	3	13	9.31	11.16	
	4	11.35	6.46	8.91	
	5	7.17	10.76	8.97	
	6	6.66	5.27	5.97	
	7	2.67	2.99	2.83	
	8	1.42	-	1.42	
LW-DR	1	22.29	156	89.15	89.15 to 2.61
	2	8.67	156	82.34	
	3	7.7	17.33	12.52	
	4	7.49	7.8	7.65	
	5	7.09	9.83	8.46	
	6	7.4	4.54	5.97	
	7	5.75	2.63	4.19	
	8	1.02	4.19	2.61	

4.3.5 Experimental and Theoretical Lateral Load Comparison

Bangladesh National Building Code 2020 (BNBC 2020) suggested allowable lateral load carrying capacity of the URM walls (Appendix). The experimental ultimate loads were compared with these allowable load capacities of URM walls as per BNBC (2020) shown in Figures 4.33 and 4.34.

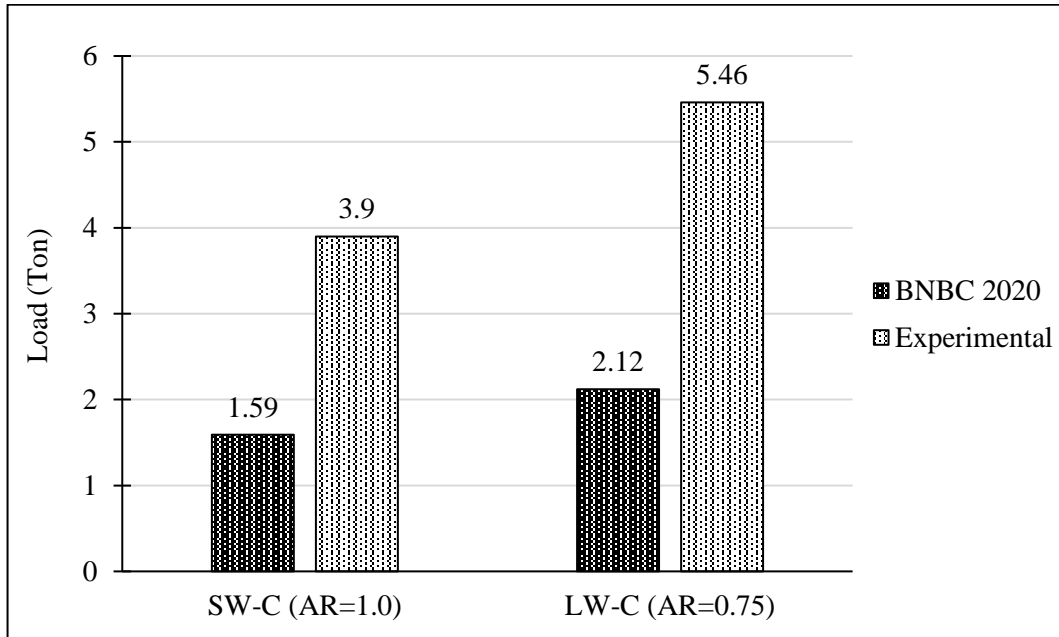


Figure 4.33 Comparison between theoretical and experimental load

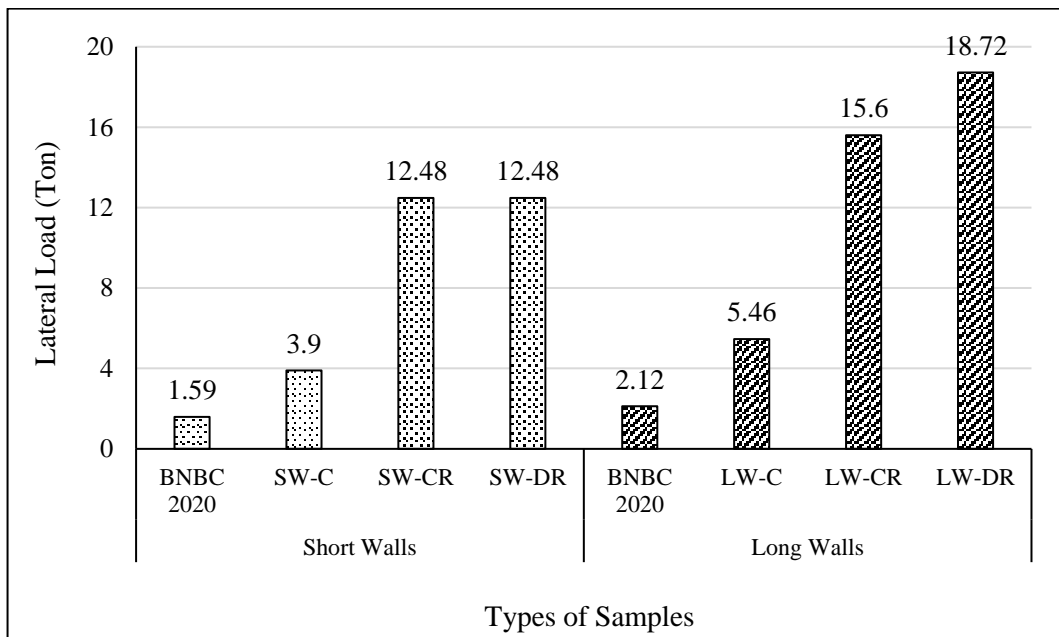


Figure 4.34 Comparison of lateral loads of all samples with BNBC 2020

It can be clearly seen that the experimental ultimate loads are about 2.45 and 2.58 times higher than code suggested values for unretrofitted short and long walls, respectively. Figure 4.33 also depicts the change in behaviour of masonry walls with varying aspect ratio. Additionally, the code suggests that the capacity of the long wall should increase by a factor 1.33 when compared to short wall for the two aspect ratios wherein, experimental lateral resistance of unreinforced walls increased approximately 1.40 times as the aspect ratio changed from 1 to 0.75.

4.3.6 In-plane Deformation Profile of the Wall Samples

The displacement data were collected at top of the wall and at the mid-point of the far end as well. With the help of these data the approximate deflected profile of the wall could be predicted for every maximum top displacement. Figures 4.35 to 4.40 illustrate the deflected profile of walls.

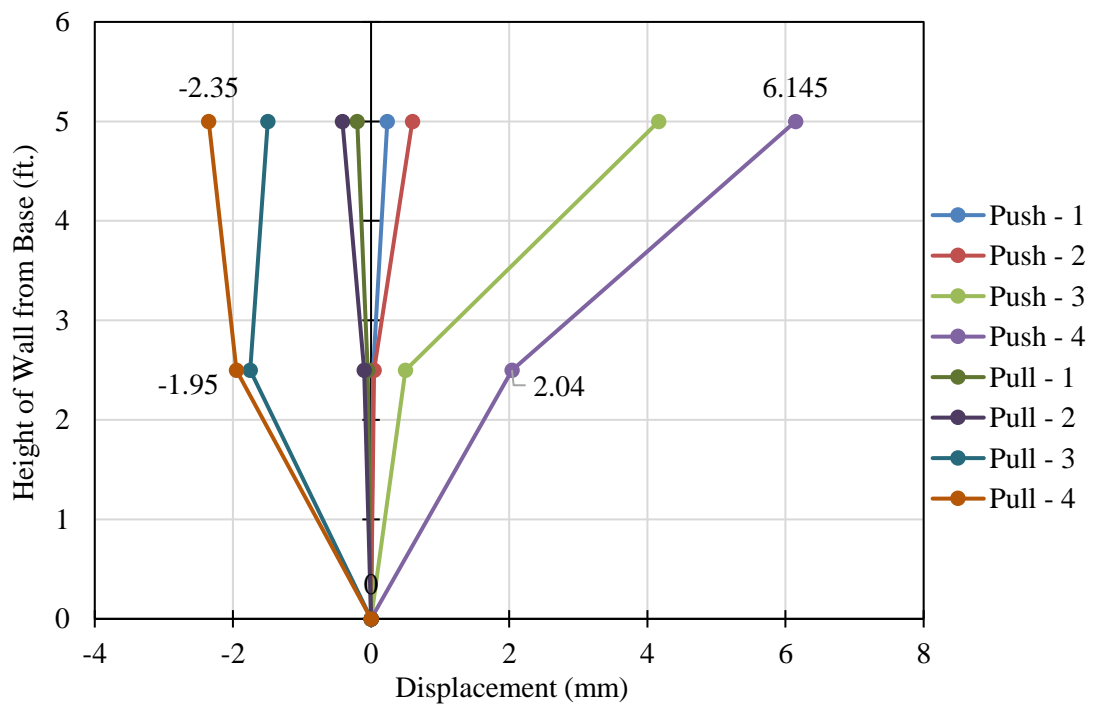


Figure 4.35 Approximate deflected shape of SW-C sample

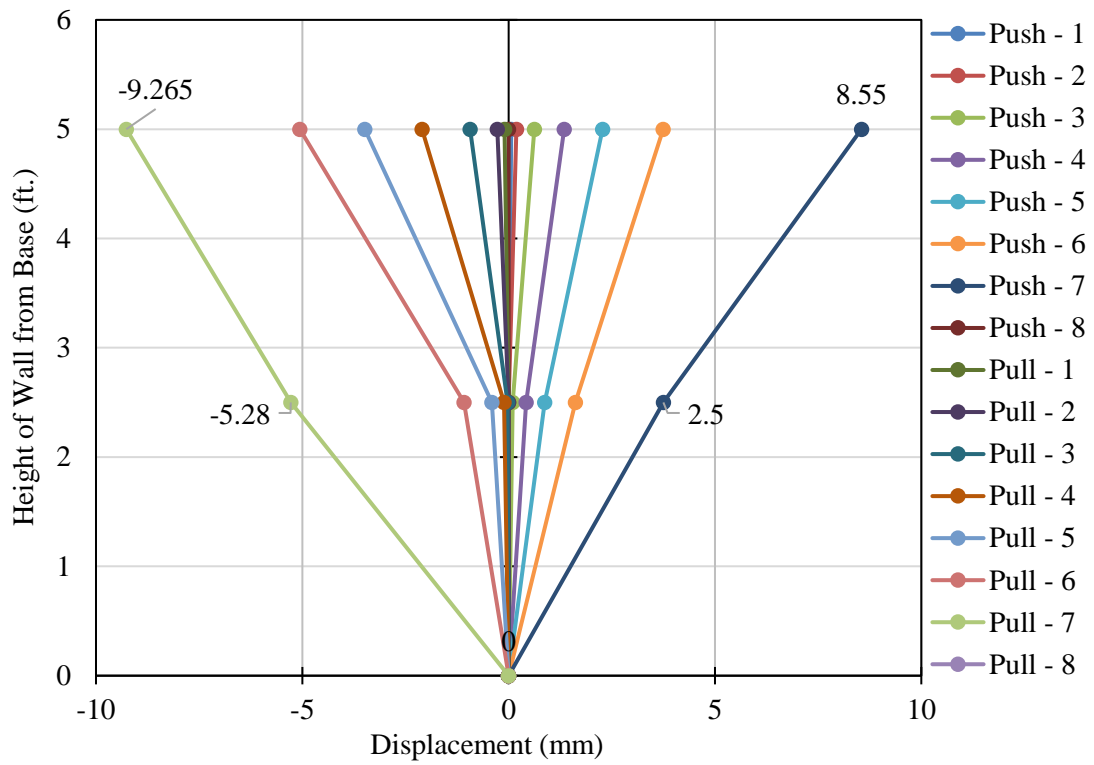


Figure 4.36 Approximate deflected shape of SW-CR sample

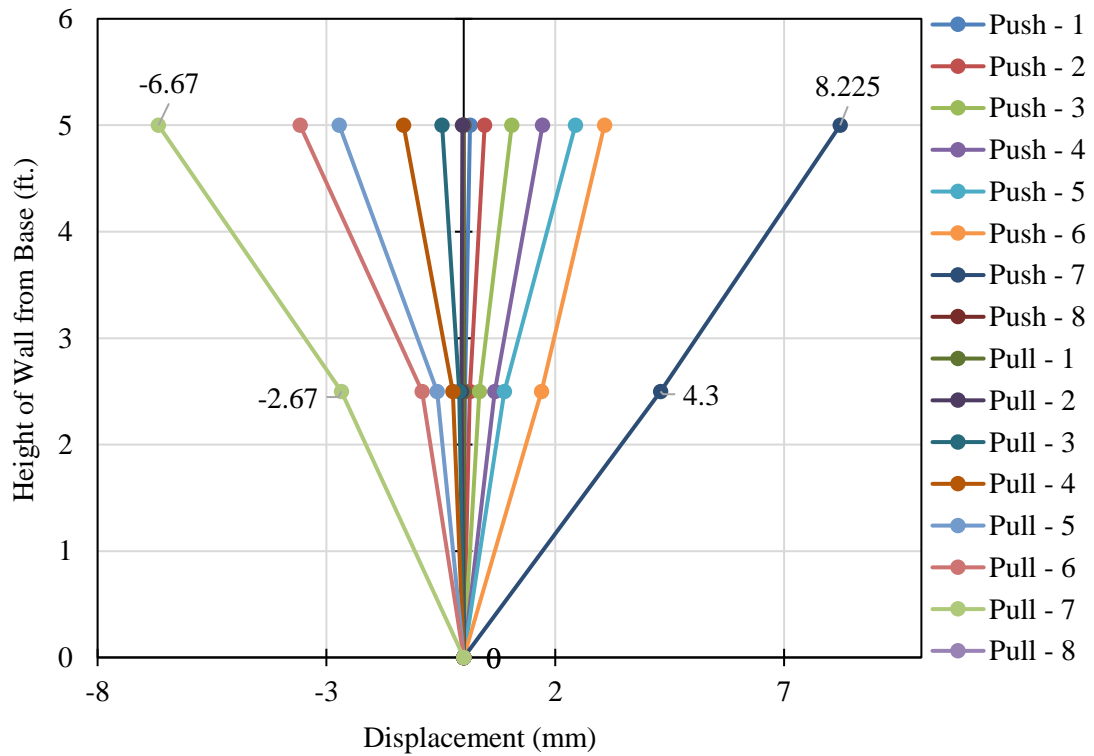


Figure 4.37 Approximate deflected shape of SW-DR sample

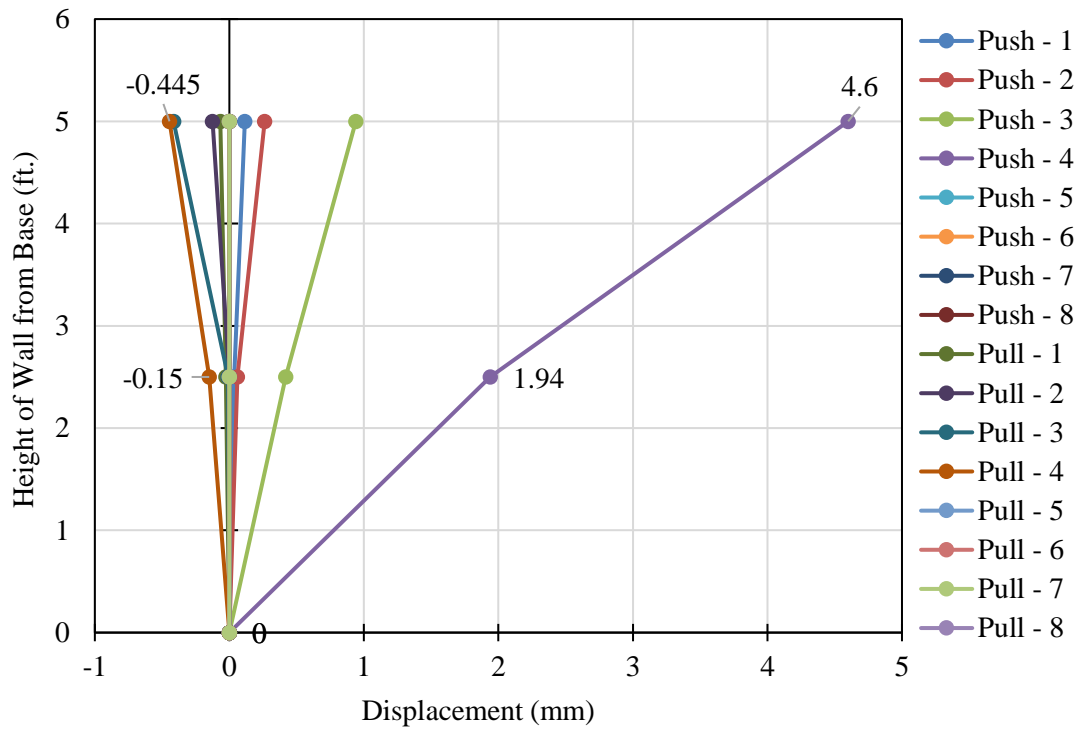


Figure 4.38 Approximate deflected shape of LW-C sample

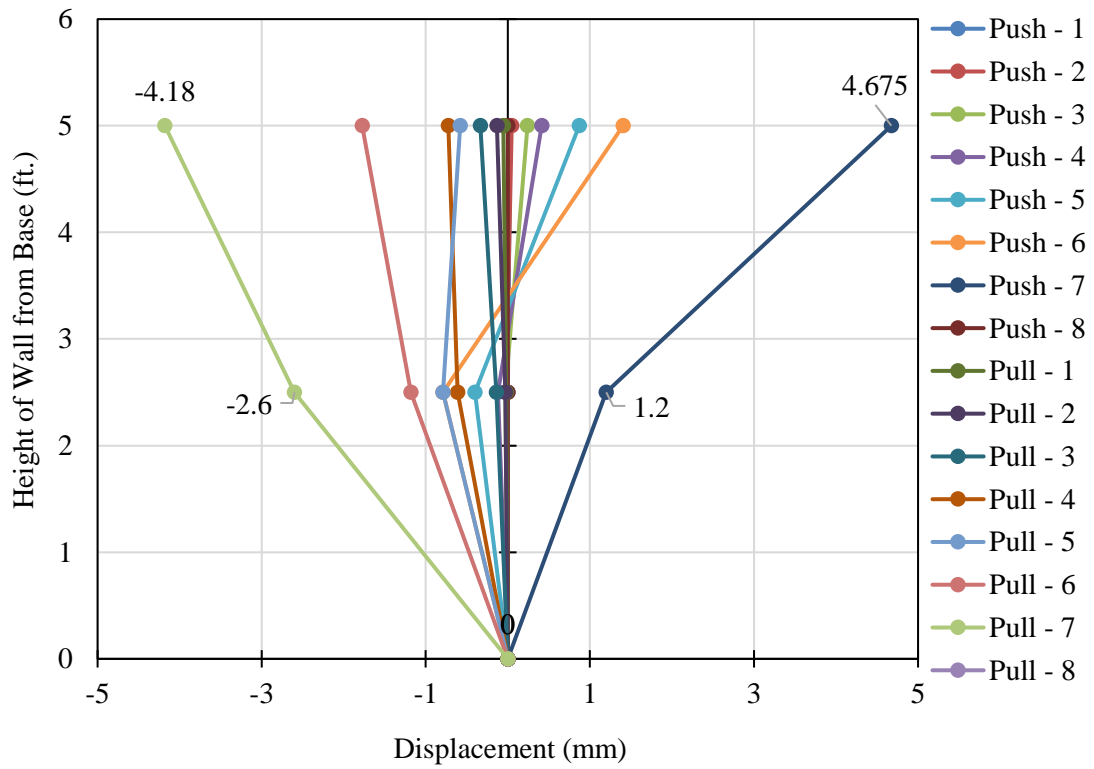


Figure 4.39 Approximate deflected shape of LW-CR sample

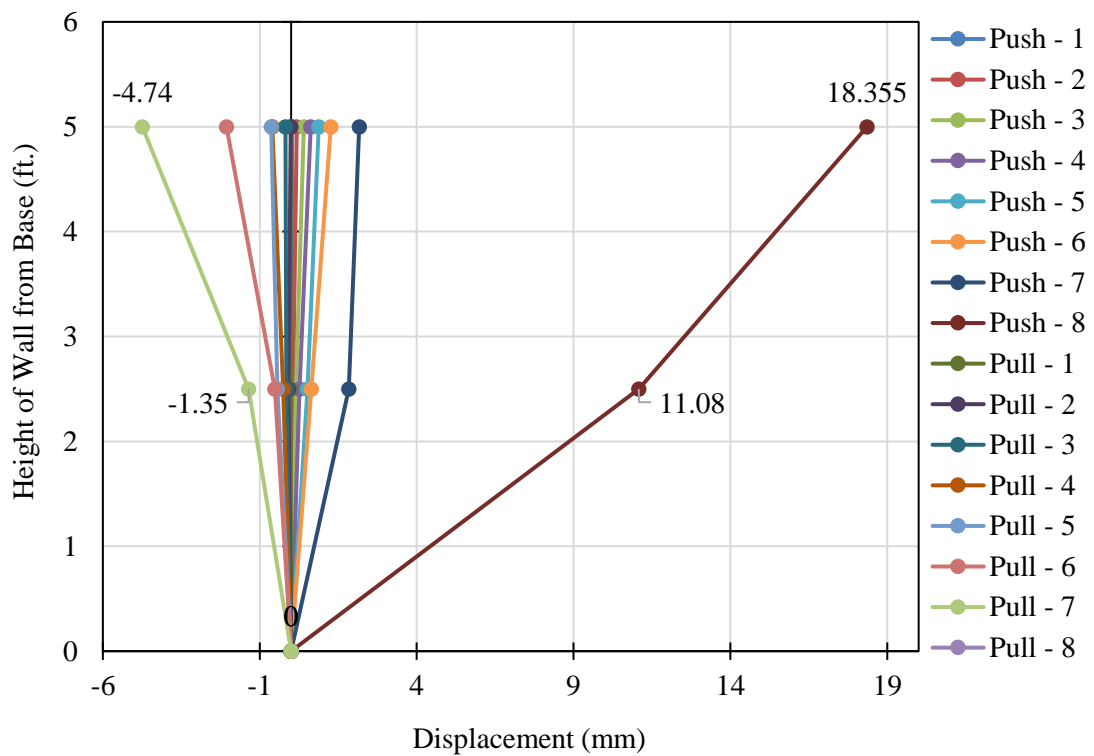


Figure 4.40 Approximate deflected shape of LW-DR sample

4.4 Comparison of Obtained Result to Literature

The exclusive study of literatures gave an insight of possible failure mechanism and response of URM walls before and after retrofitting. Considering the geometries and vertical stress level (0.21 N/mm^2) of the samples tested in this research work and comparing them to those available in literature, following observations can be made:

The control specimens of this experimental programs failed mainly in rocking mode where the rocking action started in a layer of mortar located a few layers above the base. The cracks formed in this state propagated to the far end corner creating a chance of toe crushing. This happened for both short wall and long wall assembly (Figures 4.1 and 4.5). Again, some other experimental programs suggest the same, however, in some of the cases the formation of diagonal shear cracks were found to be the failure mode of URM wall samples. For the retrofitted samples with RC overlay on one side, the failure mode was basically rocking and flexural compression. The separation and lifting of wall sample from the base happened thus the sample started to rotate back and forth in each cycle. The sign of delamination of

RC overlay from URM wall was also observed in some regions as illustrated in the previous sections of this chapters (Figure 4.4). The short wall sample retrofitted after failure also showed sign of multiple crack formation with the separation of RC layer and lifting of wall sample. The formation of hair-line crack on RC face just opposite to the cracks on wall side was also dominant (Figure 4.2 (c)). EIGawady et al. (2007) observed rocking type of failure for URM samples as shown in Figure 4.41.

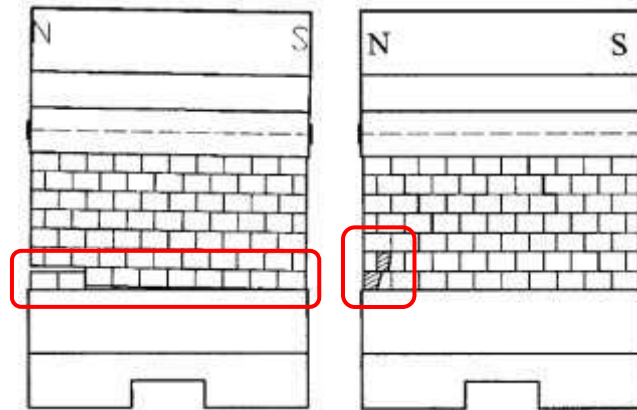


Figure 4.41 Rocking type of failure of URM walls (EIGawady et al., 2007)

Sergey and Elena (2011) conducted the same type of tests on walls with AR 0.73 (2500 x 1820 mm) and 1.21 (1500 x 1820 mm) as shown in Figure 4.42. For the first one, in control specimen, the failure was predominantly in head and bed joint and block failure at direct tension (as observed in LW-C). The retrofitting scheme followed by them was the application of RC jacket on both sides of the wall. For the retrofitted samples, the failure mode was as same as those observed in our test i.e., separation of wall from base with toe crushing and separation of RC from wall face.

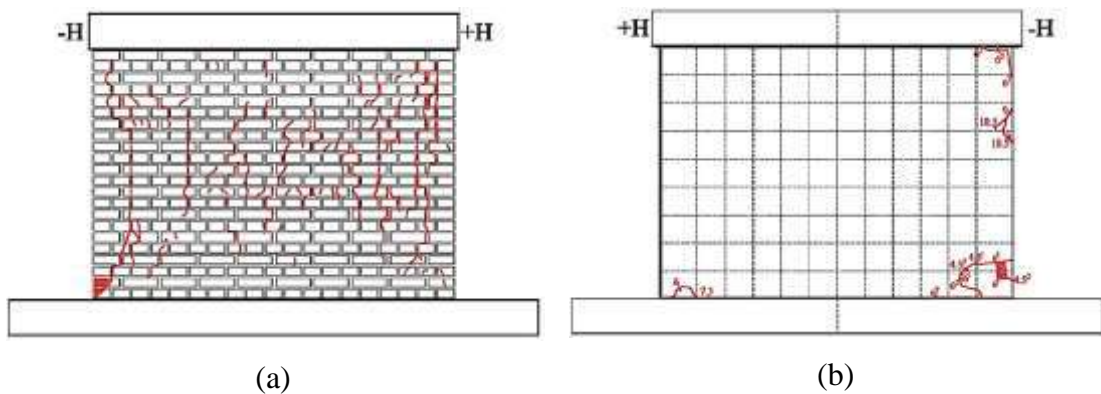


Figure 4.42 Failure of wall, (a) Control, (b) Retrofitted (Sergey and Elena, 2011)

Feng et al. (2017) tested wall samples with 3 different ARs namely 0.65 (2000 x 1300 mm), 0.75 (1750 x 1300 mm) and 0.87 (1650 x 1300 mm) which are quite close to those used in our tests. The failure mode for this URM samples as given in Figure 4.43 were flexural cracking, rocking/ toe crushing/ sliding and rocking/ sliding respectively which are relatable to the failure modes stated in this research.



Figure 4.43 Failure mode of URM walls (Feng et al., 2017)

Some other researchers (Messali et al., 2017, Mustafa et al., 2018, Mahmud et al., 2019) conducted similar type of experiments with slight difference in geometries, vertical stresses and different type of retrofitting techniques. Their experimental findings also suggest more or less same type of failure modes for control specimens.

Mohamed et al. (2007) conducted a static cyclic loading test on a set seven half-scale masonry walls and they applied FRP as retrofitting scheme. All the specimens were tested under constant gravity load and incrementally increasing in-plane loading cycles. The tested specimens had two effective moment/shear ratio, namely, 0.5 and 0.7. Figure 2.29 shows the failure pattern of the wall samples tested.

Hasnat et al. (2022) conducted a test on a full scale masonry wall of 125 mm thickness. The sample was subjected to constant gravity load during the testing under quasi-static loading. Then the tested sample was retrofitted using a single layer of ferrocement and tested in the same manner again. Another sample was directly strengthened using the same mechanism and tested in the similar way. Ferrocement laminated wall panels showed about 33% increase in lateral load capacity and directly strengthened wall samples showed about 78% increase in lateral load capacity, compared to the control. The strengthening also improved the total energy

dissipation by a factor ranging from 35.5% to 81% for the walls. The loading set up is illustrated in Figure 2.33. The walls ultimately exhibited rocking mode of failure at the wall-base slab interface and to some extent flexural compression i.e. corner crushing mode. The failure modes of wall are given in Figure 4.44.



Figure 4.44 Failure modes of wall samples (Hasnat et al., 2022)

Jamshid et al. (2018) conducted an experimental work on URM. Polypropylene (PP) band was used to evaluate their performance as a retrofitting technique. The displacement-controlled lateral deformation was investigated experimentally. The monotonic load-displacement behaviours of a URM wall and the wall retrofitted with PP band were compared. At the same time, the performance of a PP band-retrofitted building during a real earthquake was also observed. From the test it was found that the energy absorption capacity was increased by two times. The ductility capacity increased by three times. The load carrying capacity was increased by 22%. Figure 2.36 shows the after test condition of the wall samples.

Sergey and Elena (2011) tested eight walls in laboratory assembled in two series. The first series contains four unreinforced masonry walls build from solid clay bricks and lime mortar. The walls from second series are strengthened and have the same material, geometry properties and vertical load levels as the first one. The vertical stress level was 1 MPa and the lateral loading capacity was recorded to be 10.7 Ton whereas in strengthened sample the lateral load was 25.1 Ton. The application of retrofitting scheme and loading set up are shown in Figures 2.37 and 2.38.

In order to study the seismic resistance of URM walls, in-plane tests were carried out by Mustafa et al. (2018). The samples were categorized in two groups - four full-scale (233x241x25cm) and nine reduced-size specimens (100x100x25cm) made of solid clay brick and lime-cement mortar were subjected to cyclic shear and monotonic pushover loading program under constant vertical pressure. One-sided or two-sided reinforced concrete or mortar jacketing was applied to improve lateral resistance and displacement capacity. The positions of the reinforcing mesh were changed - one way of strengthening was with the orthogonal position of reinforcement mesh Q196 and “new” type of connectors made of shaped Ø5 reinforcing bars. The connectors were placed vertically (9 pieces/m²) and horizontally (4 pieces/m²) in joints and grouted with high strength quick-hardening mortar. Figure 2.41 and 2.42 show the crack patterns and crack width of URM walls and the failure mode of strengthened samples.

In the second type of strengthening, the mesh Q196 was inclined to 45° (135°) in order to follow the principal stress trajectories. Plain walls fail in shear with a typical cross-diagonal crack pattern. Jacketed walls exhibit rocking and significantly larger ductility compared to plain walls. Wallets were tested for compressive strength and elastic modulus of masonry and the results show significant variations.

The research work of Mahmoud et al. (2019) presented the results of numerical studies of full-scale unreinforced concrete block masonry walls, externally retrofitted by reinforced concrete layers focusing on the in-plane shear capacity of. At first, small-scale masonry walls were tested and their results were used to develop and calibrate numerical micro models for full-scale walls. Nonlinear pushover analyses are conducted to investigate the effects of a number of problem variables on the performance of the retrofitted walls. Numerical results reveal that wall boundary conditions affect its response considerably. Also, a significant enhancement in wall capacity and ductility is observed due to the application of the reinforced concrete layers. The set up for monotonic loading on wall samples is illustrated in Figure 2.43.

Yaghoubifar (2008) applied RC layer on one and both sides of walls as strengthening technique to study their performance under static-cyclic tests. There two URM walls,

NSBW1 and NSBW2, with different failure modes as the basic specimens as shown in Figure 4.45. The governing failure mode of unreinforced walls was rocking in NSBW1 and bed-joint sliding in NSBW2. The SSBW1 and SSBW2 were strengthened on one side and DSBW1 and DSBW2 were strengthened on both sides of the wall. The capacity and failure mode of the strengthened walls predicted with the proposed evaluation procedure are compared with the test results in Table 4.7.

Table 4.7 Predicted and experimental capacity of walls (Yaghoubifar, 2008)

Wall	Strength (kN)		Failure Mode	
	Predicted	Experimental	Predicted	Experimental
SSBW2	139	135	Diagonal tension	Diagonal tension
DSBW2	259	270	Flexural	Flexural
SSBW1	43	42	Flexural	Flexural
DSBW1	48	50	Flexural	Flexural

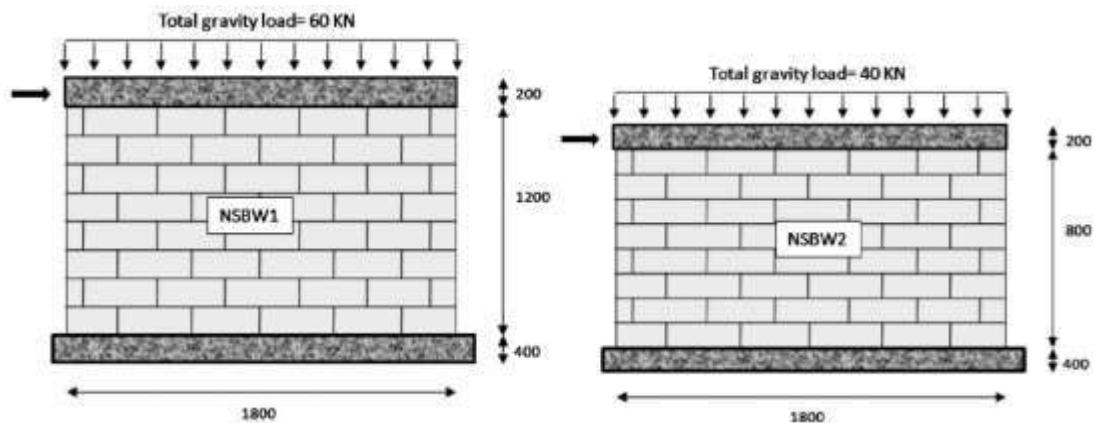


Figure 4.45 Basic URM wall specimens (Yaghoubifar, 2008)

The comparison of some of the experimental results with the tests data obtained in this research work are presented in Figures 4.46 and 4.47. The values in the parenthesis of the title in horizontal axis show the dimensions of the wall samples

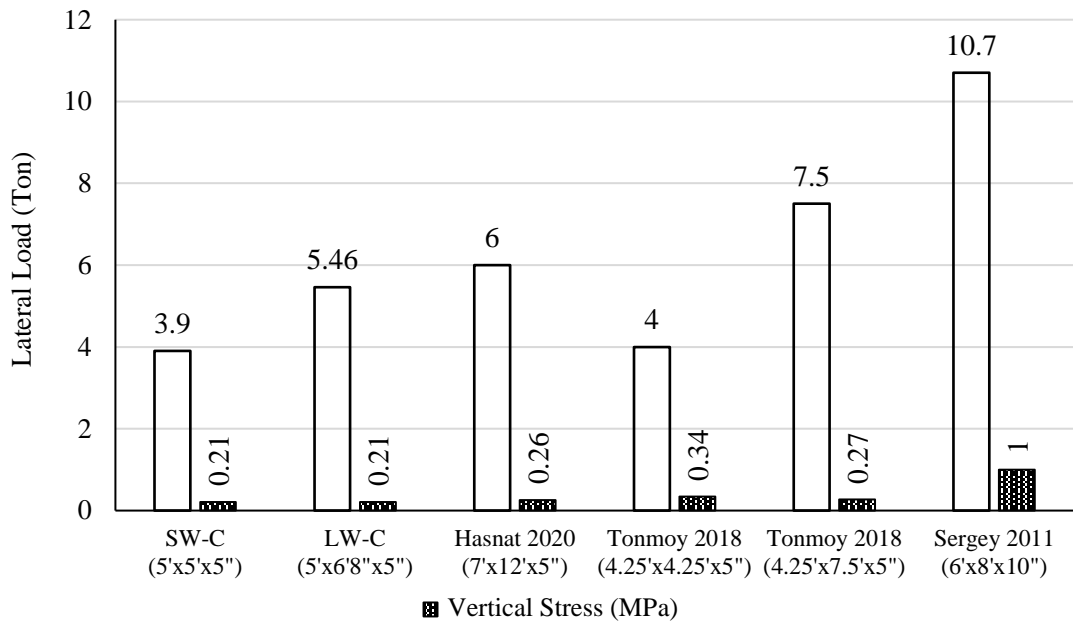


Figure 4.46 Comparison of lateral loads of control specimen

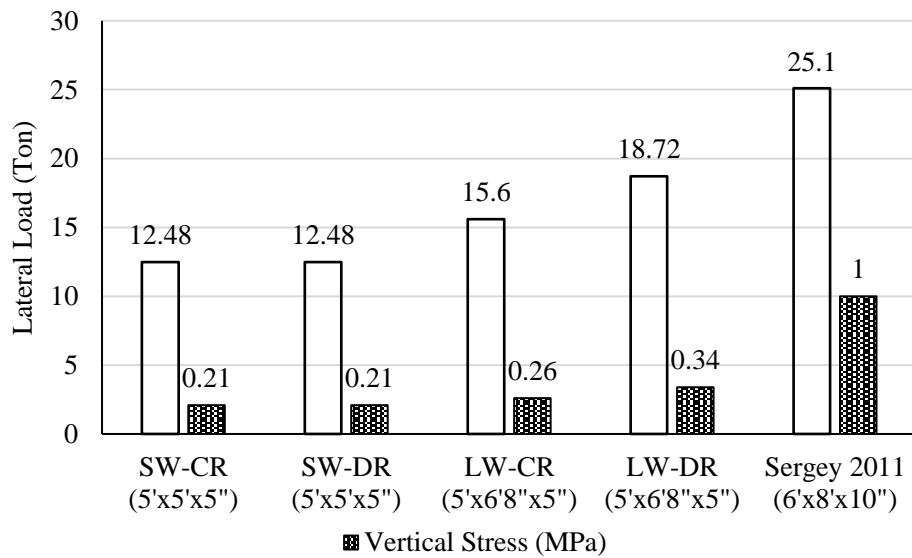


Figure 4.47 Comparison of retrofitted samples to walls jacketed on both sides

Chapter 5

CONCLUSIONS AND RECOMMENDATIONS

5.1 Summary and Conclusion

The experiment conducted in this research work focused on studying the behaviour of URM walls under cyclic loading with simultaneously acting gravity load on it. In this study, the URM walls were retrofitted and strengthened using RC overlay on one face only. The effect of aspect ratio (height to length) is studied using wall samples of two different aspect ratios namely 1.0 and 0.75. Total 6 cyclic tests were conducted on 4 (four) wall samples. The control specimens were tested and then retrofitted followed by the same testing repeated. Half scale burnt clay bricks were used as masonry units for the construction of those half-scale walls. Conventional mortar with typical 1:4 cement-sand ratio was used. The RC jacket contained 6 mm dia. bars @75 mm (3 in.) c/c in both directions and the concrete was prepared with 1:1.2:1.7 ratio of cement, sand and 5mm downgrade aggregates with a specified amount of a water-reducing admixture (Master Glenium). The test set up and testing procedure including the detailed data analysis of the structures are reported in the previous chapters. On the basis of the experimental investigation, following concluding remarks can be drawn:

- i) The control samples of short walls failed due to the generation of horizontal cracks a few layers above the base which ended up propagating towards the toe. Same type of failure was observed for long wall control specimen as well. However, the retrofitted samples showed a variety of failure modes. Short walls failed by a combined action of rocking and flexural compression i.e., corner crushing. Some diagonal cracks were also formed for retrofitted sample with aspect ratio 1.0. Again, the strengthened samples of long walls also showed the same type of failure modes. Thus, the RC overlay changed the failure mode remarkably.
- ii) For short walls, the ultimate load carrying capacity was increased by approximately 3.2 times in both the retrofitted (SW-CR) and strengthened samples (SW-DR). The strengthened sample (SW-DR) undergoes a large amount of deformation (1.2 times of SW-CR and 2.2 times of control

specimen). For long walls, strengthening increased the capacity by almost 3.43 times and for retrofitting it was 2.86 times whereas the displacement was increased by 2.73 times and 1.64 times respectively.

- iii) The energy dissipation capacity for short wall was increased by almost 9.1 times and 11.56 times for retrofitted and directly strengthened samples respectively. For long walls, these values are 2.93 and 12.34 times for LW-CR and LW-DR respectively.
- iv) The reinforcement with concrete jacketing improved the ductility by 4.3 times, 7.45 times for short wall retrofitted after failure and directly strengthened respectively. For long walls, the increase in ductility was 3.4 times and 8.9 times respectively for retrofitted and directly strengthened samples.
- v) Hysteretic damping for short wall assemblies ranges from 7.85% to 16.61% which belongs to the retrofitted sample SW-CR. For the control specimen of long wall (LW-C), the hysteretic damping ranges approximately from 5% to 13.7%.
- vi) The long walls showed an improved response as compared to the short wall samples.
- vii) The experimental lateral load carrying capacity for short and long walls are almost 2.45 and 2.58 times corresponding to the BNBC code provision.

5.2 Future Recommendations

The following recommendation are made for further investigations in this research:

- i) The test was conducted on half-scale masonry walls using half-scale masonry units. Therefore, a full-scale wall test is suggested for the same.
- ii) The number of parameters to be investigated could be modified and/or increased (such as bond type in wall, detailing and type of RC, variation in vertical stress, out-of-plane response of wall, etc.) and the number of wall samples can be increased to have a better comparison.
- iii) The variation in aspect ratio such as a high and slender wall with aspect ratio greater than 1.0 or a very long wall with aspect ratio of 0.5 can be a point of interest as well.

- iv) To assess more practical application of strengthening and obtaining more accurate behaviour, walls with opening could be investigated for the same.
- v) Further studies could be carried out with finite element modelling that simulates the behaviour of in-plane strengthened masonry walls. This can give a better insight to the practical use of the retrofitting scheme.
- vi) The performance of RC overlay is recommended to compare with some other strengthening and retrofitting technique keeping all other parameters unchanged.
- vii) The test was conducted on masonry walls itself and the point of interest was in-plane cyclic loading test only. A shake-table test on a half-scale or full-scale masonry room is also suggested using the same retrofitting scheme to know the effect of RC overlay on the actual dynamic behaviour of the masonry structure.

REFERENCES

Akhter, S. H. (2010) “Earthquakes of Dhaka. Environment of Capital Dhaka—Plants Wildlife Gardens Parks Air Water and Earthquake”. Asiatic Society of Bangladesh, pp. 401-426

Alam, M.S., and Amanat, K.M. (2004) “FE Modeling Scheme to Simulate the Retrofitting Effect of Masonry Infill with Ferrocement Overlay,” Proceedings of the 2nd International Conference on Protection of Structures against Hazards, Singapore, pp. 297-301.

Al-Zaman ,M. D., and Monira, N. J. (2017) “A Study of Earthquakes in Bangladesh and The Data Analysis of The Earthquakes That Were Generated in Bangladesh and Its’ Very Close Regions for The Last Forty Years (1976-2016)”, Journal of Geology & Geophysics, Vol. 6, No. 4, pp. 300, DOI: 10.4172/2381-8719.1000300.

Amanat, K.M., Alam, M.M.M. and Alam, M.S. (2007). “Experimental Investigation of the Use of Ferrocement Laminates for Repairing Masonry In-filled RC Frames,” Journal of Civil Engineering (IEB), Issue 2, Vol. 35, pp. 71-80.

Ansary, M. A., and Arefin, M. R. (2020) “Assessment of Predominant Frequencies in Dhaka City, Bangladesh Using Ambient Vibration”, Springer, Asian Journal of Civil Engineering, Vol. 21, pp. 91-104.

Ansary, M.A. (2003) “HOUSING REPORT: Single-storey brick masonry house (EMSb1)” World Housing Encyclopedia, Report No. 91.

Bhattacharya, S., Nayak, S. and Dutta, S. C. (2014) “A critical review of retrofitting methods for unreinforced masonry structures,” International Journal on Disaster Risk Reduction, 7, 51-67.

Biswas, R. N., Islam, M. N., and Islam, M. N. (2018) “Modeling on Management Strategies for Spatial Assessment of Earthquake Disaster Vulnerability In Bangladesh”, Springer, Modeling Earth Systems and Environment, Vol. 4, pp. 1377–1401,

CDMP (2009) “Earthquake Vulnerability Assessment of Dhaka, Chittagong and Sylhet City Corporation Area,” Comprehensive Disaster Management Programme (CDMP), Ministry of Disaster Management and Relief, Dhaka.

ElGawady, M.A., Lestuzzi, P. and Badoux, M. (2006) “Retrofitting of Masonry Walls Using Shotcrete,” Proceedings of NZSEE Conference available at www.nzsee.org.nz/db/2006/Paper45.pdf.

ElGawady, M.A., Lestuzzi, P. and Badoux, M. (2007) “Static Cyclic Response of Masonry Walls Retrofitted with Fiber-Reinforced Polymers,” *Journal of Composites for Construction*, Vol. 11, pp. 50-61.

FEMA P-774 (2009) “Unreinforced Masonry Buildings and Earthquakes”, Applied Technology Council (ATC), California, October 2009.

Feng, W., Wang, H. T., Li, G., Jia, J. Q. and Li, H. N. (2017) “Seismic performance of traditional abode masonry walls subjected to in-plane cyclic loading,” *Materials and Structures*, 50:69.

Gattesco, N. and Boem, I. (2017) “Out-of-plane behaviour of reinforced masonry walls: Experimental and numerical study,” *Composites part B* 128, 39-52.

Gencil, O. (2015) “Characteristics of fired clay bricks with pumice additive”. *Energy Build.* 2015, 102, 217–224.

Ghiassi, B., Soltani, M. and Tasnimi, A. A. (2012) “Seismic evaluation of masonry structures strengthened with reinforced concrete layer,” *J. Struct. Eng.*, 138(6), 729-743.

Hasnat, A., Ahsan, R. and Yashin, S. M. (2022) “Quasi-static in-plane behaviour of full-scale unreinforced masonry walls retrofitted using ferro-cement overlay”, *Asian Journal of Civil Engineering*, <https://doi.org/10.1007/s42107-022-00447-7>.

Hendry, A.W., Sinha, B.P., and Davies, S.R. (1997) “Design of masonry structures,” E and FN Spon, London.

Hindustan Times (2015), <https://www.hindustantimes.com/india/five-major-earthquakes-to-have-struck-india/story-0TIxSQULO1tYXGTEcOlqQL.html>. (Date of access: 25/06/2022).

Hose Y. and Seible F. (1999) “Performance Evaluation Database for Concrete Bridge Components, and Systems under Simulated Seismic loads,” PEER Report 1999/11, Pacific Earthquake Engineering Research Center College of Engineering, University of California, Berkley, U.S.A.

Islam, M. A. and Ahsan, R. (2019) “Performance of unreinforced masonry wall in shaking table test”, International Conference on Disaster Risk Management, Dhaka, Bangladesh, January 12-14.

Jamshid, Z.H., Hossein, G., Sanket, N., Sreekanta, D. (2019) “Experimental and Field Performance of PP Band–Retrofitted Masonry: Evaluation of Seismic Behaviour” Journal of Performance of Constructed Facilities, Volume 33 Issue 1.

Khair, M.A. (2005) “Finite Element Analysis of Unreinforced Masonry Walls subjected to In-plane Loads,” M.Sc. Engg. Thesis, Department of Civil Engineering, Bangladesh University of Engineering and Technology, Dhaka.

Khajeheian, M. K. and Maheri, M. R. (2017) “Seismic behaviour factor for unreinforced concrete block masonry walls retrofitted with RC layers,” Iran J Sci Technol Trans Civ Eng., 41:389–404.

Khan, A. A. (2018) “The Geo-Genetic Status of Earthquake-Related Hazards and The Role of Human And Policy Dimensions in Impact Mitigation”, Environmental Hazards, Vol.17, No.4, pp. 276–291.

Kit Miyamoto, H., and Amir S.J.G. (2012) “Urban Earthquake Damage Assessment and Reconstruction: 2010 Haiti Earthquake.” World Conference on Earthquake Engineering, Lisboa.

Khoo, C. L. and Hendry, A. W. (1973), “A failure Criteria for Brickwork in Axial Compression,” Proceedings, Third International Brick and Masonry Conference, Essen, Germany, pp. 139-145.

Lang, K. (2000) “Seismic vulnerability of existing buildings.” PhD dissertation, Institute of Structural Engineering, Department of Civil, Environmental and Geomatics Engineering, Swiss Federal Institute of Technology, Zurich, Switzerland.

Lotfi, H. R. and Shing, P. B. (1994), “Interface Model Applied to Fracture of Masonry Structures,” Jr. of Structural Engineering, 120(1), pp. 63-80.

Lourenco, P.B., 2014, “Masonry Structures: Overview,” Encyclopedia of Earthquake Engineering, DOI 10.1007/978-3-642-36197-5_111-1.

Macabuag, J., Guragain, R. and Bhattacharya, S. (2012) “Seismic retrofitting of non-engineered masonry in rural Nepal,” Structures and Buildings.

Mahmoud, R. M., Khajeheian, M. K. and Vatanpour, F. (2019) “In-plane seismic retrofitting of hollow concrete masonry wall with RC layers,” *Structures*, vol. 20, pp. 425-436.

McNary, W. S. and Abram, D. P. (1985) “Mechanics of Masonry Compression”, *Journal of Structural Engineering/ Volume 111 Issue 4*.

Messali, F., Metelli G. and Plizzari, G. (2017)“Experimental results on the retrofitting of hollow brick masonry walls with reinforced high performance mortar coating,” *Construction and Building Materials*, vol. 141, pp. 619–630.

Moffet, P. (2016) “Report: The Sustainability of Masonry in Construction Today” *Masonry Worx*, April.

Mohamed A. E., Lestuzzi, P. and Marc, B. (2007) "Static and cyclic response of masonry wall retrofitted with fiber-reinforced polymers," *J. Compos Constr* 11(1): 50-61.

Mustafa H., Fadil B. and Senad M. (2018) “EXPERIMENTAL TESTING OF SOLID BRICK MASONRY WALLS,” 16th European Conference on Earthquake Engineering, 18-21 June.

Nakagawa, T., Narafu, T., Imai, H. (2012) “Collapse behaviour of a brick masonry house using a shaking table and numerical simulation based on the extended distinct element method.” *Bulletin of Earthquake Engineering*, Vol. 10, pp. 269–283.

Nayak, S. and Dutta, S. C. (2016) “Improving seismic performance of masonry structures with openings by polypropylene bands and L-shaped reinforcing bars,” *J. Perform. Constr. Facil.*, American Society of Civil Engineering (ASCE), 30(2), 04015003.

Priestley, M. J. N., Seible, F. and Calvi, G. M. (1996) “Seismic Design and Retrofit of Bridges,” New York: John Wiley & Sons, Inc.

Rodrigues, H., Furtado, A., Vila-Pouca, N., Varum, H., and Barbosa, A. R. (2018) “Seismic Assessment of a School Building in Nepal and Analysis of Retrofitting Solutions”, Springer, *International Journal of Civil Engineering*, Vol. 16, pp. 1573–1589.

Sakalle, R., Tiwari, N. and Reshi, S. H. (2018) “Seismic Analysis of Old Masonry Buildings using Equivalent Static Method”, *International Journal for Research in*

Applied Science & Engineering Technology (IJRASET) ISSN: 2321-9653, Volume 6 Issue X.

Saleem, M. U., Numada, M., Amin M. N. and Meguro, K. (2016) "Shake table test on FRP retrofitted masonry building model," J. Compos. Constr. American Society of Civil Engineering (ASCE), 20(5).

Sar, D., and Sarkar, P. (2013) "Seismic Evaluation of Existing Unreinforced Masonry Buildings," Proceedings of the International Symposium on Engineering under Uncertainty: Safety Assessment and Management (ISEUSAM - 2012), pp.1267-1276.

Sanket N. and Shekhar C.D. (2016) "Improving Seismic Performance of Masonry Structures with Openings by Polypropylene Bands and L-Shaped Reinforcing Bars", J. Perform. Constr. Facil., 30(2): 04015003.

Sergey C. and Elena D.J. (2011) "Experimental Evaluation of In-Plane Shear Behaviour of Unreinforced and Strengthened Brick Masonry Walls", Conference Paper.

Shah, S. M. A., Shahzada, K., Gencturk, B. and Memon, S. A. (2017) "Retrofitting of full scale masonry building using ferro-cement overlay," J. Perform. Constr. Facil. American Society of Civil Engineering (ASCE), 31(5), 04017079.

Silva, V., Amo-Oduro, D., Calderon, A., et al., (2020) "Development of a global seismic risk model," Earthquake Spectra. Vol. 36, Issue 1, pp.372-394. doi:10.1177/8755293019899953.

Yaghoubifar, A. (2008). "Experimental and analytical investigation on the behaviour of strengthened brick walls by steel bars and concrete." M.Sc. thesis, Dept. of Civil Engineering, Tarbiat Modares Univ., Tehran, Iran.

Zerin, A. I. (2018) Experimental Investigation of the In-plane Cyclic Response of Infilled Reinforced Concrete Frame and Their Possible Retrofit Measures, M.Sc. Thesis, Department of Civil Engineering, Bangladesh University of Engineering and Technology.

APPENDIX

Table A.1 Load-deformation data for specimen SW-C (Control)

Cycle	Load (Ton)	Top Disp. (mm)	Mid Disp. (mm)	Remarks
Cycle-1 (0.78 Ton)	0.00	0.00	0.00	
	0.39	0.08	0.00	
	0.78	0.24	0.03	
	0.39	0.17	0.03	
	0.00	0.10	0.03	
	-0.39	-0.04	0.00	
	-0.78	-0.20	-0.05	
	-0.39	-0.17	-0.05	
Cycle-2 (1.56 Ton)	0.00	0.01	-0.05	
	0.78	0.23	-0.04	
	1.56	0.60	0.05	
	0.78	0.45	0.04	
	0.00	0.26	0.03	
	-0.78	-0.02	-0.05	
	-1.56	-0.42	-0.10	
	-0.78	-0.28	-0.10	
Cycle-3 (3.12 Ton)	0.00	0.04	-0.10	
	0.78	0.35	-0.02	
	1.56	0.72	0.03	
	2.34	1.50	0.28	
	3.12	4.17	0.50	1 st Crack
	2.34	3.16	0.35	
	1.56	2.09	-0.55	
	0.78	0.88	-0.97	
	0.00	0.43	-1.14	
	-0.78	0.21	-1.25	
	-1.56	-0.12	-1.35	
	-2.34	-0.72	-1.51	
	-3.12	-1.50	-1.75	
	-2.34	-1.35	-1.73	
-1.56	-1.04	-1.64		
-0.78	-0.66	-1.53		
0.00	-0.31	-1.44		
Cycle-4 (3.90 Ton)	0.78	0.04	-1.37	
	1.56	0.55	-1.20	
	2.34	1.62	-0.80	
	3.12	4.02	0.69	
	3.51	5.09	1.35	

Cycle	Load (Ton)	Top Disp. (mm)	Mid Disp. (mm)	Remarks
(Cont.)	3.90	6.15	2.04	
	3.51	6.08	2.04	
	3.90	5.68	1.86	
	2.34	3.64	0.95	
	1.56	1.55	-0.32	
	0.78	0.98	-0.72	
	0.00	0.26	-1.02	
	-0.78	0.02	-1.12	
	-1.56	-0.31	-1.23	
	-2.34	-0.82	-1.37	
	-3.12	-1.19	-1.62	
	-3.51	-1.59	-1.76	
	-3.90	-2.35	-1.95	
	-3.51	-2.14	-1.90	
	-3.12	-1.86	-1.80	
	-2.34	-1.51	-1.75	
	-1.56	-1.07	-1.51	
	-0.78	-0.47	-1.40	
	0.00	-0.08	-1.26	
Cycle-5 (3.12 Ton- Partial)	0.78	0.55	-1.07	
	1.56	1.22	-0.90	
	2.34	3.30	1.25	
	3.12	4.97	2.25	

Table A.2 Load-deformation data for specimen SW-CR

Cycle	Load (Ton)	Top Disp. (mm)	Mid Disp. (mm)	Remarks
Cycle-1 (0.78 Ton)	0.00	0.00	0	
	0.39	0.03	0	
	0.78	0.06	0	
	0.39	0.06	0	
	0.00	0.03	0	
	-0.39	-0.03	0	
	-0.78	-0.10	0	
	-0.39	-0.10	0	
	0.00	-0.09	0	
Cycle-2 (1.56 Ton)	0.78	0.04	0	
	1.56	0.19	0	
	0.78	0.19	0	
	0.00	0.09	0	
	-0.78	-0.10	0	
	-1.56	-0.28	0	

Cycle	Load (Ton)	Top Disp. (mm)	Mid Disp. (mm)	Remarks
(Cont.)	-0.78	-0.24	-0.01	
	0.00	-0.11	-0.01	
Cycle-3 (3.12 Ton)	0.78	0.08	0	
	1.56	0.21	0	
	2.34	0.39	0.02	
	3.12	0.62	0.1	
	2.34	0.62	0.1	
	1.56	0.60	0.1	
	0.78	0.45	0.1	
	0.00	0.29	0.18	
	-0.78	0.15	0.08	
	-1.56	-0.08	0.06	
	-2.34	-0.45	0	
	-3.12	-0.94	-0.03	
	-2.34	-0.93	-0.03	
	-1.56	-0.75	-0.03	
	-0.78	-0.47	-0.03	
	0.00	-0.19	-0.03	
Cycle-4 (3.90 Ton)	0.78	0.13	-0.03	
	1.56	0.33	0	
	2.34	0.51	0.02	
	3.12	0.68	0.1	
	3.90	0.98	0.25	
	4.68	1.35	0.42	
	3.90	1.35	0.42	
	3.12	1.27	0.42	
	2.34	1.14	0.42	
	1.56	0.96	0.37	
	0.78	0.82	0.3	
	0.00	0.60	0.23	
	-0.78	0.45	0.17	
	-1.56	0.22	0.12	
	-2.34	-0.19	0.08	
	-3.12	-0.78	0.02	
	-3.90	-1.48	-0.05	
	-4.68	-2.10	-0.11	
	-3.90	-2.10	-0.11	
	-3.12	-1.95	-0.11	
-2.34	-1.71	-0.11		
-1.56	-1.46	-0.11		
-0.78	-0.99	-0.11		
0.00	-0.61	-0.105		

Cycle	Load (Ton)	Top Disp. (mm)	Mid Disp. (mm)	Remarks
Cycle-5 (3.12 Ton)	0.78	-0.13	-0.08	
	1.56	0.47	0	
	2.34	0.73	0.1	
	3.12	0.95	0.17	
	3.90	1.22	0.3	
	4.68	1.39	0.42	
	5.46	1.74	0.6	
	6.24	2.28	0.87	
	5.46	2.25	0.87	
	4.68	2.06	0.85	
	3.90	1.86	0.76	
	3.12	1.71	0.69	
	2.34	0.98	0.56	
	1.56	0.79	0.45	
	0.78	0.59	0.36	
	0.00	0.34	0.25	
	-0.78	0.14	0.16	
	-1.56	-0.05	0.13	
	-2.34	-0.94	0.05	
	-3.12	-1.44	-0.01	
	-3.90	-1.92	-0.11	
	-4.68	-2.49	-0.2	
	-5.46	-2.94	-0.3	
	-6.24	-3.49	-0.41	
	-5.46	-3.49	-0.41	
	-4.68	-3.33	-0.41	
	-3.90	-3.02	-0.41	
	-3.12	-2.03	-0.41	
-2.34	-1.82	-0.4		
-1.56	-1.45	-0.39		
-0.78	-1.18	-0.38		
0.00	-0.80	-0.38		
Cycle-6 (9.36 Ton)	1.56	0.52	-0.12	
	3.12	1.00	0.1	
	4.68	1.53	0.4	
	6.24	2.01	0.67	
	7.80	2.73	1.03	
	9.36	3.75	1.62	
	7.80	3.70	1.62	
	6.24	3.44	1.52	
	4.68	3.08	1.34	
	3.12	2.56	1.07	

Cycle	Load (Ton)	Top Disp. (mm)	Mid Disp. (mm)	Remarks
(Cont.)	1.56	2.05	0.68	
	0.00	0.95	0.28	
	-1.56	0.65	0.1	
	-3.12	-0.02	-0.04	
	-4.68	-1.95	-0.2	
	-6.24	-2.77	-0.38	
	-7.80	-3.85	-0.63	
	-9.36	-5.06	-1.08	
	-7.80	-4.99	-1.08	
	-6.24	-4.49	-1.06	
	-4.68	-4.00	-1.02	
	-3.12	-3.26	-0.92	
	-1.56	-1.71	-0.74	
	0.00	-0.60	-0.55	
Cycle-7 (12.48 Ton)	1.56	0.11	-0.22	
	3.12	0.75	0.11	
	4.68	1.53	0.61	
	6.24	2.19	0.94	
	7.80	3.22	1.26	
	9.36	4.51	1.7	
	10.92	7.05	2.7	
	12.48	8.55	3.75	
	10.92	7.59	3.15	
	9.36	6.57	2.93	
	7.80	6.15	2.64	
	6.24	5.67	2.37	
	4.68	5.06	1.96	
	3.12	4.38	1.54	
	1.56	3.56	1.02	
	0.00	1.90	0.12	
	-1.56	0.70	-0.54	
	-3.12	-1.07	-0.86	
	-4.68	-2.43	-1.83	
	-6.24	-3.53	-2.58	
	-7.80	-4.64	-2.93	
	-9.36	-5.26	-3.38	
	-10.92	-7.04	-4.05	
	-12.48	-9.27	-5.28	
-10.92	-9.27	-5.28		
-9.36	-8.80	-5.27		
-7.80	-8.12	-5.07		
-6.24	-7.48	-4.82		

Cycle	Load (Ton)	Top Disp. (mm)	Mid Disp. (mm)	Remarks
(Cont.)	-4.68	-6.54	-4.56	
	-3.12	-5.05	-4.24	
	-1.56	-3.84	-4.07	
	0.00	-0.24	-3.55	
Cycle-8 (11.70 Ton - Partial)	1.56	3.69	-2.4	
	3.12	5.45	-1.7	
	4.68	6.83	-1.05	
	6.24	7.94	-0.4	
	7.80	8.87	0.28	
	9.36	9.83	0.84	
	10.92	10.55	1.7	
	11.70	11.30	2.25	

Table A.3 Load-deformation data for specimen SW-DR

Cycle	Load (Ton)	Top Disp. (mm)	Mid Disp. (mm)	Remarks
Cycle-1 (0.78 Ton)	0.00	0.00	0	
	0.39	0.05	0	
	0.78	0.14	0.03	
	0.39	0.13	0.03	
	0.00	0.06	0.02	
	-0.39	0.04	0.02	
	-0.78	-0.01	0	
	-0.39	-0.01	0	
	0.00	0.04	0	
Cycle-2 (1.56 Ton)	0.78	0.25	0.07	
	1.56	0.46	0.13	
	0.78	0.40	0.12	
	0.00	0.28	0.04	
	-0.78	0.17	-0.01	
	-1.56	-0.03	-0.05	
	-0.78	0.02	-0.05	
	0.00	0.16	-0.05	
Cycle-3 (3.12 Ton)	0.78	0.35	0.05	
	1.56	0.49	0.12	
	2.34	0.74	0.21	
	3.12	1.05	0.34	
	2.34	1.05	0.33	
	1.56	0.93	0.26	
	0.78	0.78	0.12	
	0.00	0.63	0.06	
	-0.78	0.51	0.01	
	-1.56	0.30	-0.02	
	-2.34	-0.01	-0.06	
	-3.12	-0.47	-0.1	
	-2.34	-0.43	-0.1	

Cycle	Load (Ton)	Top Disp. (mm)	Mid Disp. (mm)	Remarks
(Cont.)	-1.56	-0.22	-0.10	
	-0.78	0.02	-0.08	
	0.00	0.24	-0.07	
Cycle-4 (3.90 Ton)	0.78	0.47	0.03	
	1.56	0.69	0.13	
	2.34	0.93	0.23	
	3.12	1.14	0.35	
	3.90	1.40	0.48	
	4.68	1.72	0.68	
	3.90	1.75	0.67	
	3.12	1.66	0.58	
	2.34	1.51	0.48	
	1.56	1.36	0.39	
	0.78	1.16	0.26	
	0.00	0.93	0.15	
	-0.78	0.75	0.07	
	-1.56	0.67	0.05	
	-2.34	0.29	0.01	
	-3.12	-0.26	-0.04	
	-3.90	-0.84	-0.1	
	-4.68	-1.32	-0.24	
	-3.90	-1.32	-0.21	
	-3.12	-1.15	-0.21	
	-2.34	-0.91	-0.18	
	-1.56	-0.59	-0.15	
	-0.78	-0.25	-0.15	
0.00	0.10	-0.12		
Cycle-5 (3.12 Ton)	0.78	0.41	-0.05	
	1.56	0.76	0.05	
	2.34	1.12	0.19	
	3.12	1.34	0.3	
	3.90	1.55	0.42	
	4.68	1.85	0.53	
	5.46	2.06	0.68	
	6.24	2.44	0.89	
	5.46	2.43	0.885	
	4.68	2.36	0.81	
	3.90	2.18	0.66	
	3.12	2.03	0.56	
	2.34	1.86	0.435	
	1.56	1.65	0.32	
	0.78	1.46	0.22	
	0.00	1.10	0.005	
	-0.78	0.94	-0.06	
	-1.56	0.78	-0.11	
	-2.34	0.34	-0.15	
	-3.12	-0.83	-0.25	
-3.90	-1.37	-0.29		

Cycle	Load (Ton)	Top Disp. (mm)	Mid Disp. (mm)	Remarks
(Cont.)	-4.68	-1.82	-0.36	
	-5.46	-2.17	-0.43	
	-6.24	-2.72	-0.58	
	-5.46	-2.67	-0.58	
	-4.68	-2.60	-0.59	
	-3.90	-2.50	-0.57	
	-3.12	-2.38	-0.54	
	-2.34	-2.24	-0.53	
	-1.56	-2.10	-0.44	
	-0.78	-1.91	-0.31	
0.00	-1.70	-0.28		
Cycle-6 (9.36 Ton)	1.56	-1.13	0.09	
	3.12	-0.60	0.485	
	4.68	0.01	0.72	
	6.24	0.65	0.97	
	7.80	2.02	1.32	
	9.36	3.08	1.7	
	7.80	2.83	1.6	
	6.24	2.53	1.35	
	4.68	2.18	1.12	
	3.12	2.01	1.03	
	1.56	1.63	0.8	
	0.00	0.53	0.32	
	-1.56	0.07	0.11	
	-3.12	-0.43	-0.03	
	-4.68	-1.23	-0.22	
	-6.24	-2.07	-0.43	
	-7.80	-2.67	-0.65	
	-9.36	-3.58	-0.91	
	-7.80	-3.56	-0.91	
	-6.24	-3.30	-0.88	
-4.68	-2.94	-0.79		
-3.12	-2.58	-0.69		
-1.56	-2.19	-0.38		
0.00	-1.89	-0.18		
Cycle-7 (12.48 Ton)	1.56	-1.15	0.18	
	3.12	-0.47	0.565	
	4.68	0.18	0.985	
	6.24	1.12	1.36	
	7.80	2.01	1.675	
	9.36	3.50	2.1	
	10.92	6.03	2.92	
	12.48	8.23	4.3	
	10.92	8.15	4.28	
	9.36	8.01	4.13	
	7.80	7.65	3.82	
	6.24	7.21	3.595	
4.68	6.62	3.18		

Cycle	Load (Ton)	Top Disp. (mm)	Mid Disp. (mm)	Remarks
(Cont.)	3.12	5.93	2.78	
	1.56	5.16	2.3	
	0.00	3.25	1.22	
	-1.56	2.15	1	
	-3.12	0.44	0.6	
	-4.68	-1.17	0.13	
	-6.24	-2.31	-0.3	
	-7.80	-3.24	-0.65	
	-9.36	-4.10	-0.95	
	-10.92	-5.14	-1.35	
	-12.48	-6.67	-2.67	
	-10.92	-6.67	-2.67	
	-9.36	-6.57	-2.67	
	-7.80	-6.22	-2.62	
	-6.24	-5.56	-2.54	
	-4.68	-4.80	-2.18	
	-3.12	-3.93	-1.89	
	-1.56	-2.84	-1.78	
	0.00	-1.25	-1.2	
Cycle-8 (10.14 Ton - Partial)	1.56	1.44	-0.1	
	3.12	2.95	0.7	
	4.68	4.52	1.49	
	6.24	5.88	2.32	
	7.80	7.30	3.2	
	9.36	9.75	4.8	
	10.14	13.43	6.45	

Table A.4 Load-deformation data for specimen LW-C (Control)

Cycle	Load (Ton)	Top Disp. (mm)	Mid Disp. (mm)	Remarks
Cycle-1 (0.78 Ton)	0.00	0.00	0.00	
	0.39	0.03	0.00	
	0.78	0.12	0.04	
	0.39	0.10	0.04	
	0.00	0.05	0.01	
	-0.39	-0.01	0.00	
	-0.78	-0.07	-0.03	
	-0.39	-0.06	-0.02	
	0.00	-0.03	-0.02	
Cycle-2 (1.56 Ton)	0.78	0.12	-0.02	
	1.56	0.26	0.06	
	0.78	0.20	0.06	
	0.00	0.07	0.05	
	-0.78	-0.02	0.04	
	-1.56	-0.13	0.00	
	-0.78	-0.11	0.00	
	0.00	-0.04	0.00	

Cycle	Load (Ton)	Top Disp. (mm)	Mid Disp. (mm)	Remarks
Cycle-3 (3.12 Ton)	0.78	0.14	0.04	
	1.56	0.29	0.12	
	2.34	0.62	0.20	
	3.12	0.94	0.42	
	2.34	0.81	0.42	
	1.56	0.60	0.35	
	0.78	0.41	0.25	
	0.00	0.22	0.11	
	-0.78	0.12	0.08	
	-1.56	-0.02	0.07	
	-2.34	-0.15	0.05	
	-3.12	-0.42	-0.01	
	-2.34	-0.42	-0.01	
	-1.56	-0.38	-0.01	
	-0.78	-0.27	-0.01	
	0.00	-0.17	0.03	
Cycle-4 (3.90 Ton)	0.78	0.04	0.12	
	1.56	0.21	0.20	
	2.34	0.46	0.33	
	3.12	0.93	0.46	
	3.90	2.16	1.10	
	4.68	4.60	1.94	
	3.90	4.35	1.97	
	3.12	3.77	1.63	
	2.34	2.95	1.14	
	1.56	2.25	0.84	
	0.78	1.80	0.63	
	0.00	1.46	0.46	
	-0.78	1.28	0.40	
	-1.56	1.11	0.33	
	-2.34	0.85	0.24	
	-3.12	0.48	0.17	
	-3.90	0.01	0.04	
	-4.68	-0.45	-0.15	
	-3.90	-0.45	-0.15	
	-3.12	0.15	-0.15	
-2.34	0.32	-0.12		
-1.56	0.47	-0.08		
-0.78	0.59	-0.03		
0.00	0.77	0.03		
Cycle-5 (3.12 Ton)	0.78	1.01	0.13	
	1.56	1.33	0.27	
	2.34	1.98	0.50	
	3.12	2.94	0.89	
	3.90	3.97	1.46	
	4.68	5.03	2.03	
	5.46	6.72	2.91	
	4.68	6.72	2.91	

Cycle	Load (Ton)	Top Disp. (mm)	Mid Disp. (mm)	Remarks
(Cont.)	3.90	6.18	2.68	
	3.12	5.30	2.19	
	2.34	4.18	1.66	
	1.56	3.28	1.18	
	0.78	2.54	0.78	
	0.00	2.07	0.60	
	-0.78	1.87	0.51	
	-1.56	1.66	0.37	
	-2.34	1.31	0.23	
	-3.12	0.69	0.10	
	-3.90	0.23	-0.11	
	-4.68	-0.27	-0.30	
-5.46	-0.92	-0.55		

Table A.5 Load-deformation data for specimen LW-CR

Cycle	Load (Ton)	Top Disp. (mm)	Mid Disp. (mm)	Remarks
Cycle-1 (0.78 Ton)	0.00	0.00	0.00	
	0.39	0.01	0.00	
	0.78	0.03	0.00	
	0.39	0.03	0.00	
	0.00	0.01	-0.01	
	-0.39	-0.02	-0.02	
	-0.78	-0.06	-0.02	
	-0.39	-0.06	-0.02	
Cycle-2 (1.56 Ton)	0.00	-0.05	-0.02	
	0.78	0.00	-0.02	
	1.56	0.05	-0.02	
	0.78	0.05	-0.02	
	0.00	-0.02	-0.03	
	-0.78	-0.06	-0.03	
	-1.56	-0.13	-0.03	
	-0.78	-0.13	-0.03	
Cycle-3 (3.12 Ton)	0.00	-0.13	-0.03	
	0.78	-0.05	-0.04	
	1.56	0.01	-0.04	
	2.34	0.11	-0.04	
	3.12	0.24	-0.03	
	2.34	0.22	-0.02	
	1.56	0.18	-0.02	
	0.78	0.11	-0.02	
	0.00	0.01	-0.04	
	-0.78	-0.05	-0.06	
	-1.56	-0.13	-0.07	
	-2.34	-0.21	-0.13	
-3.12	-0.34	-0.14		
-2.34	-0.33	-0.14		

Cycle	Load (Ton)	Top Disp. (mm)	Mid Disp. (mm)	Remarks
(Cont.)	-1.56	-0.32	-0.13	
	-0.78	-0.29	-0.13	
	0.00	-0.24	-0.13	
Cycle-4 (3.90 Ton)	0.78	-0.12	-0.13	
	1.56	-0.02	-0.13	
	2.34	0.02	-0.13	
	3.12	0.11	-0.13	
	3.90	0.22	-0.12	
	4.68	0.41	-0.12	
	3.90	0.37	-0.12	
	3.12	0.34	-0.16	
	2.34	0.29	-0.17	
	1.56	0.23	-0.17	
	0.78	0.13	-0.18	
	0.00	0.00	-0.35	
	-0.78	-0.11	-0.37	
	-1.56	-0.19	-0.45	
	-2.34	-0.30	-0.49	
	-3.12	-0.49	-0.52	
	-3.90	-0.60	-0.60	
	-4.68	-0.73	-0.61	
	-3.90	-0.72	-0.61	
	-3.12	-0.69	-0.61	
	-2.34	-0.64	-0.61	
	-1.56	-0.59	-0.61	
	-0.78	-0.54	-0.61	
0.00	-0.48	-0.61		
Cycle-5 (3.12 Ton)	0.78	-0.42	-0.41	
	1.56	-0.13	-0.41	
	2.34	0.21	0.41	
	3.12	0.40	-0.41	
	3.90	0.49	-0.41	
	4.68	0.61	-0.40	
	5.46	0.75	-0.39	
	6.24	0.87	-0.40	
	5.46	0.87	-0.40	
	4.68	0.81	-0.40	
	3.90	0.72	-0.40	
	3.12	0.68	-0.40	
	2.34	0.59	-0.42	
	1.56	0.50	-0.49	
	0.78	0.42	-0.50	
	0.00	0.31	-0.55	
	-0.78	0.22	-0.57	
	-1.56	0.14	-0.59	
	-2.34	0.10	-0.64	
	-3.12	0.05	-0.65	
-3.90	-0.07	-0.72		

Cycle	Load (Ton)	Top Disp. (mm)	Mid Disp. (mm)	Remarks
(Cont.)	-4.68	-0.22	-0.77	
	-5.46	-0.38	-0.78	
	-6.24	-0.58	-0.79	
	-5.46	-0.58	-0.79	
	-4.68	-0.57	-0.79	
	-3.90	-0.52	-0.79	
	-3.12	-0.48	-0.79	
	-2.34	-0.43	-0.79	
	-1.56	-0.38	-0.79	
	-0.78	-0.32	-0.79	
0.00	-0.23	-0.79		
Cycle-6 (9.36 Ton)	1.56	0.03	-0.79	
	3.12	0.33	-0.79	
	4.68	0.50	-0.79	
	6.24	0.68	-0.79	
	7.80	0.89	-0.79	
	9.36	1.41	-0.79	
	7.80	1.39	-0.79	
	6.24	1.26	-0.79	
	4.68	1.14	-0.80	
	3.12	0.93	-0.80	
	1.56	0.66	-0.80	
	0.00	0.43	-0.85	
	-1.56	0.30	-0.93	
	-3.12	0.15	-0.95	
	-4.68	-0.15	-0.98	
	-6.24	-0.52	-1.02	
	-7.80	-1.00	-1.09	
	-9.36	-1.78	-1.18	
	-7.80	-1.79	-1.38	
	-6.24	-1.68	-1.35	
-4.68	-1.52	-1.35		
-3.12	-1.29	-1.35		
-1.56	-1.03	-1.35		
0.00	-0.72	-1.35		
Cycle-7 (12.48 Ton)	1.56	0.00	-1.35	
	3.12	0.27	-1.35	
	4.68	0.55	-1.15	
	6.24	0.82	-1.07	
	7.80	1.18	-0.89	
	9.36	1.64	-0.56	
	10.92	2.51	-0.06	
	12.48	4.68	1.20	
	10.92	4.55	1.20	First crack
	9.36	4.43	1.20	
	7.80	4.28	1.20	
	6.24	3.98	1.20	
4.68	3.56	0.99		

Cycle	Load (Ton)	Top Disp. (mm)	Mid Disp. (mm)	Remarks
(Cont.)	3.12	3.03	0.72	
	1.56	1.98	0.06	
	0.00	0.61	-0.43	
	-1.56	0.27	-0.65	
	-3.12	0.05	-0.67	
	-4.68	-0.45	-0.80	
	-6.24	-0.95	-1.10	
	-7.80	-1.59	-1.97	
	-9.36	-2.24	-2.15	
	-10.92	-3.05	-2.36	
	-12.48	-4.18	-2.60	
	-10.92	-4.17	-2.60	
	-9.36	-4.12	-2.60	
	-7.80	-3.92	-2.60	
	-6.24	-3.67	-2.60	
	-4.68	-3.28	-2.60	
	-3.12	-2.93	-2.60	
	-1.56	-2.29	-2.60	
0.00	-1.65	-2.60		
Cycle-8 (15.60 Ton - Partial)	1.56	-0.65	-2.55	
	3.12	-0.09	-2.80	
	4.68	0.68	-1.95	
	6.24	1.42	-1.40	
	7.80	2.16	-1.05	
	9.36	3.10	-0.35	
	10.92	3.94	0.20	
	12.48	5.60	0.81	
	14.04	7.34	2.10	
	14.82	8.48	2.95	
	15.60	11.00	4.60	Failure

Table A.6 Load-deformation data for specimen LW-DR

Cycle	Load (Ton)	Top Disp. (mm)	Mid Disp. (mm)	Remarks
Cycle-1 (0.78 Ton)	0.00	0.00	0.00	
	0.39	0.01	0.00	
	0.78	0.04	0.01	
	0.39	0.04	0.01	
	0.00	0.03	0.01	
	-0.39	0.02	0.00	
	-0.78	-0.01	-0.02	
	-0.39	0.00	-0.03	
	0.00	0.00	-0.03	
Cycle-2 (1.56 Ton)	0.78	0.08	0.01	
	1.56	0.18	0.06	
	0.78	0.17	0.06	
	0.00	0.10	0.01	

Cycle	Load (Ton)	Top Disp. (mm)	Mid Disp. (mm)	Remarks
(Cont.)	-0.78	0.06	-0.03	
	-1.56	-0.01	-0.09	
	-0.78	-0.01	-0.09	
	0.00	0.01	-0.07	
Cycle-3 (3.12 Ton)	0.78	0.10	-0.01	
	1.56	0.18	0.04	
	2.34	0.30	0.10	
	3.12	0.41	0.15	
	2.34	0.40	0.15	
	1.56	0.33	0.14	
	0.78	0.24	0.09	
	0.00	0.18	0.01	
	-0.78	0.13	-0.03	
	-1.56	0.05	-0.08	
	-2.34	-0.04	-0.18	
	-3.12	-0.18	-0.15	
	-2.34	-0.18	-0.15	
	-1.56	-0.17	-0.14	
	-0.78	-0.14	-0.12	
	0.00	-0.06	-0.09	
Cycle-4 (3.90 Ton)	0.78	0.06	-0.05	
	1.56	0.17	0.00	
	2.34	0.27	0.07	
	3.12	0.39	0.13	
	3.90	0.50	0.19	
	4.68	0.63	0.27	
	3.90	0.62	0.27	
	3.12	0.58	0.27	
	2.34	0.48	0.27	
	1.56	0.40	0.25	
	0.78	0.30	0.15	
	0.00	0.23	0.06	
	-0.78	0.20	-0.01	
	-1.56	0.12	-0.06	
	-2.34	0.02	-0.09	
	-3.12	-0.18	-0.13	
	-3.90	-0.42	-0.19	
	-4.68	-0.60	-0.25	
	-3.90	-0.60	-0.25	
	-3.12	-0.59	-0.25	
-2.34	-0.52	-0.22		
-1.56	-0.43	-0.19		
-0.78	-0.34	-0.17		
0.00	-0.24	-0.14		
Cycle-5 (3.12 Ton)	0.78	-0.07	-0.09	
	1.56	0.11	-0.02	
	2.34	0.24	0.05	
	3.12	0.37	0.12	

Cycle	Load (Ton)	Top Disp. (mm)	Mid Disp. (mm)	Remarks
(Cont.)	3.90	0.42	0.20	
	4.68	0.61	0.28	
	5.46	0.74	0.37	
	6.24	0.88	0.52	
	5.46	0.88	0.52	
	4.68	0.83	0.49	
	3.90	0.76	0.44	
	3.12	0.68	0.41	
	2.34	0.59	0.37	
	1.56	0.48	0.28	
	0.78	0.43	0.20	
	0.00	0.37	0.09	
	-0.78	0.28	0.00	
	-1.56	0.22	-0.05	
	-2.34	0.13	-0.11	
	-3.12	0.06	-0.16	
	-3.90	-0.09	-0.22	
	-4.68	-0.22	-0.26	
	-5.46	-0.44	-0.35	
	-6.24	-0.64	-0.44	
	-5.46	-0.64	-0.45	
	-4.68	-0.63	-0.45	
	-3.90	-0.56	-0.39	
	-3.12	-0.49	-0.40	
	-2.34	-0.38	-0.37	
	-1.56	-0.24	-0.33	
-0.78	-0.15	-0.30		
0.00	-0.08	-0.28		
Cycle-6 (9.36 Ton)	1.56	0.05	-0.21	
	3.12	0.23	-0.12	
	4.68	0.40	0.01	
	6.24	0.63	0.19	
	7.80	0.94	0.39	
	9.36	1.27	0.64	
	7.80	1.26	0.65	
	6.24	1.18	0.60	
	4.68	1.03	0.50	
	3.12	0.85	0.39	
	1.56	0.16	0.25	
	0.00	0.00	0.12	
	-1.56	-0.11	0.03	
	-3.12	-0.29	-0.06	
	-4.68	-0.61	-0.16	
	-6.24	-1.00	-0.25	
-7.80	-1.53	-0.38		
-9.36	-2.06	-0.52		
-7.80	-2.06	-0.53		
-6.24	-1.97	-0.51		

Cycle	Load (Ton)	Top Disp. (mm)	Mid Disp. (mm)	Remarks
(Cont.)	-4.68	-1.76	-0.45	
	-3.12	-1.57	-0.40	
	-1.56	-1.31	-0.35	
	0.00	-0.87	-0.29	
Cycle-7 (12.48 Ton)	1.56	-0.44	-0.18	
	3.12	-0.23	-0.07	
	4.68	0.10	0.15	
	6.24	0.29	0.31	
	7.80	0.57	0.52	
	9.36	0.90	0.75	
	10.92	1.42	1.15	
	12.48	2.17	1.84	
	10.92	2.17	1.84	
	9.36	1.88	1.58	
	7.80	1.82	1.57	
	6.24	1.74	1.52	
	4.68	1.56	1.35	
	3.12	1.33	1.17	
	1.56	1.01	0.97	
	0.00	0.65	0.76	
	-1.56	0.50	0.65	
	-3.12	0.13	0.38	
	-4.68	-0.51	0.14	
	-6.24	-1.10	-0.07	
	-7.80	-1.75	-0.30	
	-9.36	-2.52	-0.55	
	-10.92	-3.94	-0.94	
	-12.48	-4.74	-1.35	
	-10.92	-4.74	-1.34	
	-9.36	-4.31	-1.24	
-7.80	-4.19	-1.16		
-6.24	-3.99	-1.11		
-4.68	-3.76	-1.07		
-3.12	-3.39	-0.98		
-1.56	-3.00	-0.89		
0.00	-2.23	-0.79		
Cycle-8 (12.48 Ton - Partial)	1.56	-1.20	-0.77	
	3.12	-0.59	-0.66	
	4.68	-0.10	-0.48	
	6.24	0.29	-0.17	
	7.80	0.62	0.01	
	9.36	0.83	0.21	
	10.92	1.59	0.93	
	12.48	2.42	1.69	
	14.04	2.93	1.86	First crack
	15.60	4.28	2.55	
	17.16	5.78	3.60	
18.72	18.36	11.08	Ultimate	

Cycle	Load (Ton)	Top Disp. (mm)	Mid Disp. (mm)	Remarks
(Cont.)	17.16	17.65	10.26	
	15.60	17.58	10.19	
	14.04	17.45	10.10	
	12.48	17.14	9.93	
	10.92	16.52	9.53	
	9.36	15.23	8.95	
	7.80	14.30	8.25	
	6.24	12.42	7.10	
	4.68	10.94	6.22	
	3.12	9.38	5.30	
	1.56	7.01	3.80	
	0.00	5.52	2.52	
	-1.56	5.05	2.08	
	-3.12	3.96	1.45	
	-4.68	2.85	0.98	
	-6.24	1.26	0.58	
	-7.80	-0.15	0.10	
	-9.36	-0.92	-0.55	
	-10.92	-1.23	-1.70	
	-12.48	-2.98	-3.80	

Calculation of average compressive strength and shear strength according to BNBC 2020:

The formula used from BNBC 2020 are equation (6.7.1) and –

Unreinforced masonry walls, columns and reinforced masonry wall:

$$F_a = \frac{f'_m}{5} \left[1 - \left(\frac{h'}{42t} \right)^3 \right] \quad (6.7.1)$$

Shear Stress for Shear Walls, F_v

Unreinforced masonry, clay units:

$$F_v = 0.025 \sqrt{f'_m} \leq 0.40 \text{ N/mm}^2$$

The parameters are calculated according to the equations given above.

For unreinforced masonry walls, according to BNBC 2020

Allowable Compressive Strength:

$$F_a = \frac{f'_m}{5} \left[1 - \left(\frac{h'}{42t} \right)^3 \right]$$

For short walls,

$$F_a = \frac{11.1}{5} \left[1 - \left(\frac{1500}{42 * 125} \right)^3 \right] = 2.17 \text{ MPa}$$

$$P_a = 2.17 * (1500 * 125) = 41.45 \text{ Ton}$$

For long walls,

$$F_a = \frac{11.1}{5} \left[1 - \left(\frac{1500}{42 * 125} \right)^3 \right] = 2.17 \text{ MPa}$$

$$P_a = 2.17 * (2000 * 125) = 55.50 \text{ Ton}$$

Allowable Shear Strength:

For clay units

$$F_v = 0.025 \sqrt{f'_m} \leq 0.40 \text{ N/mm}^2$$

Where,

$$\begin{aligned} f'_m &= \text{Specified compressive strength of masonry at the age of 28 days} \\ &= 11.1 \text{ MPa} \end{aligned}$$

For short wall,

Length, L= 1500 mm (5')

Thickness, t=125 mm (5")

Therefore,

$$F_v = 0.025 * \sqrt{11.01}$$

$$= 0.08 \text{ MPa}$$

$$P_v = 0.08 * (1500 * 125)$$

$$= 1.59 \text{ Ton}$$

For long wall,

$$\text{Length, } L = 2000 \text{ mm (6'-8")}$$

$$\text{Thickness, } t = 125 \text{ mm (5")}$$

Therefore,

$$F_v = 0.025 * \sqrt{11.01}$$

$$= 0.08 \text{ MPa}$$

$$P_v = 0.08 * (2000 * 125)$$

$$= 2.12 \text{ Ton}$$

The details of the parameters calculated are summarized in the following Table A.7:

Table A.7 Compressive and shear strength of masonry (BNBC 2020)

Parameters	Short Wall (1500 mm x 1500 mm)	Long Wall (2000 mm x 1500 mm)
Prism Strength (From test)	$f_m = 11.102 \text{ MPa}$	$f_m = 11.102 \text{ MPa}$
Length of wall,	$L = 1500 \text{ mm}$	$L = 2000 \text{ mm}$
Height of wall,	$h' = 1500 \text{ mm}$	$h' = 1500 \text{ mm}$
Thickness of wall,	$t = 125 \text{ mm}$	$t = 125 \text{ mm}$
Allowable Compressive Stress,	$F_a = 2.17 \text{ MPa}$	$F_a = 2.17 \text{ MPa}$
Compressive Load,	$P_a = 41.45 \text{ Ton}$	$P_a = 55.26 \text{ Ton}$
Allowable Shear stress,	$F_v = 0.08 \text{ MPa}$	$F_v = 0.08 \text{ MPa}$
Shear force,	$P_v = 1.59 \text{ Ton}$	$P_v = 2.12 \text{ Ton}$

Table A.8 28-days compressive strength data of concrete for base

Sl.	Dia. (mm)	Area (mm ²)	Observed Load (kN)	Actual Load (kN)	Strength (MPa)	Average Strength (MPa)
1	101	8011.9	278	278.4	34.7	37.2
2	102	8171.3	320	322.0	39.4	
3	101	8011.9	298	299.2	37.3	

Table A.9 Compressive strength test data for concrete of RC overlay

Wall	Days	Sample	Dia. (mm)	Area (mm ²)	Applied Load (kN)	Actual Load (kN)	Comp. Strength (MPa)	Average Strength (MPa)
LW-DR	7	1	101	8011.87	247	248.74	31.05	31.69
		2	100.5	7932.74	248	249.71	31.48	
		3	100.5	7932.74	256	258.28	32.56	
	28	1	101	8011.87	300	302.17	37.72	37.13
		2	101	8011.87	290	292.12	36.46	
		3	101	8011.87	296	298.15	37.21	
SW-DR	7	1	101	8011.87	230	231.84	28.94	29.27
		2	101	8011.87	248	249.93	31.19	
		3	101	8011.87	220	221.80	27.68	
	28	1	100.5	7932.74	295	297.15	37.46	37.17
		2	101	8011.87	285	287.10	35.83	
		3	100	7854.00	298	300.16	38.22	
SW-CR	7	1	100.5	7932.74	181	182.61	23.02	22.80
		2	100	7854.00	185	186.63	23.76	
		3	100.5	7932.74	170	171.56	21.63	
	28	1	101	8011.87	292	294.13	36.71	35.71
		2	101	8011.87	272	274.04	34.20	
		3	101	8011.87	288	290.12	36.21	
LW-CR	7	1	101	8011.87	192	193.66	24.17	25.00
		2	100	7854.00	180	181.61	23.12	
		3	100.5	7932.74	218	219.79	27.71	
	28	1	101	8011.87	230	231.84	28.94	33.24
		2	100.5	7932.74	290	292.12	36.83	
		3	101	8011.87	270	272.03	33.95	